VOL. 1 No. 5
OCTOBER 1959

JRNAL OF THE

LESS-COMMON METALS

UNIVERSITY OF HAWAII
LIBRARY
FEB 8 '61

AN INTERNATIONAL JOURNAL ON
THEIR CHEMISTRY AND METALLURGY

RS:
UTHBERTSON (Nottingham)
RBROTHER (Manchester)

RIAL ADVISORY BOARD:
ARD (Paris)
ICE COOK (Birmingham)
ROLY (Brussels)
JINGHEUZIAN (Ottawa)
LETCHER (Harwell)
GONSER (Columbus, Ohio)
NSEN (Frankfurt a.M.)
DELLI (Genoa)
EMM (Münster)
ROLL (Corvallis, Ore.)
RRAY (Harwell)
WOTNY (Vienna)
IDGEON (Toronto)
OWELL (Wembley)
ALSTON (Hyattsville, Md.)
AN ARKEL (Leyden)
WORNER (Melbourne)
NTEMA (Menlo Park, Calif.)

ELSEVIER

GENERAL INFORMATION

Types of contributions

(a) Original research work not previously published in other periodicals.
(b) Reviews on recent developments in various fields.
(c) Short communications.
(d) Bibliographical notes and book reviews.

Languages

Papers will be published in English, French or German.

Submission of papers

Papers should be sent to one of the following Editors:

Professor J. W. CUTHBERTSON (*Metallurgy*), Department of Metallurgy, The Uni
versity, University Park, Nottingham, England.
Professor F. FAIRBROTHER (*Chemistry*), The University of Manchester, Departmen
of Chemistry, Manchester 13, England.

Authors should preferably submit two copies in double-spaced typing on pages of uniforn
size. Legends for figures should be typed on a separate page. The figures should be in
form suitable for reproduction, drawn in Indian ink on drawing paper or tracing pape
with lettering etc. in thin pencil. The sheets of drawing or tracing paper should preferabl
be of the same dimensions as those on which the article is typed. Photographs should b
submitted as clear black and white prints on glossy paper.
All references should be given at the end of the paper. They should be numbered and th
numbers should appear in the text at the appropriate places.
A summary of 50 to 200 words should be included. Authors of papers in French or Germa
are encouraged to supply also a translation of the summary in English.

Reprints

Twenty-five reprints will be supplied free of charge. Additional reprints can be ordered a
quoted prices. They must be ordered on order forms which are sent together with th
proofs.

Publication

The *Journal of the Less-Common Metals* will have six issues to the volume, approx. 500 page
per volume.
Subscription price: £ 5.7.6 or $ 15.— or Dfl. 57.— per volume (post free).
For advertising rates apply to the publishers.

Subscriptions

Subscriptions should be sent to:

ELSEVIER PUBLISHING COMPANY, Spuistraat 110-112, Amsterdam-C., The Netherlands

A STUDY OF RHODIUM(III) OXALATES BY PAPER ELECTROPHORESIS, PAPER CHROMATOGRAPHY, ION-EXCHANGE CHROMATOGRAPHY AND SPECTROPHOTOMETRY

S. K. SHUKLA

Institut du Radium, Laboratoire Curie, Paris (France)

(Received August 19th, 1959)

SUMMARY

The results obtained in an investigation of rhodium(III) oxalates indicate that heating of pure rhodium(III) hydroxide with oxalic acid solution produces $RhOx_3^{-3}$ to a great extent, but that the reaction does not go to completion, other aquo-coördinated oxalato complexes of rhodium being formed in smaller quantities. Evidence is presented that in order to obtain complete conversion of rhodium(III) into potassium rhodiotrioxalate the chloride must be heated under reflux with four to five times its weight of potassium oxalate for at least 6 hours. The absorption spectrum, the stability to heating and aging at room temperature in solution, as well as the electrophoretic, paper- and ion-exchange chromatographic properties of the rhodiotrioxalate ion were studied. It was shown that the *dextro-* and *laevo-*forms of $RhOx_3^{-3}$ have identical electrophoretic mobilities.

INTRODUCTION

The stability and optical activity of the rhodium(III) oxalates are responsible for their being among the most studied compounds of the metal. LEIDIÉ[1] seems to have been the first to prepare the oxalates $M_3[Rh(C_2O_4)_3]$, where M represents Na, K, or NH_4. Their resolution into optical isomers was achieved by WERNER[2]. In 1929, DELÉPINE[3] utilised the action of potassium oxalate on potassium chlororhodites to prepare potassium rhodiodichlorodioxalates and potassium rhodiotrioxalates. LIFSCHITZ AND ROSENBOHM[4] studied the absorption spectrum of $RhOx_3^{-3}$, which showed a low band at 25,000 and a higher one at 35,000 cm^{-1}. In a solution obtained by heating a mixture of 0.1 *M* $RhCl_6^{-3}$ and 0.6 *M* K_2Ox for four hours JØRGENSEN[5] obtained the first band as the crystal field band, the other as electron transfer band and a shoulder on the red side of the latter as second crystal field band, and attributed them to $RhOx_3^{-3}$.

In our work[6-9] on the complexes that rhodium(III) forms with HCl, HBr, HNO_3, H_2SO_4 and $HClO_4$, using paper electrophoresis, paper chromatography, ion-exchange chromatography and spectrophotometry, we found that, in all the cases examined the reaction is not so simple as had previously been reported; a series of complexes occur due to the high coördinating power of rhodium(III) and it is especially difficult to get rid of chloro-groups if they are present in the starting substance. Valuable information and some quite new results were obtained by applying the above methods

References p. 342

to the study of halides, sulphates and perchlorates. The aim of the present work was to continue the investigation of complexes by applying the above methods to the rhodium oxalates.

TECHNIQUES

Paper electrophoresis

The glass plate technique, as described by LEDERER AND WARD[10], was used, with 250 V and a run of 45 minutes on paper strips 2.7 × 40 cm (Papier d'Arches No. 302). For preparative purposes we used Whatman No. 3 MM paper strips (7.5 × 40 cm) and the time of the run was also increased when necessary. In preliminary experiments it was found that a 1 *N* solution of potassium oxalate was the most suitable electrolyte for the electrophoresis of all the oxalates studied. Aquation of the rhodium oxalates occurred when solutions of oxalic acid or mixtures of oxalic acid with potassium oxalate were used as electrolytes (see later).

The bands were detected by spraying the paper with a solution of $SnCl_2$ and KI in 5 *N* HCl and heating the paper under an infra-red lamp.

Paper chromatography

The ascending technique with Whatman No. 1 paper strips was employed. The developing solvents were water, 1 *N* potassium oxalate, 1 *N* oxalic acid, methanol, ethanol, butanol, and methanol, ethanol and butanol acidified with 2% acetic acid.

Ion-exchange chromatography

Columns filled with anion-exchange resin Dowex-2 were used for investigating the nature and separation of the different ionic species formed from rhodium in the reaction mixture. After charging with the solution to be analysed, the columns were eluted with 1 *N* potassium oxalate and/or 1 *N* oxalic acid.

Whatman No. 1 paper strips impregnated with Dowex-50 resin were also employed to investigate the nature of the rhodium in the reaction mixture and the oxalates obtained.

Spectrophotometry

The absorption spectra of the solutions were measured with a spectrophotometer of Jobin and Yvon (Paris), using quartz cells.

EXPERIMENTAL RESULTS

Reaction of rhodium hydroxide with oxalic acid

According to LEIDIÉ[1] dissolution of rhodium hydroxide in hot, concentrated oxalic acid leads to the formation of rhodium oxalate. We dissolved freshly prepared and electrophoretically pure[8] (*i.e.* a single fast cationic band being obtained in $HClO_4$, which is our criterion for the purity of the hydroxide) rhodium hydroxide in concentrated oxalic acid solution and heated it at about 105°C under reflux. The hydroxide went into solution, most of it even in the cold and completely after a short heating, giving a clear yellowish red solution which was pure yellow when viewed in thin test tubes. In Fig. 1a the electropherogram of the above solution after 15 minutes

References p. 342

heating is given. It shows that the solution contains two anionic species of rhodium. It can be seen that most of the hydroxide is converted into a fast anion, whose identity with $RhOx_3^{-3}$ was established (see the following section). We consider that the slower band is due to an aquo-oxalato-complex ion of rhodium, possibly $Rh(H_2O)_2Ox_2^{-1}$. When the solution was passed through a column filled with Dowex-2 resin two bands were

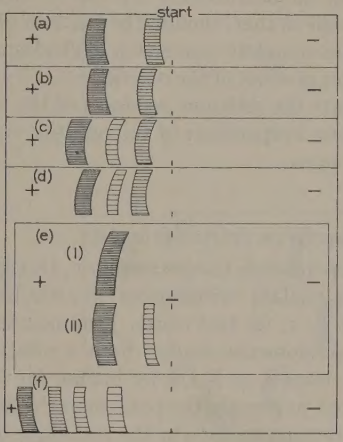

Fig. 1. Electropherograms (250 V for 45 min; electrolyte 1 *N* K_2Ox) of (a) a mixture of $Rh(OH)_3$ and oxalic acid heated for 15 min; (b) mixture (a) heated for 10 h; (c) mixture (a) heated for 12 h; (d) mixture (a) heated for 30 h; (e) an aqueous solution of crystals of potassium rhodiotrioxalate (I) and solution (b) electrophorised on the same paper (II); (f) solution (b) electrophorised for 1 h using 1 *N* oxalic acid as the electrolyte.

again obtained (Fig. 4(I)), a wide, strongly absorbed one at the top of the column and another at about 1 cm below the first. Both the complexes were so strongly absorbed on the resin at these positions that on elution with large amounts of 1 *N* potassium oxalate solution, 1 *N* oxalic acid or water neither the position of the bands could be shifted nor the substances eluted.

To investigate the influence of time of heating, we continued refluxing the solution. At different intervals, (half an hour at first and longer afterwards), samples of the solution were taken and then subjected to electrophoresis. Selected electropherograms are shown in Fig. 1. Boiling of the solution for 10 hours (Fig. 1b) did not cause any appreciable change either in the nature of the two anions or in their relative amounts. On continuing heating for two hours more we found that a third light band appeared (Fig. 1c), situated between the two other electrophoretic bands, which were still present. Fig. 1d, obtained after heating the solution for 30 hours, shows that the reaction does not give a single anionic species of rhodium. In Fig. 1f one of the electropherograms with 1 *N* oxalic acid as electrolyte, is given. It shows three to four anionic species, probably resulting from the aquation that occurs when the sample is put on the paper in the presence of oxalic acid.

The fast anionic band, which constituted the major fraction of the reaction product

References p. 342

was eluted from the electropherogram and re-electrophorised using 1 *N* potassium oxalate as the electrolyte. It gave a single anionic band with the same mobility as in the reaction mixture. With oxalic acid we again found three bands very similar to those shown in Fig. 1c. The eluted solution of the fast anionic band gave the same spectrum as that of pure $RhOx_3^{-3}$ (Fig. 6). These data as well as those of Fig. 1e which is an electropherogram of the reaction mixture after heating for 10 hours and of a solution of potassium rhodiotrioxalate crystals in water electrophorised on the same paper, leads us to believe that, though the reaction of rhodium hydroxide with oxalic acid does not end in complete conversion of rhodium into rhodium trioxalate this compound is the major product of the reaction.

Our attempts to separate the different products of the reaction by crystallisation were not successful because evaporation of the mixture even under mild conditions gave only an amorphous mass.

Action of rhodium(III) chloride on potassium oxalate

For the preparation of potassium rhodiotrioxalate, DELÉPINE[3] recommends boiling a solution of potassium oxalate with either $K_2[RhCl_5(H_2O)]$ or $K_3RhCl_6 \cdot H_2O$ in the molecular ratio of 3 : 1, for two hours. JØRGENSEN[5] obtained the solution of $RhOx_3^{-3}$ for his spectrophotometric studies from a solution 0.1 *M* with respect to $RhCl_6^{-3}$ and 0.6 *M* with respect to K_2Ox by boiling for four hours at 100°. In the present work we attempted to prepare the potassium rhodiotrioxalate from hydrated rhodium chloride and potassium oxalate by the technique of the above authors.

We prepared an aqueous solution of rhodium chloride and five times its weight of potassium oxalate. The solution was red and somewhat turbid, but became clear dark red after warming slightly. When this solution was electrophorised with 1 *N* K_2Ox as electrolyte three anionic bands were obtained of which the fastest was deep red, the slowest brown and the band in between light rose. The red constituent formed the major part, there being less of the brown and least of the rose constituent. When an aliquot of the solution was left to stand at room temperature it soon turned yellow (when viewed through a thin test tube) but still gave the three anionic species with mobilities identical to those described above (Fig. 2a). A preliminary experiment for the preparation of the trioxalate showed that the reaction is relatively slow when the solution is heated on the water bath. We, therefore, refluxed the solution and electrophorised aliquots after different periods of heating.

On heating, the red solution of rhodium chloride and potassium oxalate first passes through a stage of a dark brown turbidity, and then became yellowish red after about two to three minutes. In Fig. 2a an electropherogram made after 15 minutes refluxing is given. The fastest anionic band was visible and had a yellow colour; the two other bands appeared only after applying the reagent for rhodium. The relative distribution and the mobilities of these species of rhodium were the same as those of the starting solution. We believe that these species are $RhCl_6^{-3}$, $[RhCl_5(H_2O)]^{-2}$ and $[RhCl_4(H_2O)_2]^{-}$ respectively. The electropherogram in Fig. 2b was obtained after boiling for 1 hour and 15 minutes. It can be seen that a slight change has occurred. In the next hour of heating an appreciable change occurred, as is shown in Fig. 2c. Only two anionic bands were obtained and these differed in mobility from those in Figs. 2a and b. The anion of higher charge was yellow and formed the major part of the mixture, the

References p. 342

slower only became visible on development of the electropherogram. We suggest that after about two hours heating the two hexachloro-, $RhCl_6^{-3}$, and diaquotetrachloro, $[RhCl_4(H_2O)_2]^-$, ions react with the oxalate ion to give $RhOx_3^{-3}$ and $[RhOx_2(H_2O)_2]^-$ ions respectively, which form the rapid and slow anionic bands in the electropherogram. It is evident from Figs. 2d and e, obtained after boiling for 4 and 5 hours respectively, that, except for the decreasing concentration of the slower anionic rhodiodiaquodioxalato ion, both the colour and the mobility of the two species of rhodium have not altered much. Complete conversion into rhodiotrioxalato ion seems to be attained after refluxing the solution for 6 hours, when electrophoresis shows only a single anionic rhodium species, identical in all respects to the fast band of Figs. 2c, d and e. In order to ascertain whether further boiling of the solution gives rise to other changes, we continued heating under reflux for a further period of 24 hours. The electropherograms were always identical to that obtained after 6 hours of boiling (Fig. 2f). Heating was then discontinued and the solution was left to crystallise. Deep orange coloured, well-defined hexagonal crystals of racemic potassium rhodiotrioxalate were obtained. These crystals were found to be non-hygroscopic and very soluble in water. Both the crystals and their aqueous solution were quite stable at room temperature. Electropherograms of aqueous solutions of the crystals of potassium rhodiotrioxalate are shown in Fig. 3. With 1 *N* K_2Ox solution as the electrolyte, a fresh solution as well as one aged at room temperature for more than two and a half months gave only a single anionic band, the mobility of which was the same as that obtained with the solution from which the crystals had been prepared. Even on allowing the electrophoresis to run for 2 hours, in which time the rhodiotrioxalato ion had moved a

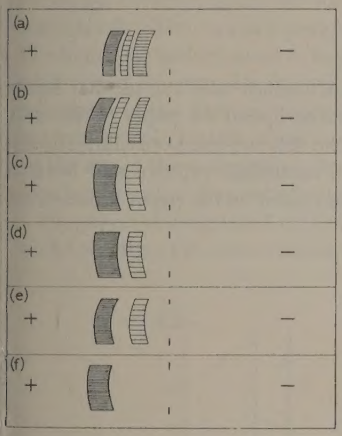

Fig. 2. Electropherograms (250 V for 45 min; electrolyte 1 *N* K_2Ox) of a mixture of $RhCl_3$ and K_2Ox solutions heated for (a) 15 min; (b) 1¼ h; (c) 2¼ h; (d) 4 h; (e) 5 h; and (f) 6 h.

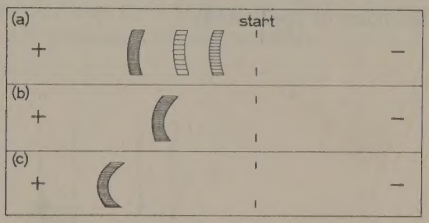

Fig. 3. Electropherograms of aqueous solutions of crystals of potassium rhodiotrioxalate. Conditions: (a) 250 V for 45 min; electrolyte 1 *N* oxalic acid; (b) 250 V for 45 min; electrolyte 1 *N* K_2Ox; (c) 250 V for 2 h; electrolyte 1 *N* K_2Ox.

References p. 342

distance of 9.5 cm on the paper, the rhodium complex did not show any signs of decomposition (Fig. 3c). However, when oxalic acid or a mixture of oxalic acid and potassium oxalate was used as electrolyte, the same solution of the crystals and also the solution that had given a single fast anionic band with 1 N K_2Ox solution, gave three and sometimes even four anionic bands of lower mobility (Fig. 3a). As already pointed out, we suppose that this is due to aquation of the $RhOx_3^{-3}$ ion in the presence of oxalic acid.

Paper chromatography

The solution of the crystals of potassium rhodiotrioxalate and the mother liquor from which they had been obtained, were chromatographed on paper. With 1 N oxalic acid, 1 N potassium oxalate and water as the solvent the potassium rhodiotrioxalate moved with the liquid front, while with methanol, ethanol and butanol as such or acidified with 2% acetic acid, the solution placed on the paper remained at the point of application.

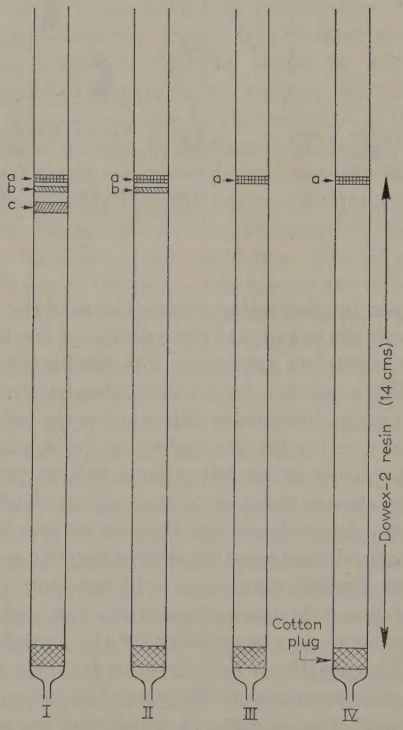

Fig. 4. Ion-exchange chromatograms on columns of Dowex-2 resin of (I) a mixture of $RhCl_3$ and K_2Ox solutions heated for 2 h; (II) the same mixture heated for 4 h; (III) the same mixture heated for 6 h; (IV) an aqueous solution of crystals of potassium rhodiotrioxalate.

References p. 342

Ion-exchange chromatography

Fig. 4 shows the chromatograms on columns filled with anion-exchange resin Dowex-2. The eluting solvent was 1 *N* potassium oxalate, 1 *N* oxalic acid or distilled water. Similar to the results obtained on electrophoresis, the mixture of the rhodium chloride and potassium oxalate solutions gave, after different periods of heating, the same number of strongly adsorbed bands. Figs. 4 (I), (II) and (III) show the ion-exchange chromatograms of solutions that had been refluxed for 2, 4 and 6 hours respectively. The oxalato-complexes of rhodium are highly adsorbed on Dowex-2. The bands (a) and (b) seem to be due to $RhOx_3^{-3}$ and $RhOx_2(H_2O)_2^-$ ions respectively, while band (c) may be due to some chloro-coördinated anionic rhodium complex because it is the first to disappear on further boiling. Fig. 4 (IV) was obtained with the solution of crystals of potassium rhodiotrioxalate; the band is so firmly adsorbed on the top of the column that prolonged elution with oxalic acid or potassium oxalate solution or water does not change its position.

On papers impregnated with the cation-exchange resin Dowex-50, $RhOx_3^{-3}$ moved with the solvent in water, oxalic acid or 1 *N* potassium oxalate solution.

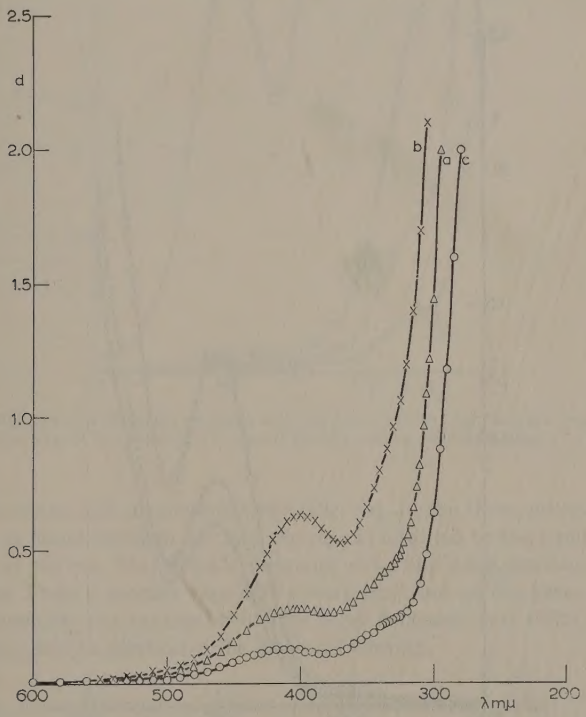

Fig. 5. Absorption spectra of (a) a solution of $RhCl_3$ and K_2Ox heated for 4 h; (b) a solution obtained by elution of the fast anionic band in the electropherogram (Fig. 2d) of solution (a); (c) a solution obtained by elution of the slower anionic band in the electropherogram (Fig. 2d) of solution (a).

References p. 342

Absorption spectra

Fig. 5a shows the spectrum of the solution of $RhCl_3$ and K_2Ox, after it had been boiled for 4 hours; by electrophoresis and ion-exchange chromatography it has been shown that it contains $RhOx_3^{-3}$ and $[RhOx_2(H_2O)_2]^-$ (Figs. 2d and 4(II)). Curve (a) of Fig. 5 has a low band at 405 mμ, a shoulder at 330 mμ and a shallow minimum at 375 mμ. When the fast electrophoretic band in the above solution (Fig. 2d) was eluted from the electropherogram with 1 *N* K_2Ox solution, it gave a curve (Fig. 5b) with only one maximum at 400 mμ and a minimum at 370 mμ. The slower anionic band of rhodium in the electropherogram of Fig. 2d gave quite a different absorption curve, with a band at 410 mμ, a higher shoulder (more prominent than the one in curve a) extending from 315 to 345 mμ, and a minimum at 380 mμ. Comparison of curves (a), (b) and (c) of Fig. 5 shows that the absorption curve (a) of the mixture of solutions is a combination of curves (b) and (c) relating to its components, for a similar curve will be obtained if the sum of the absorptions of (b) and (c) is plotted.

Fig. 6 shows the identity of the absorption curves of $RhOx_3^{-3}$ obtained from different sources: (a) solution of $RhCl_3$ and K_2Ox heated for 14 hours, (b) solution of the $RhOx_3^{-3}$ band eluted from the electropherogram of the mixture obtained by heating

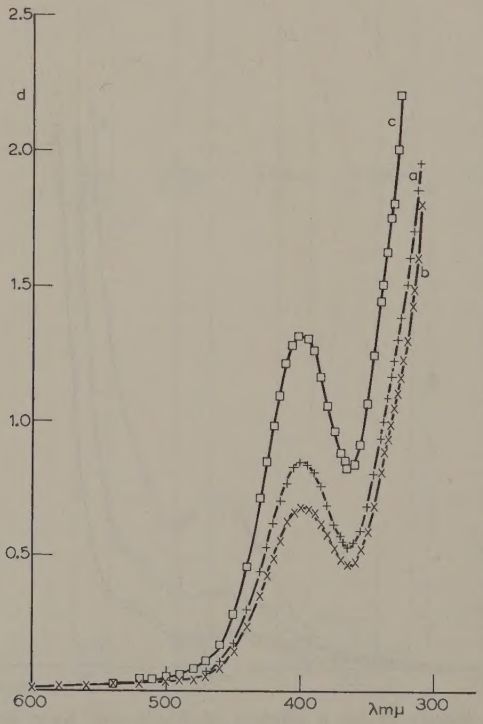

Fig. 6. Absorption spectra of (a) a solution of $RhCl_3$ and K_2Ox heated for 14 h; (b) a solution obtained by elution of the fast anionic band in the electropherogram of the mixture of $Rh(OH)_3$ and oxalic acid heated for 14 h; (c) an aqueous solution of crystals of potassium rhodiotrioxalate.

References p. 342

$Rh(OH)_3$ and oxalic acid for 14 hours and (c) aqueous solution of crystals of K_3RhOx_3. These curves are in every respect identical with curve (b) of Fig. 5.

In Fig. 7 the absorption spectra are shown of the solutions of crystals of potassium rhodiotrioxalate in water at different dilutions and in the wavelength range 200 to 500 mμ. With a concentrated solution it is difficult to go to a higher frequency

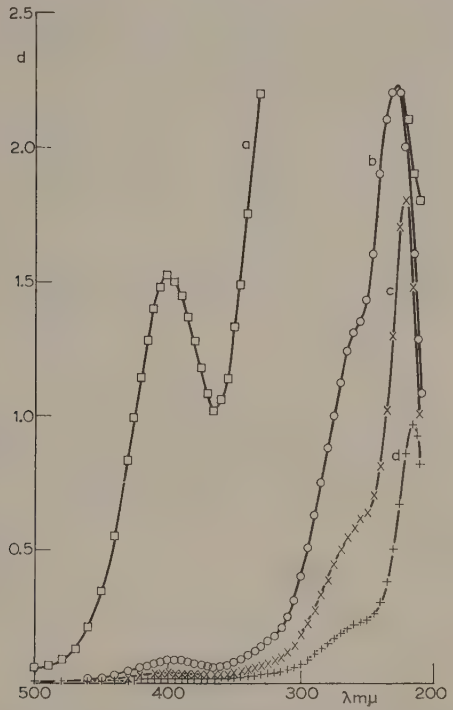

Fig. 7. Absorption spectra of dilute aqueous solutions of crystals of potassium rhodiotrioxalate. The concentrations of the solutions for the different curves were such that a > b > c > d.

region because of the high absorption there (Fig. 7a). In the three curves (b), (c) and (d) a shoulder is found between 240 and 280 mμ, in addition to the band at 400 and the minimum at 365 mμ. This shoulder becomes wider and more pronounced in more dilute solutions. There is another very high absorption band on the lower wavelength side of this shoulder; the maximum of this band decreases and shifts towards the higher frequency side on dilution of the $RhOx_3^{-3}$ solution.

Electrophoretic studies of the optical isomers of potassium rhodiotrioxalate

The resolution of racemic potassium rhodiotrioxalate into its optical isomers is achieved by allowing it to react with a boiling solution of strychnine nitrate, whereby *d*-$H_3Stry_3[Rh(C_2O_4)_3] \cdot 2H_2O$ and *l*-$H_3Stry_3[Rh(C_2O_4)_3] \cdot H_2O$ are formed. On adding

References p. 342

excess potassium iodide to the solution of these two *d*- and *l*-compounds strychnine iodide is precipitated and the two isomers of the rhodiotrioxalate remain in solution. The less soluble form of the potassium rhodiotrioxalate, which separates first on crystallisation, is the *dextro*-form. The *laevo*-form, which is the last to separate, is always accompanied by more or less racemic oxalate[11]. On account of the isomorphism of *d*-potassium rhodiotrioxalate with *d*-potassium iridiotrioxalate, DELÉPINE[12] and CHARONNAT[13] give it the formula $K_3[Rh(C_2O_4)_3] \cdot 2H_2O$ but WERNER[2] and JAEGER[14] believe that both the *d*- and the *l*-isomer have the same formula: $K_3[Rh(C_2O_4)_3] \cdot H_2O$.

Because of the difference in the solubility of the two isomers, we thought it possible that the strength with which they are attracted to strychnine might be different and hence that they might have different mobilities in the presence of strychnine. In that case it should be possible to separate the two isomers electrophoretically. Owing to the low solubility of the strychnine rhodiotrioxalate it was not possible to examine it electrophoretically. We therefore spotted the racemic potassium rhodiotrioxalate solution on the paper and used solutions of strychnine sulphate as electrolyte.

Fig. 8. Electropherograms of an aqueous solution of crystals of potassium rhodiotrioxalate. Conditions: 250 V for 4 h; electrolyte (a) a mixture of 1 *N* K_2Ox and 1% strychnine sulphate solution; (b) 1% strychnine sulphate solution.

Fig. 8 shows the electropherograms of the solution of the crystals of potassium rhodiotrioxalate (a) with a solution containing 1% strychnine sulphate and 1 *N* with respect to K_2Ox as the electrolyte, and (b) with a 1% strychnine sulphate solution as the electrolyte. It was found that in a potassium oxalate solution containing 1 to 8% of strychnine sulphate, $RhOx_3^{-3}$ always moved as one fast anion with the usual mobility, while in strychnine sulphate solution alone, it was precipitated at the point of application. This led us to the conclusion that both the *dextro*- and the *laevo*-form of $RhOx_3^{-3}$ have the same mobility.

REFERENCES

1 E. LEIDIÉ, *Ann. chim. et phys.*, [VI] 17 (1889) 305.
2 A. WERNER, *Ber.*, 47 (1914) 1954.
3 M. DELÉPINE, *Anales soc. españ. fis. y quim.*, 27 (1929) 485.
4 J. LIFSCHITZ AND E. ROSENBOHM, *Z. physik. Chem.*, 97 (1920) 1.
5 C. K. JØRGENSEN, *Acta Chem. Scand.*, 10 (1956) 500.
6 M. LEDERER, *Paper presented to the Congress on Analytical Chemistry*, Moscow, December 1957.
7 M. LEDERER, *J. Chromatog.*, 1 (1958) 279.
8 S. K. SHUKLA, *J. Chromatog.*, 1 (1958) 457.
9 S. K. SHUKLA AND M. LEDERER, *J. Less-Common Metals*, 1 (1959) 255.
10 M. LEDERER AND F. L. WARD, *Anal. Chim. Acta*, 6 (1952) 355.
11 P. PASCAL, *Nouveau traité de chimie minérale*, Tome XIX, Masson et Cie., Paris, 1958, p. 428.
12 M. DELÉPINE, *Bull. soc. chim. France*, [5] 1 (1934) 1258.
13 R. CHARONNAT, *Ann. chim. (Paris)*, [10] 16 (1931) 152.
14 F. M. JAEGER, *Rec. trav. chim.*, 38 (1919) 181.

THE CONSTITUTION OF MANGANESE BASE ALLOYS WITH METALS OF THE SECOND TRANSITION SERIES

A. HELLAWELL

Department of Metallurgy, Oxford University (Great Britain)

(Received August 27th, 1959)

SUMMARY

Binary phase diagrams have been determined for manganese base alloys with the metals yttrium, zirconium, niobium, molybdenum, ruthenium, rhodium, palladium and silver. The results are based principally on thermal analysis, supplemented by microscopical examination.

Binary phase diagrams have been published for manganese and iron base alloys with the solute elements titanium to copper of the first transition series[1]. The work has also been extended for iron base alloys to metals of the second transition series[2], while in the present work, taking manganese as solvent, binary alloys have been examined with the metals yttrium to silver in the second transition series. In this work, the main concern has been with the effect of the various solute metals upon the allotropic transformation temperatures[3], rather than with an accurate determination of each phase diagram.

METHOD

Alloys were examined by thermal analysis, supplemented by microscopical and X-ray work. The thermal analysis was carried out in apparatus described previously[1,4], using thoria refractories for the more reactive alloys (Y, Zr, Nb) and alumina for the rest. All alloys were melted under pure argon and were chemically analysed after examination.

The limits of solid solubility for the metals yttrium and zirconium in manganese is so small, that it has not been possible to give more than provisional phase diagrams in these cases.

For the alloys of the remaining metals, where the limits of solid solubilities are greater, the diagrams may be regarded as more accurate, and, in general, confirm previous work, where this exists.

The metals used were the same as those described in previous work[1,2]. The transition temperatures for the manganese were taken to be the same as in earlier work[1]. being:

$$\beta\text{Mn} \xrightarrow{1094^\circ\text{C}} \gamma\text{Mn} \xrightarrow{1135^\circ\text{C}} \delta\text{Mn} \xrightarrow{1244^\circ\text{C}} \text{liquid.}$$

References p. 347

The phase diagrams for manganese base alloys are shown in Figs. 1 and 2. Owing to the scale of the diagrams some of the narrow two-phase regions are drawn as single lines. In the cases of the Mn-Y and Mn-Zr systems, alloys containing very low solute concentrations (below 0.25 at.%) showed thermal arrests which were the same as for the pure solvent, or differed in such a way as to produce inflexions in the phase boundaries at these very low concentrations. It is thought that this effect is probably not genuine, and that it may correspond to the 'gettering' of impurities by these more reactive metals; phase diagrams have therefore been drawn without giving much weight to the arrests at these concentrations.

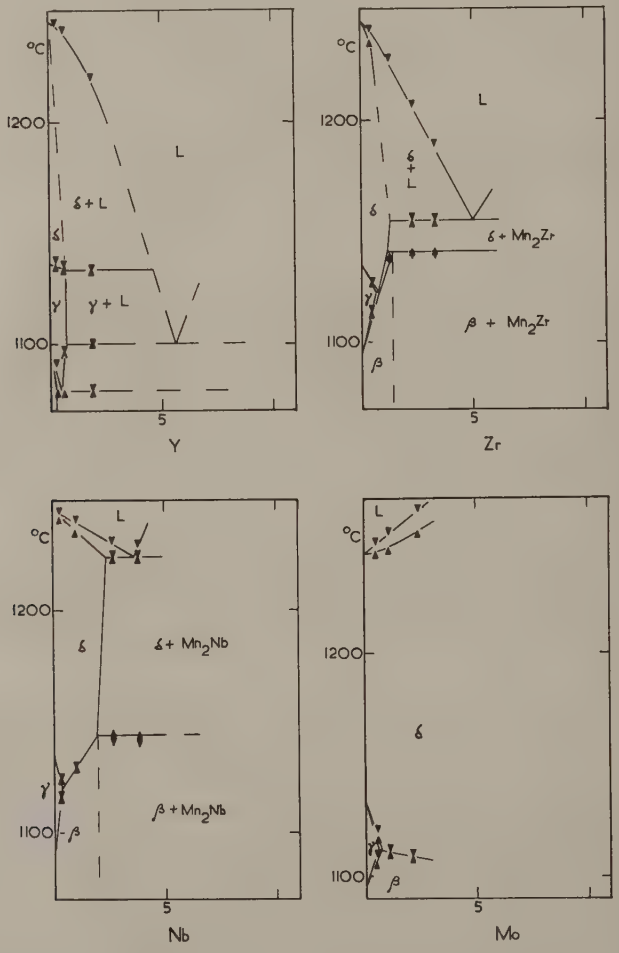

Fig. 1. Manganese base diagrams with yttrium, zirconium, niobium and molybdenum. Temperatures in °C, compositions in atomic %. Cooling arrests ▼, Heating arrests ▲, L — liquid.

References p. 347

RESULTS

Manganese–yttrium (Fig. 1)

The solubility of yttrium in γ and δ manganese only slightly exceeds 0.5 at.%, and is very small in the α and β phases. The reaction $\delta = \gamma$ + liquid occurs at 1133°C, but the solidus is too steep to be detected by thermal analysis and is represented as a broken line. There is a second horizontal at 1100°C which is probably a eutectic between the γ phase and the first compound, the eutectic point being at about 5 at.% yttrium. The third horizontal at 1079°C corresponds to the eutectoidal decomposition of the γ phase at about 0.5 at.%.

Manganese–zirconium (Fig. 1)

There is restricted solubility in all phases, extending to about 1.5 at.% in the β and δ phases, while the γ field is closed at about 0.5 at.%. The horizontal at 1155°C corresponds to a eutectic (liq. (5%) = δ (1.25%) + Mn_2Zr), the microstructures of the 2.3 and 3.3 at.% alloys contain eutectic. The compound Mn_2Zr has been identified by WALLBAUM[5].

Manganese–niobium (Fig. 1)

The liquidus and solidus fall to a eutectic horizontal at 1224°C (liq. (3.6 %) = δ (2.4%) + Mn_2Nb). The microstructures of the alloys higher in niobium show a primary plus eutectic type structure, the compound Mn_2Nb is that reported by WALLBAUM[5]. The γ field is closed at about 0.4 at.% Nb by a eutectoid ($\delta = \beta + \gamma$) at about 1120°C, while a second horizontal at 1145°C corresponds to the reaction $\beta = \delta + Mn_2Nb$.

Magnanese–molybdenum (Fig. 1)

The diagram is analogous to the Mn-Cr diagram[1] in which the β and δ fields extend to the appearance of a σ phase. In the Mn-Mo system the σ phase has been identified at 36 at.%[6]. The γ field is closed at 0.6 at.% by a peritectoid at 1112°C ($\beta = \gamma + \delta$), the resultant β/δ boundaries then fall gradually to a eutectoid, $\delta = \beta + \sigma$.

Manganese–ruthenium (Fig. 2)

The liquidus and solidus rise to a peritectic at 1268°C (liq. (7%) + δ (8.5%) = δ (8%)). The β/γ boundaries are only slightly depressed by addition of ruthenium, and in this respect the present work confirms that of RAUB[7], in which the β/γ boundaries extend almost horizontally to about 20 at.% Ru, while the α/β boundaries fall steeply.

Manganese–rhodium (Fig. 2)

The liquidus and solidus fall to a peritectic, δ (4%) + liq. (5.5%) = γ (4.5%), beyond which there is a minimum which almost coincides with the end of the peritectic. The γ field is extented, and the β/γ boundaries fall steeply, this confirms the diagram suggested by RAUB[7] and others.

Manganese–palladium (Fig. 2)

The liquidus and solidus fall to a peritectic at 1211°C, δ (3.9%) + liq. (5.7%) =

References p. 347

γ (4%), beyond which the γ liquidus and solidus fall to a minimum. The β/γ boundaries fall steeply, confirming the diagram expected by RAUB[8].

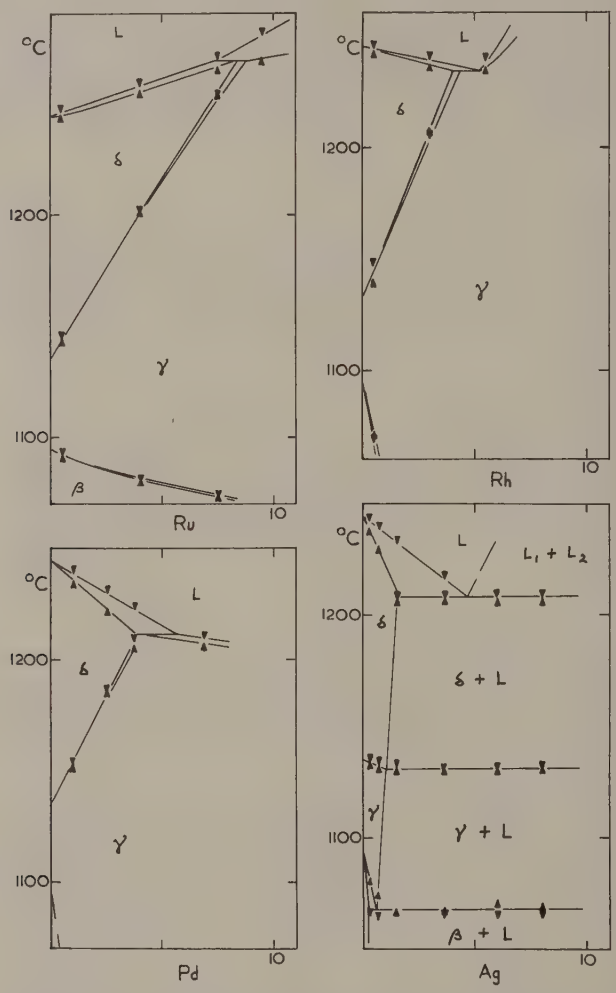

Fig. 2. Manganese base diagrams with ruthenium, rhodium, palladium and silver. Temperatures in °C, compositions in atomic %. Cooling arrests ▼, Heating arrests ▲, L — liquid.

Manganese–silver (Fig. 2)

The manganese-rich portion only is shown, while the rest of the diagram is of the form shown by RAUB AND ENGEL[9]. Solubility is restricted in all phases, reaching a maximum of about 1.5 at.% in the δ phase. The liquidus and solidus fall to a horizontal at 1208 °C,

References p. 347

beyond which there is a region of liquid immiscibility extending to about 50 at.% Ag. The portion of the diagram shown here, differs from the previous work in showing an expanded δ field, the γ/δ boundaries being depressed to a eutectoid horizontal at 1131°C. The β/γ boundaries are depressed to a second horizontal at about 1070°C, while there is a further horizontal below 1000°C which corresponds to the peritectic formation of the silver-rich solid solution, as shown by RAUB AND ENGEL[9].

ACKNOWLEDGEMENTS

Thanks are due to both the B.N.F. research association and to the B.I.S.R.A. for financial assistance in buying materials, to Mr. K. SPEIGHT of the B.I.S.R.A. laboratory, Sheffield, for carrying out the chemical analyses, and to Professor W. HUME-ROTHERY for laboratory accommodation and enthusiastic support for the present work.

REFERENCES

1 A. HELLAWELL AND W. HUME-ROTHERY, *Phil. Trans. Roy. Soc. London, Ser. A*, 249 (1957) 417.
2 W. S. GIBSON AND W. HUME-ROTHERY, *J. Iron Steel Inst. London*, 189 (1958) 243.
3 A. HELLAWELL, *J. Less-Common Metals*, 1 (1959) 110.
4 G. B. HARRIS AND W. HUME-ROTHERY, *J. Iron Steel Inst. London*, 174 (1953) 212.
5 H. J. WALLBAUM, *Z. Krist.*, 103 (1941) 391.
6 P. GREENFIELD AND P. A. BECK, *Trans. Am. Inst. Mining Met. Engrs.*, 200 (1954) 253.
7 E. RAUB, *Z. Metallk.*, 46 (1955) 282.
8 E. RAUB, *Z. Metallk.*, 45 (1954) 430.
9 E. RAUB AND A. ENGEL, *Metallforschung*, 1 (1946) 62.

DIE BEEINFLUSSUNG DER WARMVERFORMBARKEIT VON Ti–Al-LEGIERUNGEN DURCH WASSERSTOFFZUSÄTZE

H. W. SCHLEICHER UND W. JUNG-KÖNIG

Metall-Laboratorium der Metallgesellschaft AG, Frankfurt/Main (Deutschland)

(Eingegangen den 4. September 1959)

ZUSAMMENFASSUNG

Die Warmverformbarkeit von Titanlegierungen mit Al-Gehalten bis zu 10% und ihre Beeinflussung durch Wasserstoffzusätze wurde untersucht. Als Mass für die Verformbarkeit diente die Stauchung kleiner Versuchszylinder unter der Einwirkung eines Fallhammers. Die Stabilisierung der kubischen, weichen β-Phase durch den Wasserstoff bewirkt eine Erhöhung, zunehmende Wasserstoffkonzentration in dieser Phase eine Erniedrigung der Verformbarkeit. Das Maximum der Verformbarkeit ergibt sich aus dem Zusammenwirken dieser Einflüsse und ist von Al-Konzentration und Temperatur abhängig.

SUMMARY

The effect of hydrogen on the hot-workability of titanium and titanium alloys with up to 10 wt.% Al has been examined. As a measure of the deformability upsetting factors (decrease in height, in percent) were determined on small cylinders deformed by the impact of a free falling steel hammer.

Stabilization of the cubic, soft β-phase by hydrogen increases the plasticity, increasing concentrations of hydrogen in this phase reduce it. Maximum plasticity occurs under the combined effect of these influences, and depends on the Al concentration and on the temperature.

Die bekannten Versprödungserscheinungen, die durch Wasserstoff an Titan und Titanlegierungen hervorgerufen werden und in den letzten Jahren Gegenstand zahlreicher Untersuchungen[1] waren, sind vor allem in der Nähe der Raumtemperatur von Bedeutung. Wenn auch der Mechanismus, durch den der Wasserstoff seine schädigende Wirkung ausübt, noch nicht voll geklärt ist, so herrscht doch kaum Zweifel, dass die Ausscheidung der Hydridphase mit den Erscheinungen in engem Zusammenhang steht. Diese Phase tritt im unlegierten Titan bei Wasserstoffkonzentrationen, die kleiner als rund 1.3 Gew.%, entsprechend etwa 38 At.%, sind, erst unterhalb 320°C auf, so dass bei höheren Temperaturen keine Versprödung mehr entstehen kann.

Wie das zuerst von McQUILLAN[2] aufgestellte und dann von LENNING, CRAIGHEAD UND JAFFEE[1] ergänzte Zustandsdiagramm des Systems Ti–H (Abb. 1) aufzeigt, erniedrigt der Wasserstoff in starkem Masse die Umwandlungstemperatur des Titans. Der Existenzbereich der kubischen β-Phase, der beim reinen Titan erst oberhalb 882°C beginnt, wird dadurch bis zu Temperaturen von 320°C gesenkt. Da diese

Literatur S. 355

Phase im Vergleich zur hexagonalen α-Phase eine wesentlich bessere Verformbarkeit besitzt, erschien es möglich, schwierige Warmverformungen dadurch zu erleichtern, dass vor der Verformung Wasserstoff in das Werkstück eingebracht und dadurch die β-Phase zu tiefen Temperaturen stabilisiert wird. Im Anschluss an den Verformungsvorgang kann dieser Wasserstoff durch eine Hochvakuumbehandlung wieder entfernt werden.

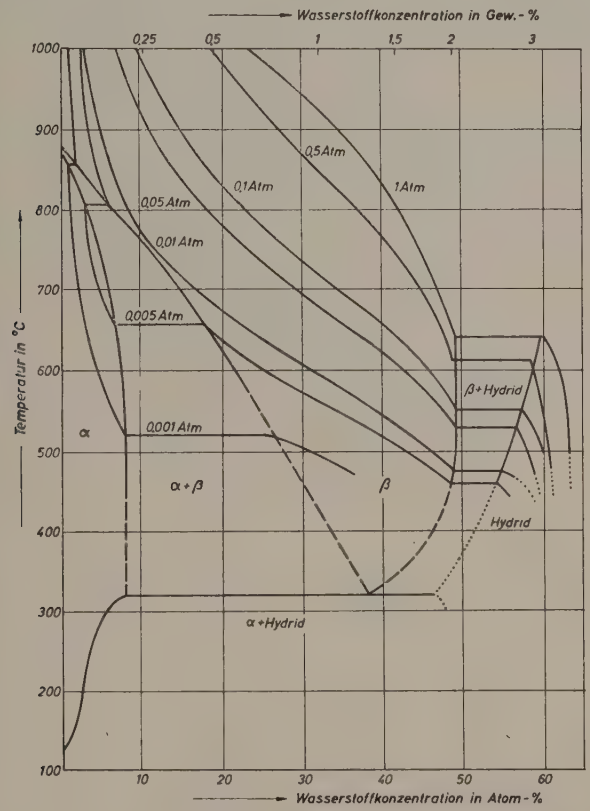

Abb. 1. System Ti–H (nach McQUILLAN und LENNING, CRAIGHEAD UND JAFFEE).

Besonders interessant ist die Wirkung des Wasserstoffs auf die Warmverformbarkeit von Titan-Aluminium-Legierungen, weil Aluminium einerseits, wie Abb. 2[3,4] zeigt, im Gegensatz zu Wasserstoff die α/β-Umwandlungstemperatur des Titans erhöht, und andererseits, wie BERGER, WILLIAMS UND JAFFEE[5] nachgewiesen haben, eine höhere Wasserstoff-Löslichkeit in der α-Phase hervorruft. Im folgenden soll über einige Versuche berichtet werden, mit denen die Beeinflussung der Verformbarkeit von Titan und Titan-Aluminium-Legierungen durch Wasserstoff näher untersucht wurde.

Literatur S. 355

VERSUCHSDURCHFÜHRUNG

Als Mass der Verformbarkeit der untersuchten Werkstoffe wurde die Stauchung ermittelt, die kleine Versuchszylinder von 11 und 12 mm Durchmesser und 12 mm Höhe unter einem von stets gleicher Höhe herabfallenden Hammer erleiden. Die Proben wurden aus Stangenmaterial hergestellt, das aus Titanschwamm mit einer mittleren Härte von HB 30/10 ≈ 115 kg/mm² und Reinstaluminium im Lichtbogenofen zweimal geschmolzen und dann auf der Strangpresse verformt worden war.

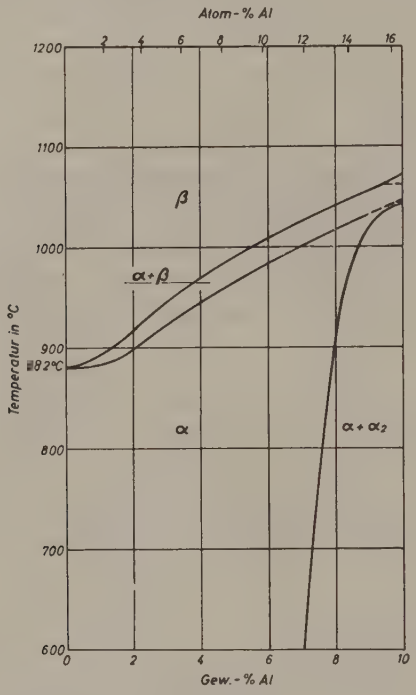

Abb. 2. Ti-reiche Seite des Systems Ti–Al.

Die Wasserstoffbehandlung der grob überdrehten Stangenabschnitte geschah in einem Quarzrohr, in das dosierte Mengen durch Erhitzen von Titanhydrid gewonnenen Wasserstoffs eingelassen werden können. Die Proben wurden bei 900°C im Laufe von 30 min beladen, dann auf 700° im Ofen abgekühlt, auf dieser Temperatur 2 h zur Homogenisierung gehalten und anschliessend ausserhalb des Ofens auf Raumtemperatur abgekühlt. Nicht beladene Vergleichsproben erhielten eine entsprechende Wärmebehandlung im Vakuum. Da die Apparatur eine kontrollierte Wasserstoffzugabe bei Sättigungsdrucken über etwa 400 mm Hg nicht erlaubte, wurde in einigen Fällen der höchste Wasserstoffgehalt durch Erhitzen in Wasserstoff von Atmosphärendruck eingestellt und die aufgenommene Menge durch Gewichtsbestimmungen ermittelt.

Literatur S. 355

Nachdem die Proben anschliessend auf das Endmass gedreht worden waren, wurden sie in einem dicht neben der Schlagapparatur stehenden Elektro-Ofen auf einer etwa 10 mm starken kleinen Stahlplatte unter einer Aufschüttung von Magnesiumoxydpulver auf die Verformungstemperatur erhitzt. Die Stahlplatte mit der durch das MgO vor rascher Abkühlung geschützten Probe wurde dann dem Ofen entnommen, rasch unter den Fallhammer gebracht und nach schnellem Abstreifen des auf der Probe liegenden Pulvers sofort gestaucht. Die Zeit von der Entfernung aus dem Ofen bis zum Aufschlag des Hammers betrug etwa 2 sec. Durch die Wärmeisolation des Oxydpulvers und die Wärmekapazität des Trägers konnte in dieser kurzen Spanne keine merkliche Abkühlung eintreten.

Zur Prüfung der Frage, ob die Dauer der Aufheizperiode, die etwa 15 min betrug, und die während dieser Zeit eintretende Oberflächenoxydation einen Einfluss auf die Stauchung ausübt, wurden einige Proben in argongefüllten Quarzampullen über verschiedene Zeiträume im Ofen belassen und nach raschem Zerschlagen des Quarzes unter den Hammer gebracht. Die erhaltenen Stauchungen stimmen mit denen der in Luft aufgeheizten Proben überein.

MESSERGEBNISSE

Abb. 3 zeigt zunächst die Abhängigkeit der Stauchung, d.h. der beim Stauchvorgang eintretenden prozentualen Abnahme der Probenhöhe, von Prüftemperatur

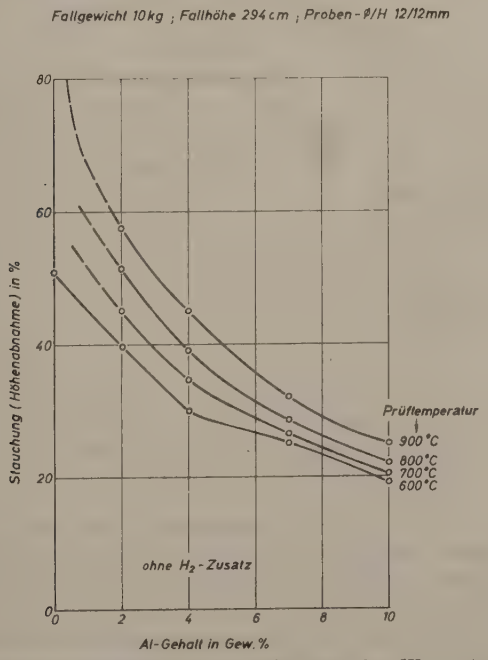

Abb. 3. Stauchung von Ti–Al-Legierungen ohne Wasserstoff.

Literatur S. 355

und Aluminiumgehalt für wasserstoffreies Material. Man sieht, wie mit steigendem Aluminiumgehalt die Stauchung kontinuierlich abnimmt und wie andererseits bei gleicher Legierungszusammensetzung ein annähernd linearer Anstieg mit der Temperatur zu beobachten ist. Der nicht ganz gleichmässige Verlauf der 600°-Kurve bei 7% Al hängt möglicherweise mit dem Auftreten der α_2-Phase[4] zusammen. Für unlegiertes Titan ist oberhalb 600°C kein Wert mehr gemessen worden, da bei den zu erwartenden hohen Verformungsgraden die Höhenabnahme keine angemessene Angabe mehr darstellen würde.

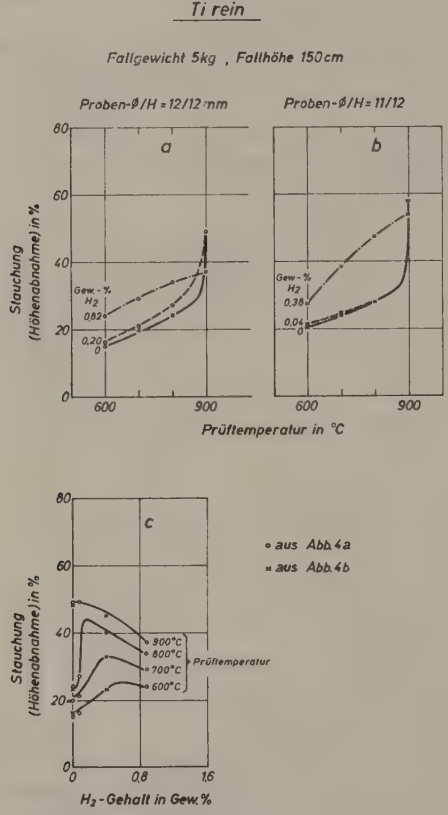

Abb. 4. Stauchung von Titan mit Wasserstoff.

Die Temperatur-Abhängigkeit der Stauchung des unlegierten Titans wurde wegen der genannten Schwierigkeiten mit geringerer Fallenergie untersucht. Die mit einem aus 150 cm Höhe herabfallenden 5 kg schweren Hammer gewonnenen Stauchwerte sind in Abb. 4a und b enthalten. Für wasserstoffreies Material steigt danach die Stauchung bis zu 800°C mit der Temperatur verhältnismässig langsam und linear an, während bei 900°C ein wesentlich höher liegender Wert gefunden wird. Diese durch

Literatur S. 355

die bei 882°C erfolgende α/β-Umwandlung verursachte Diskontinuität geht besonders deutlich auch aus Abb. 4c hervor.

Bei den wasserstoffreien Titan–Aluminium-Legierungen tritt eine plötzliche Steigerung der Verformbarkeit unterhalb 900°C nicht auf, da durch den Al-Gehalt die α-Phase aller hier untersuchten Konzentrationen bis über 900°C stabil bleibt.

Über die Auswirkung von Wasserstoffzusätzen auf die Verformbarkeit von Titan und Ti-Al-Legierungen geben die Abb. 4–8 Auskunft. Bei reinem Titan wirkt bei 900°C der Wasserstoff verfestigend, während bei den tieferen Temperaturen mit steigendem Wasserstoffgehalt ein Maximum der Verformbarkeit überschritten wird. Da der Prüfung von Reintitan zwei verschiedene Probenabmessungen zugrunde lagen, wurden die Messwerte der Abb. 4b mit dem Faktor des Querschnittverhältnisses beider Probensorten $(11/12)^2 = 0.84$ multipliziert in Abb. 4c eingetragen. Die Berechtigung dazu ergibt sich aus der verhältnismässig guten Übereinstimmung der so berichtigten Werte mit denen der Abb. 4a für den wasserstoffreien Zustand. Der Beginn der eingezeichneten Kurven ist aus den Messwerten mit Hilfe weiter unten erläuterter Überlegungen extrapoliert worden.

Bei Al-haltigen Legierungen geht nach den Abb. 5–8 die Stauchung mit zunehmendem Wasserstoffgehalt im allgemeinen ebenfalls durch ein Maximum. Das Maximum ist bei TiAl2 bei allen Temperaturen ausgeprägt, bei TiAl4 und TiAl7 ist es ab 800°C beobachtbar. Bei TiAl10 ist noch ab 800°C der Anstieg, jedoch kein Abfall der Stauchung mehr festzustellen. Da mit steigender Al-Konzentration die Löslichkeit des Wasserstoffs abnimmt, wird der überprüfbare Wasserstoff-Konzentrationsbereich immer kleiner.

DISKUSSION

Aus der 900°-Kurve der Abb. 4c geht deutlich hervor, dass sich die Verformbarkeit der β-Phase im System Titan–Wasserstoff mit steigendem Wasserstoffgehalt vermindert. Diese Beobachtung gibt die Möglichkeit, die erhaltenen Messergebnisse qualitativ zu verstehen. Im heterogenen $\alpha+\beta$-Gebiet entspricht der Zunahme des Wasserstoffgehaltes eine Erhöhung des β-Anteiles im Gefüge. Das Mengenverhältnis α-Kristalle : β-Kristalle ergibt sich aus der bekannten Hebelbeziehung. Die Wasserstoffkonzentration der β-Phase ist bei gegebener Temperatur innerhalb des ganzen heterogenen Bereiches gleich und aus dem Phasendiagramm abzulesen. Da der β-Anteil im heterogenen Gebiet mit der Konzentration linear ansteigt, muss auch die Verformbarkeit ansteigen, und zwar so lange, bis nur noch die β-Phase vorliegt. Von dieser Wasserstoffkonzentration ab reichert sich die β-Phase an Wasserstoff an, und die Verformbarkeit sinkt wieder. Die Konzentration maximaler Verformbarkeit fällt also mit der $(\alpha+\beta)/\beta$-Phasengrenze zusammen und muss sich – mindestens für das unlegierte Titan – mit sinkender Temperatur zu höheren Werten verschieben. Diesen Überlegungen entsprechend sind für reines Titan die Kurven für 600–800°C in Abb. 4c gezeichnet worden.

Die genannte Temperaturabhängigkeit der Wasserstoff-Konzentration maximaler Verformbarkeit geht für die Legierung TiAl2 aus der Abb. 5 von selbst hervor. Hier erreicht man auch bei 900°C durch Wasserstoff noch eine Erhöhung der Stauchung, da diese Legierung bei dieser Temperatur im α- oder $\alpha+\beta$-Zustand vorliegt. Bei 800°C liegt das Maximum in der Nähe von 0.4 Gew.%, d.h. die $(\alpha+\beta)/\beta$-Grenze muss bei

Literatur S. 355

einer höheren Wasserstoff-Konzentration liegen als beim unlegierten Titan, wie das auf Grund der α-stabilisierenden Wirkung des Al auch zu erwarten ist. Bei den Legierungen mit höheren Al-Gehalten ist die Verschiebung des Verformungs-Maximums nicht mehr deutlich. Zwar zeigt bei 900°C die Legierung TiAl4 ihre maximale Verformbarkeit bei einer höheren Wasserstoff-Konzentration als die Legierung TiAl2, doch scheint sich das Maximum weder bei fallender Temperatur noch bei steigender Al-Konzentration zu wesentlich höheren Wasserstoff-Konzentrationen zu verlagern. Offenbar verläuft die $(\alpha+\beta)/\beta$-Grenze bei höheren Al-Gehalten steiler als bei geringeren.

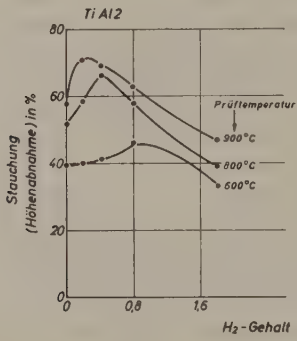

Abb. 5

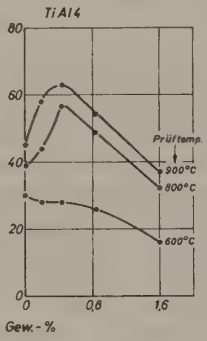

Abb. 6

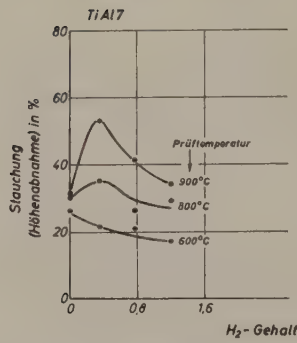

Abb. 7

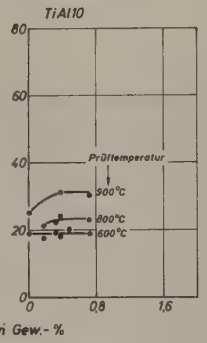

Abb. 8

Abb. 5–8. Stauchung von Ti–Al-Legierungen mit Wasserstoff. Fallgewicht 10 kg; Fallhöhe 294 cm; Proben-φ/H 12/12 mm.

Die Tatsache, dass bei 600°C bei höheren Al-Konzentrationen der Wasserstoff die Verformbarkeit nicht mehr verbessert, könnte zunächst vermuten lassen, dass bei dieser tiefen Temperatur die β-Phase durch Wasserstoff nicht mehr stabilisiert werden kann. Der Verlauf der 600°-Kurve der Legierung TiAl4 in Abb. 6 deutet aber darauf hin, dass diese Vermutung nicht zutrifft. Offenbar wird hier zunächst die α-Phase durch den Wasserstoff verfestigt, wie das auch bei Raumtemperatur

Literatur S. 355

in einem mit dem Al-Gehalt zunehmenden Ausmass von BERGER *et al.*[5] gefunden wurde. Beim Übergang in das ($\alpha+\beta$)-Gebiet hat diese Phase dann etwa die gleiche Verformbarkeit wie die sich ausscheidende β-Phase, so dass das gegenseitige Mengenverhältnis beider Bestandteile ohne Einfluss auf die Gesamtverformung bleibt, was sich in einem annähernd horizontalen Verlauf der Kurve äussert. Reichert sich nach Überschreiten des heterogenen Bereiches die β-Phase weiter an Wasserstoff an, so fällt die Verformbarkeit weiter ab. Diese Deutung wird durch metallographische Befunde unterstützt. Wenn auch die Gefügebilder der Stauchproben infolge der bei der Abkühlung auf Raumtemperatur auftretenden Ausscheidungen nicht leicht zu beurteilen sind, so weisen sie doch darauf hin, dass in dem interessierenden Konzentrationsgebiet die β-Phase noch durch Wasserstoff stabilisiert werden kann und dass z.B. bei der Legierung TiAl7 selbst bei 500° durch Wasserstoff noch β-Phase gebildet wird.

Bei höheren Temperaturen ist die Löslichkeit des Wasserstoffs in der α- und β-Phase kleiner, und die Verfestigung beider Phasen bleibt geringer. Dadurch steigt die durch Wasserstoffzusatz erzielbare Verformungserleichterung an.

Zu einer genauen Analyse des Verhaltens der Legierung TiAl10 reichen die vorliegenden Messwerte nicht aus. Sie dürfte auch kaum ohne eine genauere Kenntnis des 3-Stoffsystems Ti–Al–H gelingen.

LITERATUR

[1] z.B., G. A. LENNING, C. M. CRAIGHEAD UND R. I. JAFFEE, *Trans. AIME*, 200 (1954) 367; Hydrogen contamination in titanium and titanium alloys, *WADC Technical Report 54–616*, Teil 1–4 (1955–1957), mit zahlreichen Beiträgen verschiedener Autoren; H. W. SCHLEICHER UND U. ZWICKER, *Z. Metallk.*, 47 (1956) 570; L. W. BERGER, W. S. MYLER UND R. I. JAFFEE, *Trans. AIME*, 212 (1958) 40; R. D. DANIELS, R. J. QUIGG UND A. R. TROIANO, *ASM Preprint*, No. 86 (1958); K. CLAUS, *Z. Metallk.*, 49 (1958) 201.

[2] A. D. MCQUILLAN, *Proc. Roy. Soc. London*, A 204 (1950) 309.

[3] M. HANSEN UND K. ANDERKO, *Constitution of Binary Alloys*, McGraw Hill, New York, 1958.

[4] K. SAGEL, E. SCHULZ UND U. ZWICKER, *Z. Metallk.*, 47 (1956) 529.

[5] L. W. BERGER, D. N. WILLIAMS UND R. I. JAFFEE, *Trans. AIME*, 212 (1958) 509.

SOME MEASUREMENTS ON THE THERMOELECTRIC POWER OF PLUTONIUM METAL

J. A. LEE AND R. O. A. HALL

Atomic Energy Research Establishment, Harwell, Berks. (Great Britain)

(Received September 4th, 1959)

SUMMARY

The thermal e.m.f. of a plutonium–platinum thermocouple has been measured between 20°C and 630°C, and the absolute thermoelectric power of plutonium in its six allotropic modifications calculated over their stable temperature range. The implications of the results in relation to the form of the density of states/energy curve at the Fermi surface are discussed.

INTRODUCTION

The relations between the thermoelectric power and the Peltier and Thomson coefficients are well established[1,2]. We have

$$\frac{\mathrm{d}\theta_{12}}{\mathrm{d}T} - \frac{\mathrm{d}\pi_{12}}{\mathrm{d}T} + \mu_1 - \mu_2 = 0 \tag{1}$$

$$\frac{\mathrm{d}}{\mathrm{d}T}\left(\frac{\pi_{12}}{T}\right) = \frac{\mu_1 - \mu_2}{T} \tag{2}$$

where π_{12}, μ are the Peltier and Thomson coefficients respectively defined in the usual way, and θ_{12} is the thermoelectric force between the two metals 1, 2 forming an open circuit.

Hence we have

$$\pi_{12} = T \cdot \frac{\mathrm{d}\theta_{12}}{\mathrm{d}T} \tag{3}$$

and

$$T \cdot \frac{\mathrm{d}^2\theta_{12}}{\mathrm{d}T^2} = \mu_1 - \mu_2 \tag{4}$$

Of the three thermoelectric quantities only μ, the Thomson coefficient refers to a single metal. The absolute thermoelectric power, $\mathrm{d}\theta/\mathrm{d}T$ for a metal is defined as

$$\frac{\mathrm{d}\theta}{\mathrm{d}T} = \int_{0^\circ\mathrm{K}}^{T} \frac{\mu}{T} \cdot \mathrm{d}T \tag{5}$$

To measure $\mathrm{d}\theta/\mathrm{d}T$ it is necessary to measure μ for at least one metal down to absolute zero. (For practical purposes by measurement against a superconductor below the

References p. 361

transition point, where $\mu = 0$ for the superconductor.) $d\theta/dT$ may then be found for other metals by direct measurement of the relative thermoelectric power against the standard.

$$\frac{d\theta_{12}}{dT} = \int_0^T \frac{\mu_1 - \mu_2}{T} dT = \frac{d\theta_1}{dT} - \frac{d\theta_2}{dT} \quad (6)$$

In the present investigation the absolute thermoelectric power for plutonium was determined by comparison with pure platinum, for which the absolute thermoelectric power has been determined[3].

MATERIALS

The platinum wire used was Johnson Matthey spectrographically pure material. Two samples of plutonium were used, both of the same nominal purity. Table I gives a list of the impurities determined by spectrographic analysis.

TABLE I

SPECTROGRAPHIC ANALYSIS FOR PLUTONIUM SAMPLES

	Fe	*U*	*Ni*	*Cr*	*Si*	*Ca*	*Al*	*Na*	*P*
p.p.m.	40	<50	25	<10	<25	120	~90	15	60
			Mg	*K*	*Li*	*B*	*Th*		
p.p.m.			10	100	1	<100	—100		

EXPERIMENTAL METHODS AND RESULTS

Each plutonium/platinum couple was prepared by spot welding a 9 in. length of 0.030 in. diameter plutonium wire to a similar piece of platinum wire to form the hot junction. The cold junctions were formed by spot welding both wires to copper leads. The welding operations were carried out in an argon-filled glove box, and good clean junctions were obtained.

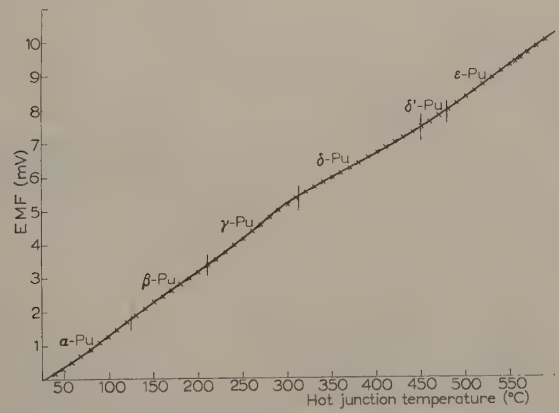

Fig. 1. E.m.f. of a plutonium/platinum thermocouple Sample A, run 1.

References p. 361

E.m.f. measurements were made with the hot junction enclosed in a massive copper block, furnace heated; the cold junctions being maintained at a constant temperature of 20°C in an oil bath, both the furnace and oil bath being enclosed in a vacuum chamber. The temperatures of the copper block and the oil bath were measured by calibrated chromel/alumel thermocouples.

Measurements were made dynamically, at a heating rate of 0.5°C/min, the hot junction temperature being raised continuously from 20°C to 630°C, so that with the hot junction at its highest temperature, all six allotropic modifications were present in dynamic equilibrium along the length of the plutonium wire. Since the interphase boundaries should stay at a constant temperature, the heating transformation temperature, the e.m.f. should be additive.

The results for the two samples, given graphically in Figs. 1, 2 are in good agreement.

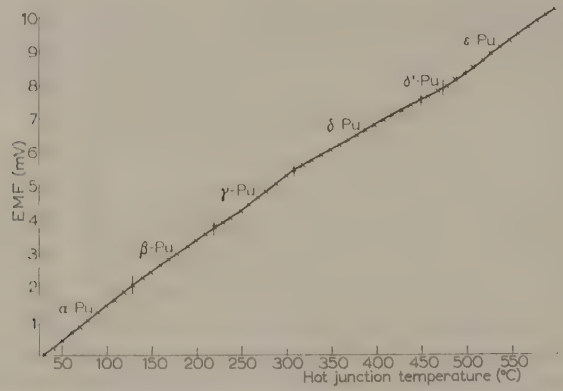

Fig. 2. E.m.f. of a plutonium/platinum thermocouple Sample B, run 1.

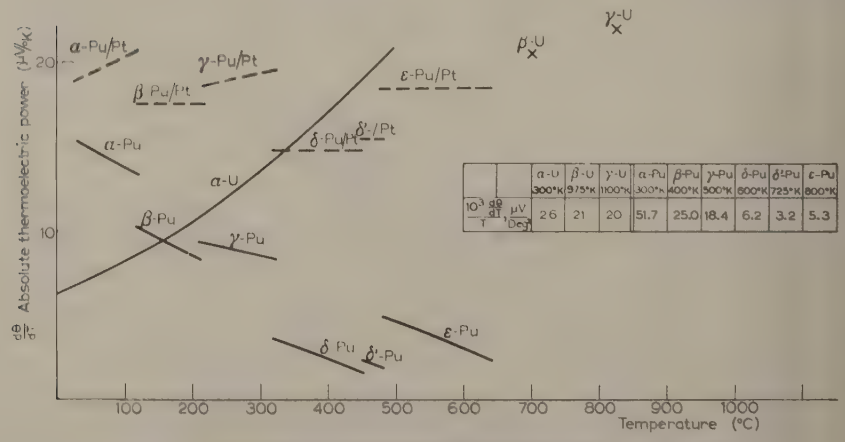

	α-U 300°K	β-U 975°K	γ-U 1100°K	α-Pu 300°K	β-Pu 400°K	γ-Pu 500°K	δ-Pu 600°K	δ'-Pu 725°K	ε-Pu 800°K
$10^3 \frac{d\Phi}{dT}$, μV/Deg	26	21	20	51.7	25.0	18.4	6.2	3.2	5.3

Fig. 3. Absolute thermoelectric power.

References p. 361

Some scatter was observed as the hot junction passed through a phase transformation, particularly at the plutonium $\alpha \rightarrow \beta$ transformation temperature where the volume change is a maximum. The slope of the curve for δ-prime is slightly greater than for the δ-phase in sample A, and slightly less in sample B.

Fig. 3 shows the thermoelectric power for the plutonium–platinum couple, calculated from the slope of the e.m.f./temperature curve, and the absolute thermoelectric powers derived from this. The scatter in the results for the relative thermoelectric power was within $\pm$ 5% from run to run, and sample to sample. Values for uranium[4] and thorium[5] are included for comparison. The absolute thermoelectric power falls from a high positive value for α-plutonium, comparable to that observed for the three allotropic modifications of uranium, through lower values for β and γ-plutonium to a minimum positive value for δ-plutonium rising again to a slightly higher value for δ-prime-plutonium.

DISCUSSION

The recent calculation by RIDLEY[6] of a Wigner-Seitz approximation to the outer electron wave functions for metallic uranium, and similar work by LEHMAN[7] on thorium and uranium, has provided us with a picture of the band structure of uranium as consisting of a smooth low density of states band and a high density of states band with approximately three electrons in each (Fig. 4).

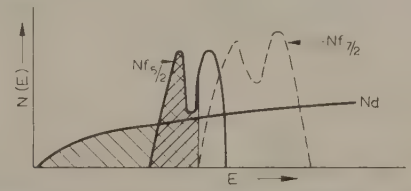

Fig. 4. Schematic representation of the band structure of uranium metal (After LOMAR AND RIDLEY).

RIDLEY's work indicates that the 7*s*, 7*p* atomic levels are raised in energy on forming the solid and are most unlikely to be occupied in the metal. The band formed from the 6*d* atomic levels is broad ~6 eV wide, and the wave function surprisingly uniform over most of the atomic cell. The 5*f* states form a narrow band 1/2 to 1 eV wide, of about the same energy as the *d* band, and which is likely to be split into two parts, the lower six states corresponding to $J = 5/2$; and the upper eight states to $J = 7/2$. In α-uranium at least the lower six may be split into three bonding and three antibonding levels.

This picture is qualitatively the same as that deduced by FRIEDEL[8], although his broad conduction band is based on 7*s*, 7*p* rather than 6*d* electrons, and his narrow high density of states band on 6*d*-5*f* hybrids rather than almost entirely 5*f*.

It seems likely that a similar picture holds for plutonium; the 5*f* band is a little narrower and the $J = 5/2$ and $J = 7/2$ states a little better separated; the *d* band probably still containing about three electrons and the *f* band five. Experimentally

References p. 361

the high paramagnetic susceptibilities and specific heats in all six allotropic modifications indicate a high density of states at the Fermi surface and the high resistivity could be attributed to the scattering of the conduction electrons into the narrow high density band.

In considering the negative expansion coefficient in the f.c. cubic δ-plutonium phase, VARLEY[9] has shown that a negative volume coefficient of expansion is possible without a change of phase, if the Fermi energy of the electron gas has a value for which the density of states of the electrons changes sufficiently rapidly with energy, particularly if this is associated with a high electronic specific heat from a large number of overlapping bands *i.e.*, the negative coefficient of expansion of δ-plutonium could be explained by a high slope of the $N(E)/E$ curve at the Fermi surface.

The thermoelectric power is very sensitive to the form of the Fermi surface. Conventional theory leads to the expression for the thermoelectric power $\mathrm{d}\theta/\mathrm{d}T$[1,10].

$$\frac{\mathrm{d}\theta}{\mathrm{d}T} = \frac{\pi^2 \cdot k^2}{3e} \left(\frac{1}{\sigma} \cdot \frac{\mathrm{d}\sigma}{\mathrm{d}\epsilon}\right)_\zeta \cdot T \qquad (7)$$

where

$$\sigma(E) = \frac{e^2}{4\pi^3\hbar^2} \cdot \int \tau(K) \cdot \left(\frac{\mathrm{d}E}{\mathrm{d}K_z}\right)^2 \cdot \frac{\mathrm{d}S}{|\nabla E|} \qquad (8)$$

The subscript ζ in equation (7) means that the derivative is evaluated at the Fermi surface; $\tau(K)$ is the relaxation constant; and K is the wave vector defined so that $\hbar K$ is the momentum. The other symbols have their usual significance; e is negative.

This expression is valid for both pure metals and alloys, whatever the relations between E and K, at temperatures greater than the Debye temperature θ_D. We would expect it to hold for plutonium where a value $\theta_D \simeq 113^\circ\mathrm{K}$ may be deduced from its melting point, and a value $\theta_D \simeq 180^\circ\mathrm{K}$ from its elastic constants.

The thermoelectric power depends therefore on the way in which the mean free path and the effective mass of the electrons which determine $\sigma(E)$ vary with energy. Qualitatively if the electrons with higher energy have a greater mean free path, smaller effective mass etc., than those with less energy the thermoelectric power will be negative. If the converse is the case, positive.

JONES[10] has shown that for a single zone of standard form a reasonable argument leads to a solution of (7) of the form

$$\frac{\mathrm{d}\theta}{\mathrm{d}T} = \frac{\pi^2 k^2}{3e\zeta} \cdot \left[\frac{7}{2} - \frac{E}{N(E)} \cdot \frac{dN(E)}{\mathrm{d}E}\right] \cdot T \qquad (9)$$

where ζ is the Fermi energy.

The second term in the brackets is equal to 1/2 for free electrons and is of this order for tightly bound electrons near the bottom of an energy band *i.e.*, $\mathrm{d}\theta/\mathrm{d}T$ is negative, since e is negative. But where the Fermi surface lies close to the zone boundaries, *i.e.*, $\mathrm{d}N(E)/\mathrm{d}E$ is large and positive, the second term may be greater than 7/2 leading to a positive value of $\mathrm{d}\theta/\mathrm{d}t$.

For an inverted band of standard form, for which E may be replaced by A-E

References p. 361

where A is the energy at the top of the band, a positive value of $d\theta/dT$ corresponds to a negative slope $dN(E)/dE$. This simulates the behaviour of tightly bound electrons near the top of an energy band and nearly free electrons with wave vectors near the boundary of a Brillouin zone.

To a first approximation we may discuss plutonium on a two-zone picture. Bearing in mind the experimental data the position is analogous to the case for uranium which FRIEDEL has discussed in some detail[8] *i.e.*, we have two possibilities. Either the Fermi surface is overlapped by a single narrow band with a high density of states, or the Fermi surface is overlapped by both a narrow band and a broad conduction band.

If the former is the case, this corresponds to a single band of inverted form and we would expect, a high positive value for the thermoelectric power to correspond to a large negative slope of the density of states curve.

In the latter case, that indicated by RIDLEY, the conductivity will be to a large extent inversely proportional to the probability of transition from the conduction band to the narrow band[11] and, we would expect that a high positive thermoelectric power corresponds in this case to a narrow band with a high positive slope $dN(E)/dE$ and *vice versa*.

We have seen that the absolute thermoelectric power, $d\theta/dT$ of α-plutonium is high and positive, of a similar order to that for α-U *i.e.*, the slope of the density of states curve is high, its sign depending on whether or not a conduction band, in addition to a narrow band, overlaps the Fermi surface. The magnitude of $d\theta/dT$ falls to a low positive value for δ, δ-prime and α-plutonium and it would therefore appear that the slope of the density of states curve must be relatively small in these phases *i.e.*, the VARLEY criterion for a negative volume expansion coefficient is not fulfilled for δ-plutonium and an alternative explanation must be sought.

ACKNOWLEDGEMENTS

The authors wish to thank their colleague M. J. NOTLEY for preparation of the plutonium wire samples, and F. T. BIRKS of the Chemistry Division for spectrographic analysis. They also wish to thank Dr. M. B. WALDRON for his encouragement and helpful discussion.

REFERENCES

1 A. H. WILSON, *Theory of Metals and Alloys*, Cambridge University Press, London, 1953.
2 H. N. V. TEMPERLEY, *Changes of State*, Cleaver Hume Press, London, 1956.
3 G. MASING, *Handbuch der Metallphysik*, Vol. 1. Akademische Verlagsgesellschaft m.b., 1935 Leipzig, p. 398.
4 A. DAHL AND M. S. VAN DUSEN, *Natl. Bur. Standards U.S.*, 39 (1947) 53.
5 H. BONDINE, JR., *Phys. Rev.*, 102 (1956) 1459.
6 E. C. RIDLEY, *Proc. Roy. Soc. London*, A 243 (1958) 422. *Proc. Roy. Soc. London*, A 247 (1958) 199.
7 W. LEHMAN, N.A.A. S.R. 1839, U.S. Atomic Energy Commission (1957).
8 J. FRIEDEL, *J. Phys. and Chem. Solids*, 1 (1956) 175.
9 J. H. O. VARLEY, *Proc. Roy. Soc. London*, A 237 (1956) 413; *Atomic Energy Research Establ*, (*Gt. Brit.*), M/R 1878.
10 H. JONES, *Proc. Phys. Soc. London*, 68 (1955) 1191.
11 N. F. MOTT AND H. JONES, *Theory of the Properties of Metals and Alloys*, Oxford University Press, London, 1936.

THE ORDERED CRYSTAL STRUCTURE OF In_2Te_3

J. C. WOOLLEY AND B. R. PAMPLIN

Department of Physics, University of Nottingham

AND

P. J. HOLMES

Research Laboratory, Associated Electrical Industries, Aldermaston, Berks. (Great Britain)

(Received September 5th, 1959)

SUMMARY

The intermetallic semiconducting compound In_2Te_3 is based on a defect zinc-blende (or fluorite) structure, and it is possible to cause ordering of the lattice vacancies. Experimental work has been carried out to investigate the methods by which specimens in this ordered state may be produced, and the ordering temperature briefly investigated. The ordered structure has been investigated by X-ray powder methods, and analyses carried out to determine the details of atomic arrangement in the ordered structure.

It is shown that although the ordering lines can be indexed on a three-fold cubic cell, as suggested by INUZUKA AND SUGAIKE, no structure based on a cell of this size can predict correctly the observed reflections.

This problem has been studied independently in two laboratories, starting from different premises and predicting different structures. One analysis, assuming that only the normal zinc-blende atomic sites are available for ordering, predicts a body-centred orthorhombic structure with space group $Imm2$. The second view, assuming that enantiomorphous fluorite sites are possible positions of indium atoms in the ordered material, predicts a higher symmetry tetragonal structure with space group either $P4_12mcm$ or $P4_12nm$. The two analyses are presented separately, and it is then concluded that the experimental evidence available from powder work is not sufficient to enable a choice to be made between the two structures.

1. INTRODUCTION

Interest in the $A_2^{III}B_3^{VI}$ class of intermetallic compounds has recently increased, partly because of their possible semiconductor applications. The literature on the crystal structures of these materials is at present incomplete and confused, owing to the limited number of workers who have had good crystalline material for study and to the wide variety of conditions under which the samples have been prepared. The structure of In_2Te_3 has been studied independently, by means of X-ray powder photography, by J. C. WOOLLEY and B. R. PAMPLIN at Nottingham University, and by P. J. HOLMES, working on material prepared by his colleagues at the A.E.I. Research Laboratory. Although the experimental X-ray data obtained by these two groups are identical, their theoretical analyses differ considerably. These results and analyses are therefore presented here in a joint paper, for easy comparison.

References p. 376

2. CONSIDERATION OF PUBLISHED LITERATURE

There are three published papers of particular significance. HAHN AND KLINGLER[1] attributed to In_2Te_3 a zinc-blende type of crystal structure, with one third of the In sub-lattice sites vacant at random, and a lattice constant of 6.146 Å. Their powder photographs showed no lines other than those which would be expected from such a structure, and it is concluded that, as far as their specimens were concerned, their description of the structure was correct.

In a later paper, HAHN[2] stated that annealing gave rise to extra super-lattice lines, indicating some form of ordering of the vacancies. The nature of this ordering was not discussed in detail.

The third report, by INUZUKA AND SUGAIKE[3], was based on a study of single-crystal material, as well as on powder photographs, and it is understandable that conditions suited to the growth of reasonable sized single crystals also favour an ordered structure. The single-crystal work, on crystals with cubic habit, indicated a unit cell side of 18.40 Å, or three times that of the simple zinc-blende cell. Their powder photographs were indexed on this basis, and by considering the absent reflections, as well as other physical properties, the authors concluded that $F\bar{4}3m$ ($F\bar{4}3m$, No. 216) was the space group of the ordered structure.

The extra reflections which these authors observed were all weak compared with those which arise from the simple zinc-blende cell, which in the larger cell had indices which were all odd or all even multiples of 3. The fact that these lines occurred strongly is a good confirmation of the assumption that the structure is based on the zinc-blende lattice, and it seems reasonable to assume that the Te atoms, at any rate, occupy a face-centred cubic sub-lattice of 6.14 Å unit cell side. In this case, all the "extra" reflections may be attributed to the In sub-lattice.

Although in this earlier work the X-ray powder pattern has been interpreted as showing that the structure is based on the zinc-blende lattice, it should be pointed out that the indices of reflections to be expected from a fluorite lattice are similar. The relative intensities of the reflections depend only on the relative scattering powers of the atoms on the "*Ca*" and the "*F*" sites. So it is possible to consider the In_2Te_3 structure as being a fluorite structure with In in one-third of the "*F*" sites and Te in the "*Ca*" sites. In the disordered state, it would be difficult to distinguish the powder pattern of this structure from that of the previously assumed defect zinc-blende structure, especially since there is no certainly as to the completeness of the disordering.

3. PREPARATION OF MATERIALS

The In_2Te_3 used by WOOLLEY and PAMPLIN for this work was prepared by sealing the appropriate weights of In and Te in an evacuated quartz tube, melting together at a temperature above 667°C (the melting point of In_2Te_3) and quenching. X-ray photographs of the resulting ingot showed only the normal zinc-blende (or fluorite) lines, no extra lines of any kind being visible. In an attempt to produce ordering, such material was zone-melted *in vacuo* by the usual techniques, the zone being swept along the ingot at approximately 1 in./h and some ten zone sweeps being used. Although specimens taken from various points in this ingot showed extra lines in an X-ray photograph, these lines were found to be different at different points in the ingot. This was taken to indicate the occurrences of non-stoichiometry rather than

References p. 376

ordering, and this conclusion was confirmed by comparing the extra lines with lines from other possible phases (*e.g.* InTe and Te), and with lines shown by specially prepared non-stoichiometric alloys. An ingot of disordered material was then melted in a sealed tube and directionally frozen, the freezing surface traversing an ingot 9 cm long in approximately 2 days. Samples from all parts of such an ingot gave the same pattern of X-ray lines, and these did not appear to be related to other possible phases. This was taken to be the required ordering, and all of the lines observed could be suitably indexed, as shown below. A sample of the ingot was analysed by Johnson, Matthey and Co. Ltd, and the composition was given as: In 40.06 at.%, Te 59.94 at.%. It is to be noted that INUZUKA AND SUGAIKE quote the composition of their material as $I_{2.09}Te_3$.

The material used by P. J. HOLMES was prepared by Dr. J. E. PARROTT, using an essentially similar method of directional freezing at a rate of 2 to 6 in./h.

In order to show further that the lines observed in this case were due to ordering, specimens were annealed at various temperatures below the melting point (667°C), so as to determine the ordering temperature. It was found that after one day's anneal, followed by quenching in water, specimens annealed at temperatures up to 620°C retained their ordering lines, while those annealed at temperatures of 640°C and above lost the ordering lines and gave the normal disordered photograph. This was taken to confirm that the extra lines were due to ordering, and that the ordering temperature was 630 ± 10°C. It is of interest to note that this temperature is approximately the same as that quoted by APPEL[4] for a transition from zinc-blende to wurtzite structure in this material.

4. EXPERIMENTAL X-RAY DATA

The powder photographs were taken with CuKα radiation, using a calibrated Unicam 19 cm camera at Nottingham, and a 9 cm Unicam camera, with Hilger microfocus source at Aldermaston Court.

INUZUKA AND SUGAIKE have assigned to the material a cubic super-lattice structure with three times the simple lattice parameter. Since in the present work it has been found possible to assign indices of a limited number of classes (see below) to all extra lines on this basis, their findings are considered to be essentially correct in this respect. However, comparison of their measurements with those described here shows several differences of detail. Firstly, there are a fair number of weak lines which they do not record, and secondly, the indexing of a few other weak lines differs from theirs. This may indicate that their material did, in fact, have a different structure. However, it is concluded from their published data that their experimental conditions did not produce such sharp and clear pictures as the present series. It is therefore suspected that the identification and indexing of some weak extra lines by INUZUKA AND SUGAIKE may have been in error. In particular, the lines to which they assign $N(= h^2 + k^2 + l^2)$ values of 43 and 172 are accurately 44 and 171 on the present photographs, none of whose N values differ significantly from integers.

A list of lines which have been found up to $N = 531$ is given in Table I. A few very weak lines may have been lost in the tails of the very strong ones, or among the background noise level. Longer exposures, made in an attempt to make such lines clearer, and evacuating the camera to reduce the background, failed to reveal any more, and it is concluded that the reflections indexed are the only important ones of

References p. 376

the ordered structure. It is noted that this powder pattern bears no resemblance whatever to either of the patterns obtained for varieties of In_2S_3 by HAHN AND KLINGLER.

Experimentally observed intensities have been estimated visually, and grouped into eight categories, *viz.*: vvs, vs, s, m, mw, w, vw, and vvw. These are listed in Table I together with the measured values of $\sin^2\theta$, the cubic indices on the three-fold axes, and the calculated values of lattice parameter obtained from each line.

Owing to the use of a powder technique and the resulting multiple coincidence of reflections, a complete analysis of the photograph has not been possible. It was hoped, however, that only a limited number of ordered structures would be possible within the limits of the conditions imposed, and that these could then be compared with the experimental results as regards absent spectra and relative intensities.

It is at this stage that the work of the two groups diverges, and so separate theoretical developments are presented in the following sections 5 and 6, followed by a final section containing joint conclusions.

TABLE I

POWDER PHOTOGRAPHS OF ORDERED In_2Te_3 POWDER

(Reflections which are common to both ordered and disordered material are underlined). (Two values of $\sin^2\theta$ bracketed to one value of n correspond to the $K\alpha_1$ and $K\alpha_2$ values for that reflection. Bracketed values of n represent unresolved lines).

$\sin^2\theta$	$n=h^2+k^2+l^2$ on three-fold cubic axes	$h\,k\,l$	Observed intensity	Calculated unit cell parameter $3a$
0.0141	8	220	mw	18.374
0.0195	11	311	mw	18.317
0.03515	20	420	mw	18.400
0.0473	27	333	vvs	18.426
0.0561	32	440	mw	18.419
0.0612	35	531	s	18.443
0.0631	36	600	m	18.421
0.0776	44	622	m	18.364
0.0980	56	642	m	18.436
0.10305	59	553 731	s	18.453
0.1188	68	644 820	mw	18.451
0.1256	72	660	vvs	18.464
0.1401	80	840	vw	18.429
0.1447	83	753 911	m	18.470
0.1725	99	933	vs	18.452
0.1814	104	862 10,2,0	w	18.466
0.1876	{107 {108	773 951 666	w w	— —
0.2020	116	864 10,4,0	w	18.480
—	128	880	vw	—
0.2283	131	955 971 11,3,1	mw	18.473
0.2435	140	10,6,2	vw	18.491
0.2508	144	12,0,0	s	18.456
0.2645	152	10,6,4 12,2,2	w	18.488
0.2699	155	975 11,5,3	mw	18.481
0.2854	164	886 10,8,0 12,4,2	mw	18.487
0.2971 0.2990	171	993	s	{18.477 {18.463
0.3064	176	12,4,4	vw	18.483
0.3115	{179 {180	977 11,7,3, 13,3,1} 12,6,0	wd	— —

References p. 376

(continued on p. 366)

TABLE I (continued)

$\sin^2\theta$	$n=h^2+k^2+l^2$	$h\,k\,l$ on three-fold cubic axes	Observed intensity	Calculated unit cell parameter 3a
0.3479	200	10,8,6 10,10,0 14,2,0	vw	18.490
0.3557	203	11,9,1 13,5,3	vw	18.424
0.3675	212	12,8,2 14,4,0	vw	18.523
0.3752 0.3771	216	12,6,6	s	18.479 18.479
—	224	12,8,4	vvw	—
0.3948	227	11,9,5 13,7,3 15,1,1	vw	18.492
0.4100	236	10,10,6 14,6,2	vw	18.463
0.4218 0.4240	243	999 15,3,3	m	18.485 18.485
0.4304	248	12,10,2 14,6,4	vw	18.489
0.4356 0.4382	251	11,9,7 11,11,3 13,9,1 15,5,1	mw	18.489 18.479
0.4525 0.4551	260	12,10,4 14,8,0 16,2,0	w	18.463 18.456
—	272	12,8,8 16,4,0	vvw	—
0.4778	275	13,9,5 15,5,5 15,7,1	w	18.479
0.4997 0.5028	288	12,12,0	m	18.491 18.480
0.5139	296	14,8,6 14,10,0 16,6,2	vw	18.485
—	299	13,9,7 13,11,3 15,7,5 17,3,1	vvw	—
0.5350	308	12,10,8 16,6,4	vw	18.481
0.5464 0.5492	315	15,9,3	m	18.494 18.493
—	320	16,8,0	—	—
—	323 324	11,11,9 15,7,7 17,5,3 12,12,6 18,0,0	vwd	—
—	332	14,10,6 18,2,2	—	—
—	344 347	12,10,10 14,12,2 18,4,0 13,13,3 15,11,1 17,7,3	vvw	—
—	356	14,12,4 16,8,6 16,10,0 18,4,4	vvw	—
0.6243 0.6274	360	18,6,0	mw	18.496 18.496
—	371	13,11,9 15,11,5 17,9,1 19,3,1	vw	—
0.6711 0.6745	387	15,9,9	mw	18.497 18.496
—	392	14,14,0 16,10,6 18,8,2	vvw	—
—	395 396	15,11,7 15,13,1 12,9,5 19,5,3 18,6,6	vvw	—
—	404	14,12,8 16,12,2 18,8,4 20,2,0	vw	—
—	416	16,12,4 20,4,0	vvw	—
0.7270 0.7306	419	13,13,9 15,13,5 17,9,7 17,11,3 19,7,3	mw	18.491 18.492
—	428	14,14,6 18,10,2	vvw	—
—	432	12,12,12	vvw	—
—	440 443	14,12,10 18,10,4 20,6,2 15,13,7 19,9,1 21,1,1	vw	—
—	452	16,14,0 18,8,8 20,6,4	vvw	—
0.7960 0.8000	459	15,15,3 21,3,3	mw	18.503 18.493
—	464	16,12,8 20,8,0	—	—
—	467 468	15,11,11 17,13,3 19,9,5 21,5,1 18,12,0	vw	—

TABLE I (continued)

$\sin^2\theta$	$n=h^2+k^2+l^2$	$h\,k\,l$ on three-fold cubic axes	Observed intensity	Calculated unit cell parameter $3a$
—	488	16,14,6 18,10,0 22,2,0	vw	—
0.8516	491	17,11,9 19,9,7 19,11,3 21,5,5 21,7,1	mw	18.495
0.8561				18.492
—	500	16,12,10 20,8,6 20,10,0 22,4,0	vw	—
0.8742	504	18,12,6	m	18.494
0.8785				18.495
—	512	16,16,0	—	—
—	515	15,13,11 17,15,1 21,7,5	vvw	—
—	524	18,14,2 18,10,10 22,6,2	vvw	—
0.9212	531	15,15,9 21,9,3	mw	18.493
0.9255				18.496

The background on a microphotometer trace of one of P. J. H.'s photographs showed a few slight departures from a smooth curve in the regions of $N = 16$, 17, 21, 122, 136, and 399. No definite lines could, however, be brought up by any means, and these are not regarded as significant.

5. DETERMINATION OF ORDERED STRUCTURE

(J. C. WOOLLEY AND B. R. PAMPLIN)

5.1. Determination of the unit cell of the ordered structure

As indicated above, it was found possible to index all lines on a three-fold face-centred cubic unit cell, as postulated by INUZUKA AND SUGAIKE. Such a scheme indicated a very large number of absent spectra, however. It was found that, for every reflection observed, one index, h, k or l, was divisible by three, indicating that a smaller tetragonal cell could be used of dimensions $3a_0$, $3a_0$, a_0. This is a face-centred tetragonal cell and a rotation of the X and Y axes through 45° gives a smaller body-centred tetragonal cell of dimensions $3a_0/\sqrt{2}$, $3a_0/\sqrt{2}$, a_0. When the indices of the reflections were transformed to this cell, it was found that in every case one of the new h or k indices was again divisible by three, indicating the possibility of a smaller orthorhombic cell of dimensions $a_0/\sqrt{2}$, $3a_0/\sqrt{2}$, a_0. It was thus found that all reflections could be indexed on this orthorhombic cell, with the normal body-centring limitations still being observed. This data was taken to indicate that when ordering occurs, the symmetry is reduced from face-centred cubic to body-centred orthorhombic.

Assuming the atomic sites in the ordered lattice are the same as in the disordered lattice, ignoring for the moment minor distortions which may occur on ordering, the orthorhombic cell would have dimensions $a_0/\sqrt{2}$, $3a_0/\sqrt{2}$, a_0 exactly (where a_0 is the parameter of the disordered cell). The fact that the high-order reflections can still be indexed as cubic, and that these lines are not noticeably broader than usual, shows that in such an orthorhombic cell the $a:b:c$ ratio postulated above would be very closely maintained. A pseudo-cubic analysis of the present results indicates a small expansion on ordering with values of ordered $a_0/3 = 6.165$ Å and disordered $a_0 = 6.158$ Å with an accuracy of ± 0.001 Å. But the multiple coincidence of lines due to the use of the powder technique (see Table IV) masks any splitting of high-angle lines caused by anisotropic expansion on ordering. No attempt has therefore been made to try to determine the $a:b:c$ ratio more accurately.

References p. 376

TABLE II

STRUCTURE AMPLITUDES FOR SPACE GROUP *Imm*2

Conditions imposed on		F^2	Relative intensity ($f_{In} = f_{Te}$)
h	*l*		
Not divisible by 3	No condition imposed	$(2f_{In})^2$	1
Odd, divisible by 3	Doubly even	$(4f_{In} - 6f_{Te})^2$	1
Even, divisible by 3	Singly even		
Divisible by 3	Odd	$(4f_{In})^2 + (6f_{Te})^2$	13
Odd, divisible by 3	Singly even	$(4f_{In} + 6f_{Te})^2$	25
Even, divisible by 3	Doubly even		

5.2. Determination of the space group of the ordered structure

In attempting to predict the ordered structure, the conditions imposed were as follows:

(a) It was assumed that the atomic sites in the ordered structure are the same as those in the disordered zinc-blende structure, and such an arrangement of sites must satisfy the symmetry properties of the particular space group considered, *i.e.* the ordered space group must be a sub-group of $F\bar{4}3m$.

(b) It was assumed that all of the lattice vacancies take part in the ordering, *i.e.* in the ordered structure one site in three on the In lattice is different from the other two.

(c) It was also assumed that no Te atom would be left with less than two In nearest neighbours. Since in normal zinc-blende structure each atom is four-fold coördinated, and hence in disordered In_2Te_3 a Te atom has on the average $2\frac{2}{3}$ In neighbours, it was considered that a minimum of two nearest neighbours was reasonable from the point of view of bonding.

Assuming the three-fold cubic face-centred cell postulated by INUZUKA AND SUGAIKE, and taking the atomic sites for the normal disordered structure (*i.e.* A lattice 000, face-centred, and B lattice $\frac{1}{4}\frac{1}{4}\frac{1}{4}$, face-centred) it was seen that only one face-centred cubic structure could be found which satisfied conditions (a) and (b) above, and that one was ruled out by condition (c). If a three-fold cubic primitive cell is assumed, 20 possible ordered structures can be found which satisfy conditions (a) and (b), but only one of these satisfies condition (c) also. Again, however, the experimental X-ray results show absent spectra which would not be predicted by this primitive cell.

Turning to space groups of lower symmetry, no body-centred tetragonal group could be found which would allow ordering satisfying all three conditions (a), (b) and (c). Thus, from the data given in the previous section, body-centred orthorhombic space groups were considered. Assuming the same atomic sites as in the initial disordered structure, a sub-group of $F\bar{4}3m$ is required, which suggests *Imm*2, the only orthorhombic body-centred space group which enables conditions (a), (b) and (c) above to be satisfied. With a unit cell of dimensions $a_0/\sqrt{2}$, $3a_0/\sqrt{2}$, a_0 and cell origin on any atomic site, the available atomic sites are:

A lattice 0 0 0, 0 $\frac{1}{3}$ 0, and 0 $\frac{2}{3}$ 0, body-centred

B lattice $\frac{1}{2}$ 0 $\frac{1}{4}$, 0 $\frac{1}{6}$ $\frac{3}{4}$, and 0 $\frac{5}{6}$ $\frac{3}{4}$, body-centred.

A cell has been chosen with the In atoms on the B lattice. The three quoted B lattice

References p. 376

sites are equivalent in the disordered structure, but with *Imm*2 symmetry only two of these sites are equivalent. Thus, with two lattice vacancies per cell, these must take the remaining site and its equivalent body-centring site. The cell has been chosen so that these particular sites are at o $\frac{1}{6}$ $\frac{3}{4}$ and $\frac{1}{2}$ $\frac{5}{6}$ $\frac{1}{4}$. Such an ordered lattice is shown in Fig. 1 with the orthorhombic cell marked, and also the disordered cell indicated. It is seen that the Z axis stays common to both cells, but that the X and Y axes of the orthorhombic cell are the [110] and $\bar{1}10$ directions of the cubic cell.

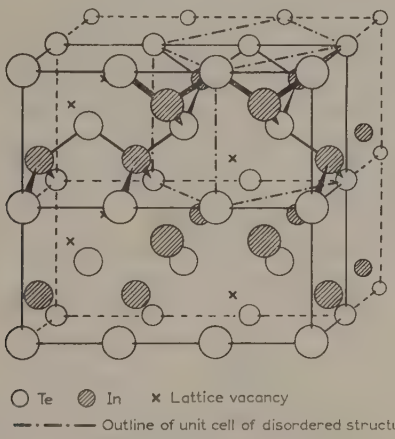

Fig. 1. Possible orthorhombic structure for In_2Te_3.

In such an ordered lattice, every third plane of atoms parallel to the (010) orthorhombic face is completely vacant of In atoms, while the two adjacent planes contain no lattice vacancies. As a result, the Te atoms in every third plane of atoms are coordinated by two In neighbours and two lattice vacancies, while the Te atoms in the other planes each have three In atoms and one lattice vacancy as nearest neighbours.

Assuming the ordering postulated above, the relative intensities of the various reflections can be calculated[5,6]. The intensity of each line is given by:

$$I = \psi(\theta)\, A\, \Sigma\, (p\, F^2_{hkl})$$

where, because the scattering factors of In and Te are close enough to be treated as equal, $\psi(\theta)$ can contain not only the normal trigonometrical factors but also the variation of f, the atomic scattering factor, with θ rather than including this variation in F^2_{hkl}. A is the absorption factor, p the multiplicity, and the summation is over the various reflections which coincide in θ. With the sites postulated above, F^2_{hkl} can be calculated in the usual way. It is found that four different types of reflection occur, and these are tabulated in Table II. Assuming in this structure $f_{Te} = f_{In}$, the relative intensities of all possible reflections with $\theta < 75°$ have been calculated and are shown in Table IV (calculated intensities scaled so that the largest intensity is listed as 1000). In these calculations the factor A has been ignored.

References p. 376

It is seen that at low θ all observed lines are predicted, and there are no predicted lines which are not observed. At high θ, a few of the predicted lines are not observed, but these are ones of very low predicted intensity. Within the limits discussed below, it is found that there is reasonable agreement between observed and predicted intensities. Hence, it appears that the ordered structure could well be that structure postulated above which has the space group *Imm*2.

5.3. Comparison of predicted and experimental results

In comparing the predicted and observed intensities, several points must be remembered. Firstly, the effect of absorption, which will be large in In_2Te_3, has not been taken into account in determining the predicted values. This will have most effect on the low θ reflections, and would therefore account for the apparent discrepancy in the relative ratios of observed to predicted values when, for example, lines $N = 8$ to 20 are compared with lines $N = 32$ to 68.

The assumption made above, that in this case we can write $f_{In} = f_{Te}$, is only correct if the structure is completely homopolar, for any degree of ionicity will tend to increase f_{Te} and reduce f_{In}. This effect is, however, of no great importance as only the zinc-blende type lines have a contribution from the Te atoms. Thus, only the ratio of the intensities of the ordered lines compared with the zinc-blende type lines will be changed: the ratio of intensities of one ordered line to another will be unaffected. Incomplete ordering has a similar effect.

In addition to these points, there is a general fall in the ratio of observed to predicted values as θ increases. Thus, the predicted intensities of lines $N = 27$, 99, and 531 are very similar, but the observed intensities are vvs, vs, and mw respectively. It is found that this applies not only to the ordered structure, but that the same effect is observed with disordered In_2Te_3. Such a reduction in intensity with increasing θ can probably be attributed to the effects produced by the presence of vacancies in the lattice. Since in any In_2Te_3 structure the lattice vacancy coordination of the Te atoms will differ from atom to atom, all Te atoms cannot be considered identical and will show small differences in scattering factor and in thermal vibration etc. In addition, the Te atoms, and probably the In atoms which surround them, will show small deviations from the ideal zinc-blende type atomic sites. The effect of such factors will be larger the higher the reflections considered, and so could account for the observed reduction in intensity with increasing θ.

In the ordered structure, these deviations could be to some extent more systematic, and so could possibly explain some differences between predicted and observed intensities for reflections which differ little in Bragg angle, *e.g.* lines with $N = 32$ and 36 and lines with $N = 296$ and 299. One obvious deviation of this type which could be postulated is in the case of the planes of atoms parallel to the (010) orthorhombic plane. Here the spacing between a plane of atoms which contains lattice vacancies and an adjacent plane might be expected to be greater than the spacing between two adjacent planes of atoms, neither of which contain vacancies. A second possibility would be that Te atoms coordinated by two In atoms and two vacancies would be situated at a different distance from the In atoms than those Te atoms having three In atoms and one vacancy as nearest neighbours. Approximate calculations to take such deviations into account tend to show that the intensities predicted in this way would be in better agreement with experiment. As pointed out above,

References p. 376

however, the experimental data obtained by the powder method do not justify these refinements in calculation.

6. DETERMINATION OF ORDERED STRUCTURE

(P. J. HOLMES)

6.1. The choice of a space-group for the ordered structure

In this analysis, as in section 5.1, the unit cell has been reduced from the three-fold cubic cell to the face-centred cell of dimensions $3a_0$, $3a_0$, a_0, since no cubic structure would fit the results. So as to emphasise the relationship to the face-centred cubic Te sub-lattice, the possible further reduction to a smaller tetragonal cell has not been carried out. The same conditions were imposed as in 5.2, with the exception that the restriction of In atoms to sites of the zinc-blende type was relaxed, and the possibility that these atoms might lie in the alternate positions (enantiomorphous sites) was considered. Thus the search was for an ordered array of atoms on one-third of the F sites of a fluorite (CaF_2) lattice, rather than of atoms on two-thirds of the sites on a zinc-blende lattice.

The observed powder reflections, indexed on this unit cell, are of four types, *viz*:

h,k odd multiples of 3, l odd
h,k even multiples of 3, l even
h,k odd and not multiples of 3, l odd
h,k even and not multiples of 3, l even

The first two types coincide with the reflections from the simple f.c.c. lattice of Te atoms, so need not necessarily occur as reflections from the In sub-lattice.

Narrowing down the tetragonal space groups which permit such reflections, using the assumed atomic coordinates, six (namely Nos. 89, 123, 125, 127, 132 and 136) were found which would fit on a systematic basis (*i.e.* all indices even or all odd, odd values of $h + k + l$ permitted)[6]. The special positions were then examined to see which combinations could give the observed special absences as well as the systematic ones. The last two of the six space groups mentioned ($P4_2/mcm$ and $P4_2nm$) have combinations of 24 positions per unit cell which satisfy these requirements (Table III). These are, for both:

2 of o o o type
2 of o o $\frac{1}{2}$ type
4 of o $\frac{1}{2}$ o type
4 of $\frac{1}{3}$ $\frac{1}{3}$ o type
4 of $\frac{1}{6}$ $\frac{1}{6}$ o type
8 of $\frac{1}{3}$ $\frac{1}{6}$ o type

These groupings are similar in respect of the arrangement of the first and last eight atoms, while the remaining ones are in related positions in the two groups, as is shown by comparison of:

$\frac{1}{3}$ $\frac{1}{3}$ o, $-\frac{1}{3}$ $\frac{1}{3}$ o, $-\frac{1}{6}$ $\frac{1}{6}$ $\frac{1}{2}$, $\frac{1}{6}$ $-\frac{1}{6}$ $\frac{1}{2}$ in No. 136

and

$\frac{1}{3}$ $\frac{1}{3}$ o, $-\frac{1}{3}$ $\frac{1}{3}$ o, $-\frac{1}{3}$ $\frac{1}{3}$ $\frac{1}{2}$, $\frac{1}{3}$ $-\frac{1}{3}$ $\frac{1}{2}$ in No. 132

Thus, the two structures are equivalent. No other combinations of 24 atoms within

References p. 376

TABLE III

STRUCTURE AMPLITUDES FOR SPACE GROUP 136, $P4_2/mnm$

$h + k + l = 2n \quad A = 8 \cos 2\pi lz\,[\cos 2\pi hx \cos 2\pi ky + \cos 2\pi kx \cos 2\pi hy]$
$h + k + l = 2n+1 \quad A = -8 \cos 2\pi lz\,[\sin 2\pi hx \sin 2\pi ky + \sin 2\pi kx \sin 2\pi hy]$
$= 0$ for h or $k = 0$ or 3

Whence 001, 021, 030, 210, 311, 320, 331 = 0

	$h+k+l=2n$											$h+k+l=2n+1$*			
Special position	000	011	020	031	110	210	211	310	321	330	220	221 441	241	111 551	511
000	2	2	2	2	2	2	2	2	2	2	2	0	0	0	0
0 0 ½	2	−2	2	−2	2	−2	−2	2	−2	2	2	0	0	0	0
0 ½ 0	4	0	4	0	−4	0	0	−4	0	−4	4	0	0	0	0
⅓ ⅓ 0	4	−2	−2	4	1	1	1	−2	−2	4	1	−3	3	−3	3
⅙ ⅙ 0	4	2	−2	−4	1	−1	−1	−2	2	4	1	−3	3	−3	3
⅓ ⅙ 0	8	0	−4	0	−2	0	0	4	0	−8	2	6	−6	−6	6
Total	24	0	0	0	0	0	0	0	0	0	12	0	0	−12	12

* The behaviour of terms containing sines differs from those containing cosines, as regards equivalence

(1, 7, 13, 19 are equivalent
2, 8, 14, 20 ,, ,,
4, 10, 16 ,, ,,
5, 11, 17 ,, ,,).

these groups would satisfy the requirements of absent spectra, and other choices of tetragonal unit cell for the In sub-lattices lead to the same conclusions.

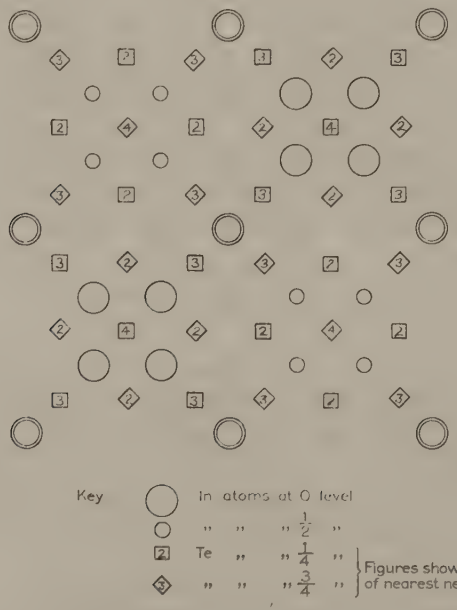

Fig. 2. Possible tetragonal structure for In_2Te_3.

References p. 376

The coordinates of the In atoms obtained in this analysis are thus:

000, $\frac{1}{2}\frac{1}{2}\frac{1}{2}$, 00$\frac{1}{2}$, $\frac{1}{2}\frac{1}{2}$0
0$\frac{1}{2}$0, $\frac{1}{2}$00, 0$\frac{1}{2}\frac{1}{2}$, $\frac{1}{2}$0$\frac{1}{2}$
$\frac{1}{3}\frac{1}{3}$0, $-\frac{1}{3}-\frac{1}{3}$0, $-\frac{1}{6}\frac{1}{6}\frac{1}{2}$, $\frac{1}{6}-\frac{1}{6}\frac{1}{2}$
$\frac{1}{6}\frac{1}{6}$0, $-\frac{1}{6}-\frac{1}{6}$0, $-\frac{1}{3}\frac{1}{3}\frac{1}{2}$, $\frac{1}{3}-\frac{1}{3}\frac{1}{2}$
$\frac{1}{3}\frac{1}{6}$0, $\frac{1}{6}\frac{1}{3}$0, $-\frac{1}{3}-\frac{1}{6}$0, $-\frac{1}{6}-\frac{1}{3}$0, $-\frac{1}{6}\frac{1}{3}\frac{1}{2}$, $-\frac{1}{3}\frac{1}{6}\frac{1}{2}$, $\frac{1}{6}-\frac{1}{3}\frac{1}{2}$, $\frac{1}{3}-\frac{1}{6}\frac{1}{2}$

The Te atoms lie on a face-centred cubic sub-lattice, based on $\frac{1}{12}\frac{1}{12}\frac{1}{4}$ as origin, reducing the overall symmetry to space group $P4_2nm$. The structure is illustrated in Fig. 2.

Relative intensities were calculated for the reflections from such a structure, of the form τpF^2, where the function τ includes with the normal geometrical factor[5] and the variation of atomic scattering factor with θ, p is the multiplicity factor, and F is the structure amplitude (see Table III). These results are given in Table IV and compare favourably with the visually estimated relative intensities. The reservations made in section 5.3, as to how good a fit can be expected, are equally valid here.

TABLE IV

COMPARISON OF OBSERVED AND CALCULATED RELATIVE INTENSITIES*

N	*Observed intensity*	*Tetragonal h k l*	*Calculated intensity***	*Orthorhombic h k l*	*Calculated intensity***
8	mw	220	246	020	70
11	mw	111	325	011	100
20	mw	420	170	110	50
27	vvs	331	1000	031 101	1000
32	mw	440	42	040	16
35	s	511	131	121	60
36	m	600 002	47	002 130	40
44	m	222	50	022	22
56	m	422	80	112	31
59	s	711 551	107	051 141	45
68	mw	820 442	55	042 150	24
72	vvs	660 602	970	060 132 200	800
80	vw	840	22	220	10
83	m	751 113	62	013 211	26
99	vs	931 333	440	033 103 161 231	550
104	w	10,2,0 822	45	152 240	20
107	w	771 513	42	071 123	20
108	w	662	14	062 202	13
116	w	10,4,0 842	35	170 222	17
128	vw	880	5	080	2
131	mw	11,1,1 213 553	48	053 143 251	25
140	vw	10,2,2	15	242	9
144	s	12,0,0 004	138	004 260	300
152	w	10,4,2 224	20	024 172	12
155	mw	11,5,1 753	26	181 213	15
164	mw	10,8,0 882 424	24	082 114 310	14
171	s	991 933	150	091 163 233 301	250
176	vw	444	6	044	3
179	wd	13,1,1 11,7,1 773	26	073 271 321	15
180		12,6,0 12,0,2 604	17	134 190 262 330	19
200	vw	14,2,0 10,10,0 10,8,2	18	0,10,0 280 312	10
203	vw	13,5,1 11,1,3	21	253 341	11
212	vw	14,4,0 824	14	154 350	8
216	s	12,6,2 664	320	064 192 204 332	360
224	vvw	844	9	224	4

References p. 376 (continued on p. 374)

TABLE IV (continued)

N	*Observed intensity*	*Tetragonal h k l*	*Calculated intensity***	*Orthorhombic h k l*	*Calculated intensity***
227	vw	13,7,1 11,5,3 115	20	015 183 1,10,1	11
236	vw	14,2,2 10,10,2	12	0,10,2 282	6
243	m	15,3,1 993 335	130	035 093 105 291 303 361	200
248	vw	14,4,2 10,2,4	14	244 352	8
251	mw	13,1,3 11,7,3 515 11,11,1	22	0,11,1 125 273 323	15
260	w	16,2,0 14,8,0 10,4,4	13	174 1,11,0 370	8
272	vvw	16,4,0 884	5	084 2,10,0	5
275	w	13,5,3 715 555	15	055 145 343	9
288	m	12,12,0	108	0,12,0 264	100
296	vw	16,2,2 14,10,0 14,8,2	14	1,11,2 372 420	9
299	vvw	17,1,1 13,11,1 13,7,3 755	21	1,10,3 215 381 411	13
308	vw	16,4,2 10,8,4	11	2,10,2 314	6
315	m	15,3,3 935	74	165 1,12,1 235 293 363 431	250
320	—	16,8,0	2	440	2
323	vwd	17,5,1 11,11,3 775	12	075 0,11,3 2,11,1	6
324		18,0,0 12,12,2 12,6,4 006	10	006 0,12,2 194 334 390 402	12
332	—	14,10,2 226	7	026 422	5
344	vvw	14,2,4 10,10,4 426	13	0,10,4 116 284	8
347		17,7,1 13,13,1 11,1,5	13	0,13,1 255 451	8
356	vvw	16,10,0 14,8,2 14,4,4 446	15	046 1,13,0 354, 442	10
360	mw	18,6,0 18,0,2 066	170	136 2,12,0 392 460	250
371	vw	19,1,1 17,1,3 13,11,3 11,5,5	18	185 383 3,10,1 413	13
387	mw	15,9,3 935	66	095 1,12,3 305 433	130
392	vvw	16,10,2 14,14,0 826	10	0,14,0 156 1,13,2	8
395	vvw	19,5,1 17,5,3 13,1,5 11,7,5	18	275 2,11,3 325 471	13
396		18,6,2 666	7	066 206 2,12,2 462	10
404	vw	20,2,0 16,2,4 14,8,4 846	16	1,11,4 226 374 3,11,0	12
416	vvw	20,4,0 16,4,4	8	2,10,4 480	5
419	mw	19,7,1 17,11,1 17,7,3 13,13,3 13,5,5	21	0,13,3 1,14,1 2,13,1 345 453	15
428	vvw	14,14,2 10,2,6	8	0,14,2 246	6
432	vvw	12,12,4	62	0,12,4 404	100
440	vw	14,10,4 10,4,6 20,2,2	15	176 3,11,2 424	12
443		13,7,5 19,1,3 117	12	017 1,10,5 3,10,3	10
452	vvw	16,14,0 886 20,4,2	10	086 482 510	8
459	mw	15,15,1 15,3,5 337 21,3,1	140	037 0,15,1 107 295 365 3,12,1 491 501	320
464	—	16,8,4 20,8,0	8	2,14,0 444	6
467	vw	11,11,5 17,13,1 19,5,3 517	20	0,11,5 227 473 521	13
468		18,12,0 12,0,6 18,0,4	9	1,15,0 266 394 530	14
488	vw	16,14,2 10,0,6 18,10,0 22,2,0	16	316 4,10,0 512	12
491	mw	17,11,3 19,7,3 19,11,1 557 717	29	057 147 1,14,3 2,13,3 541	22
500	vw	16,10,4 20,8,2 20,10,0 22,4,0	21	1,13,4 2,14,2 3,13,0 550	15
504	m	18,12,2 18,6,4 12,6,6	580	196 1,15,2 2,12,4 336 464 532	800
512	—	16,16,0	2	0,16,0	1
515	vvw	13,11,5 17,1,5 577	25	217 385 415	18
524	vvw	14,2,6 10,10,6 22,2,2	24	0,10,6 286 4,10,2	16
531	mw	15,15,3 15,3,5 21,9,1 21,3,3 937	485	0,15,3 167 1,12,5 237 2,15,1 3,12,3 435 493 503 561	800

* The absorption factor, which varies with θ and is difficult to calculate exactly, has been omitted from both sets of calculated intensities.

** Strongest low-angle reflection taken as 1000 in each case.

An interesting feature is found when the positions of the In atoms in this structure relative to the Te positions are considered. It will be seen that there are four Te atoms per unit cell ($\frac{1}{4}\,\frac{1}{4}\,\frac{1}{4}$, $\frac{1}{4}\,\frac{1}{4}\,\frac{1}{2}$, $\frac{1}{4}\,\frac{1}{2}\,\frac{3}{4}$, $\frac{1}{2}\,\frac{1}{4}\,\frac{3}{4}$) whose In neighbours are all on the same side, so that the Te atom is at the apex of a square pyramid. It seems very probable that the equilibrium position of this atom, determined by the very one-sided bonding, would not be exactly coincident with its ideal position on the f.c.c. Te sub-lattice. The effect of a small displacement would be felt more strongly in the higher-index reflections from this sub-lattice (*i.e.* $3h, 3k, l$), and if the displacement was along the axis of the pyramid, reflections from planes parallel to the C axis would not be affected. Any attempt to detect this effect from powder photographs, or even from a nominally single crystal, would be tedious, and might be negatived by antiphase effects, as outlined in the next paragraph. However, such a structure, having polarity along the C axis, could very well show the piezo-electric effects reported by INUZUKA AND SUGAIKE.

A question which remains is whether this tetragonal structure pervades the whole of a single crystal of ordered In_2Te_3. It seems likely, since the axes of the cell are in exact ratio, that a real ordered crystal, grown carefully but with no special orientation arrangements, could consist of a random arrangement of domains, with the C axis lying in each direction along each of the three "cube" axes in different parts of the crystal. When a single-crystal X-ray photograph is obtained from such a specimen in any symmetrical orientation, each permitted reflection would appear from one of the six types of domain, and the overall diffraction pattern would display cubic symmetry.

However, with a very small seed and slow directional crystallisation, a crystal displaying only tetragonal symmetry should be obtainable.

7. CONCLUSIONS

The study of Table IV shows that in general the two sets of calculated intensities agree equally well with the observed results: the main difference between the two sets appears to be in the relative values of the intensities of the weak ordering lines compared with the very strong zinc-blende type lines. An absolute comparison of these intensities is difficult unless the degree of ordering is known precisely. Thus it appears that the present experimental data cannot be used to decide between the two postulated structures. The fundamental difference between the two methods of approach is that in one case only zinc-blende type sites have been used, while the other analysis makes use of the enantiomorphous sites, as in the fluorite structure. The second method involves a relaxation of the conditions imposed by the first, and enables a unit cell of higher symmetry to be described. The use of the additional sites does, however, introduce difficulties in explaining the interatomic bonding scheme. On the other hand, the orthorhombic structure predicted by the first approach might be expected to show very pronounced layering properties, and as was pointed out above, might also show some deviation from the ideal simple $a:b:c$ ratio.

An extension of this work would involve the use of single-crystal techniques. The problem here, however, is to produce a single crystal of the necessary size and structural uniformity for the work, and also of stoichiometric composition. Although the work of INUZUKA AND SUGAIKE was with a single crystal, their quoted composition

References p. 376

indicates considerable deviation from stoichiometry, and it may well be that the ideal ordered structure is sensitive to composition.

ACKNOWLEDGEMENTS

J. C. W. and B. R. P. are indebted to Professor L. F. BATES for the facilities of his laboratory, and they wish to thank Dr. S. WALLWORK of Nottingham University for stimulating discussions. Their work forms part of an investigation carried out for the Admiralty.

P. J. H. wishes to acknowledge the helpful comments of Mr. R. L. ROUSE and Dr. J. E. PARROTT whose interest in indium telluride prompted this investigation, and of Drs. J. S. HALLIDAY and A. G. KNAPTON. The preparation and measurement of the X-ray photographs was undertaken by Mr. I. C. JENNINGS. The work from the A.E.I. Research Laboratory is published by permission of its Director, Dr. T. E. ALLIBONE, F. R. S.

REFERENCES

1 H. HAHN AND W. KLINGLER, *Z. anorg. Chem.*, 260 (1949) 97.
2 H. HAHN, *Angew. Chem.*, 64 (1952) 203.
3 H. INUZUKA AND S. SUGAIKE, *Proc. Japan Acad.*, 30 (1954) 383.
4 J. APPEL, *Dissertation*, Brunswick, 1955.
5 N. F. M. HENRY, H. LIPSON AND W. A. WOOSTER, *The Interpretation of X-ray Diffraction Photographs*, Macmillan and Co., London, 1953, p. 204.
International Tables of X-ray Crystallography, Kynoch Press, Birmingham, 1952.

A SURVEY OF THE RHENIUM–CARBON SYSTEM

J. E. HUGHES*

Research Laboratory, Associated Electrical Industries, Aldermaston, Berks. (Great Britain)

(Received September 10th, 1959)

SUMMARY

Alloys of rhenium and carbon form a simple eutectic system at 16.9 at.% carbon, 2480°C. The solid solubility of carbon in rhenium is 11.7 at.% at the eutectic temperature, falling to 4.2 at. % at 1800°C. No rhenium carbide was detected in the system.

Rhenium is an expensive metal and the possible world supply is small[1]. It retains its strength to high temperatures to a remarkable degree[2] and has a melting point (3180°C) higher than any other metal but tungsten. Because of these properties the metal or certain of its alloys[3] may find applications as valves, heaters, filaments, contacts, high-temperature springs, etc. It is probable that in such applications the rhenium will be in contact with other materials and the behaviour at high temperatures of systems containing rhenium is therefore of interest. We have determined the high-temperature part of the constitutional diagram of the system rhenium–carbon, which is one such system.

Previous work on the reactions of rhenium with carbon was contradictory, and no agreement whether a stable carbide exists had been reached. The liquidus and high temperature area of the diagram have not previously been studied and no equilibrium diagram has been published.

SCHENK, KURZEN AND WESSELKOCK[4] reported no reaction between rhenium and carbon and the rehnium–methane reaction too slight for observation, and AGTE[5] reported that rhenium formed no carbide, but TROPSCH AND KASSLER[6] believed one to be formed when rhenium was exposed to carbon monoxide. TRZEBIATOWSKI[7] found the carburizing effect of a gas to depend upon the particular sample of rhenium studied.

In the present work the alloys were prepared by melting small compacts of rhenium powder and graphite in argon on the water-cooled copper hearth of an arc furnace[8]. The rhenium used was a fine powder of 99.9 + % purity supplied by Johnson, Matthey and Co. Ltd., London. Alloys of high carbon content were prepared by melting rhenium on a graphite block in the same furnace; these were analysed and used as "master alloys" for the preparation of further alloys.

---

* Present address: Siemens Edison Swan Limited, Research Laboratory, West Road, Templefields, Harlow, Essex, Great Britain.

References p. 381

Chemical analyses were made by a dry combustion method developed for this work. The conventional combustion in a stream of oxygen was difficult because the hot gases carry over the volatile rhenium heptoxide even when cooled traps are inserted in the apparatus. The oxidation was therefore carried out in a static system. The sample (0.2–0.5 g) rested in a quartz tube attached to a 500 ml bulb filled with oxygen. The sample was heated to 1000° and after it had all sublimed from the hot zone the apparatus was allowed to cool to room temperature. The carbon dioxide formed was displaced by oxygen into an excess of decinormal baryta solution and so estimated. The apparatus was checked with samples of calcium carbonate.

The liquidus was determined in the arc furnace by adjusting the arc power so that the top half of a bead of alloy which was about 5 mm in diameter was molten and the lower half solid, and focusing an optical pyrometer on the liquid–solid interface. Observed temperature readings were calibrated against observation on pure metals of high melting points. This procedure has been used extensively in this Laboratory[9], but a notable feacture of the present system was the clarity of the solid–liquid junction (Fig. 2).

Solid alloys were examined by metallography and X-ray diffraction. Considerable

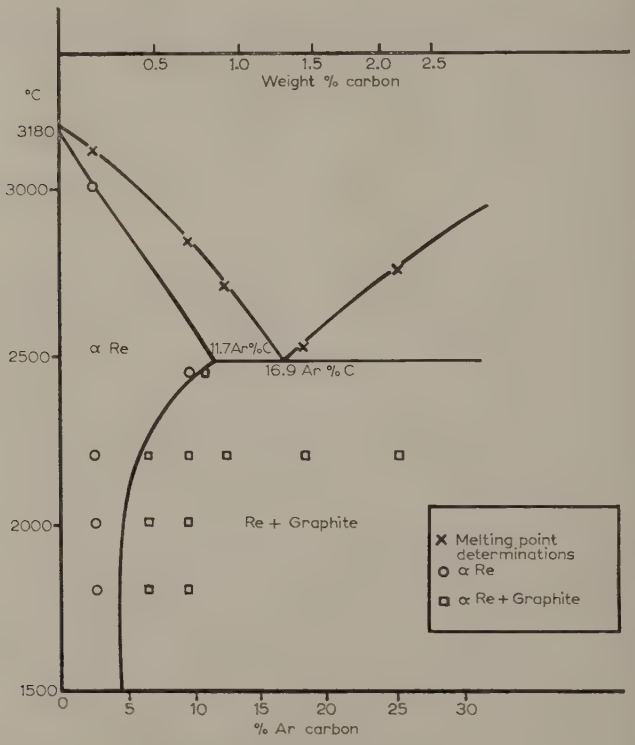

Fig. 1. Rhenium–carbon system.

References p. 381

use was made of the technique of arc furnace quenching in which the alloy under examination was melted, homogenized just below the solidus temperature, then cooled to the quenching temperature and held there for the requisite time (usually 10 min) before quenching was achieved by flooding the furnace chamber with water. This technique was suitable for temperatures of quenching in the range 1500°C to 2400°C.

Fig. 2. The solid–liquid junction in rhenium. Twice natural size.

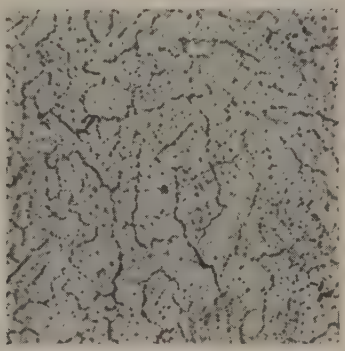

Fig. 3. Intergranular and precipitated graphite. Unetched. Furnace-cooled. X 400D.

The rhenium–carbon system above 1500°C is given in Fig. 1. It shows a eutectic at 16.9 at.% carbon and 2480 ± 50°C. At this temperature the solid solubility of carbon in rhenium is 11.7 at.% At 1800°C the solid solubility is 4.2 at.% Observations upon which this is based are summarised in Table I.

TABLE I

Alloy at. % C	*Treatment*	*Remarks*
2.7	Furnace-cooled	Melting point 3120°C
9.4	Furnace-cooled	Melting point 2850°C
12.5	Furnace-cooled	Melting point 2710°C
18.2	Furnace-cooled	Melting point 2530°C
25.1	Furnace-cooled	Melting point 2770°C
2.7	Powder compact. Heated to 2800°C	No indication of melting
2.7	Powder compact. Heated to 2900°C	No indication of melting
2.7	Powder compact. Heated to 3000°C	Top of compact fused
9.4	Annealed 2450°C — 10 min, Water-quenched	α-rhenium
10.7	Annealed 2450°C — 10 min, Water-quenched	α-rhenium + graphite
2.7	Annealed 2200°C — 10 min, Water-quenched	α-rhenium
6.8	Annealed 2200°C — 10 min, Water-quenched	α-rhenium + graphite
9.4	Annealed 2200°C — 10 min, Water-quenched	α-rhenium + graphite
12.5	Annealed 2200°C — 10 min, Water-quenched	α-rhenium + graphite
18.2	Annealed 2200°C — 10 min, Water-quenched	α-rhenium + graphite
25.1	Annealed 2200°C — 10 min, Water-quenched	α-rhenium + graphite
2.7	Annealed 2000°C — 10 min, Water-quenched	α-rhenium
6.8	Annealed 2000°C — 10 min, Water-quenched	α-rhenium + graphite
9.4	Annealed 2000°C — 10 min, Water-quenched	α-rhenium + graphite
2.7	Annealed 1800°C — 10 min, Water-quenched	α-rhenium
6.8	Annealed 1800°C — 10 min, Water-quenched	α-rehnium + graphite
9.4	Annealed 1800°C — 10 min, Water-quenched	α-rhenium + graphite

References p. 381

The presence of carbon dissolved in the rhenium led to an expansion of the lattice and increase in hardness. In an alloy of 20 at.% carbon quenched from 2400°C the "*a*" parameter increased from 2.760 Å to 2.792 Å. There was less influence on the "*c*" parameter which increased from 4.458 to 4.471. The V.P.N. of pure rhenium is approximately 150 at room temperature but this was increased to 350–500 by the presence of the maximum amount of soluble carbon. Carbon in excess of the solubility limit led to little further change in hardness.

Carbon from solution was deposited on cooling in a number of characteristic ways. When there was a small amount of carbon it appeared as a discontinuous graphitic grain boundary film; in alloys of higher carbon content the intergranular film was completed and carbon precipitation also occurred within the crystals, occasionally outlining a sub-boundary structure (Fig. 3).

Carbon in excess of the eutectic composition occurred in a number of forms depending mainly on rate of cooling. Large primary graphite flakes, the orientations of which were determined by the cooling gradients in the arc furnace, were the most common forms (Fig. 4) but spherical graphite with an accompanying concentric ring structure was also noted (Fig. 5). Such structures are similar to those which have been induced in certain nickel-carbon, cobalt-carbon and cast iron type alloys[10,11].

Heat treatments for extended periods at 1800°C on alloys of a range of carbon contents failed to reveal any new phases and it was concluded that above 1800°C no carbide existed.

Fig. 4. Primary graphite flakes. Furnace-cooled. X 200D.

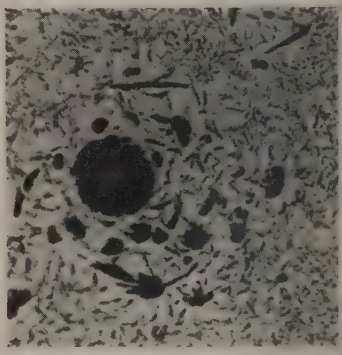

Fig. 5. Spherulitic graphite. Furnace cooled. Etched nitric acid + HF. X 450D.

CONCLUSIONS

Liquid rhenium is able to dissolve large quantities of carbon but the solid solubility is more restricted. The equilibrium diagram is in the form of a eutectic, very similar in form to the cobalt-carbon and nickel-carbon systems. The eutectic composition is 16.9 at.% carbon at 2480°C. At this temperature the solid solubility of carbon in rhenium is 11.7 at.% dropping to 4.2 at.% at 1800°C.

References p. 381

ACKNOWLEDGEMENTS

The author wishes to thank Dr. G. A. GEACH, Head of the Physical Metallurgy Section for suggesting this work, and Dr. T. E. ALLIBONE, F.R.S., Director of the Laboratory for permission to publish this paper.

REFERENCES

1 C. A. HAMPEL, *Rare Metals Handbook*, Reinhold Publ. Corp., New York, 1954.
2 C. T. SIMS, C. M. CRAIGHEAD AND R. I. JAFFEE, *J. Metals*, 7 (1955) 168.
3 G. A. GEACH AND J. E. HUGHES, *Plansee Seminar Proc.*, Pergamon Press, London, 1955.
4 R. SCHENK, F. KURZEN AND H. WESSELKOCK, *Z. anorg. u. allgem. Chem.*, 203 (1931) 159.
5 K. AGTE, *U.S. Patent No.* 1,854,970, 19th April (1932).
6 H. TROPSCH AND R. KASSLER, *Zpr. Ust. Vēd. Výzk. Uhlí.*, 2 (1932) 13.
7 W. TRZEBIATOWSKI, *Z. anorg. u. allgem. Chem.*, 233 (1937) 376.
8 D. SUMMERS-SMITH, *Metallurgia*, 42 (1950) 153.
9 D. SUMMERS-SMITH, *A.E.I. Research Report No. A126*, 1951.
10 H. MORROGH AND W. J. WILLIAMS, *J. Iron Steel Inst. London*, 155 (1947) 521.
11 H. MORROGH AND W. J. WILLIAMS, *J. Iron Steel Inst. London*, 158 (1948) 306.

ORDERING IN CoPt—FePt ALLOYS

J. C. WOOLLEY AND B. BATES

Department of Physics, University of Nottingham (Great Britain)

(Received October 21st, 1959)

SUMMARY

The effects of ordering in alloys of Co–Fe–Pt which belong to the pseudo-binary system CoPt–FePt have been studied as an initial step in the investigation of their possible permanent magnet properties. Six alloys having equal increments of composition have been investigated, and the lattice parameter values for both the ordered and disordered states have been determined for all alloys except FePt itself where the disordered state could not be obtained. Further work has been carried out on alloys of less than 25 at. % iron (*i.e.* less than 50 mol. % FePt). X-ray techniques have been used to estimate the ordering temperatures, and then the type of ordering reaction (continuous or discontinuous) occurring at various temperatures has been investigated. For these lower percentage iron alloys, possible values of percentage disregistry between the ordered and disordered structures have been calculated. The influence of the measured parameters on the possible production of hard magnetic materials from these alloys is briefly discussed.

INTRODUCTION

In recent years, considerable progress has been made in the study of hard magnetic materials, leading to the discovery of many new permanent magnet alloys. The work carried out in this field, both on the theoretical and experimental sides, has recently been reviewed by WOHLFARTH[1].

Among these new materials are binary alloys of cobalt–platinum and iron–platinum. In each case, alloys at or near the equiatomic composition are found to possess remarkable permanent magnet properties under certain conditions of heat treatment. CoPt, because of its higher coercivity and the greater ease with which the required conditions can be produced, is the more suitable of the two binary alloys as a permanent magnet material, and has been developed commercially.

The important magnetic properties of these alloys are associated in each case with an order–disorder transformation. The equilibrium diagram of the Co–Pt system[2] shows that the equiatomic alloy CoPt undergoes an ordering transformation from a disordered face-centred cubic structure to an ordered face-centred tetragonal structure of the AuCu type, with an ordering temperature of 825°C. The ordering reaction extends for some atomic percent on either side of the stoichiometric CoPt composition. LIPSON *et al.*[3] showed that the Fe–Pt diagram is similar, the equiatomic alloy FePt also having the same ordered face-centred tetragonal structure, and they assumed that the high-temperature structure for this alloy is disordered face-centred cubic, although at a higher temperature than 1100°C. This could not

References p. 389

be checked by quenching, however, because the ordering reaction is very rapid, and hence the disordered structure could not be retained.

From studies of the effects of isothermal ageing on various Co–Pt alloys in the ordered range[4,5], it appears that the optimum magnetic properties of these alloys are associated with the formation of nuclei of the ordered phase in the disordered material. At this incipient stage of development, the nuclei of the ordered phase remain coherent with the disordered matrix, resulting in the occurrence of large localised lattice strains. Modern theories of coercivity[1] would attribute the high coercivity values of these alloys to the localised strains produced in this way. Further annealing of the alloys causes the regions of ordered structure to break away as separate phases; hence the coherency strains are relieved and the hard magnetic properties lost.

NEWKIRK *et al.*[2,4] have given some experimental evidence to show that when the two structures are coherent, the cohabiting planes are (110) for the disordered structure and (101) for the ordered structure, with the directions $[001]_{\text{disordered}}$ and $[010]_{\text{ordered}}$ being parallel. They have also further argued that the above planes are the most likely combination from the viewpoint of their areas, in that calculations from the lattice parameter values show that this combination would give rise to a minimum disregistry in the lattice.

One further metallurgical point of interest in the production of suitable magnetic materials is the nature and rate of the development of the ordered phase at different temperatures of annealing. NEWKIRK *et al.* found that the nature of the ordering reaction in CoPt could take one of two distinct forms, depending upon the temperature concerned. If alloys annealed at temperatures around 700°C are investigated by X-ray methods, it is found that the main cubic lines gradually broaden into bands and slowly change in position as the ordered structure develops. As ordering advances, the tetragonal lines emerge from the band and eventually assume their final positions. For alloys annealed at lower temperatures, *e.g.* 500°C, the cubic lines remain sharp while the tetragonal lines slowly appear in their final positions and are also sharp. As ordering progresses, the tetragonal lines increase in intensity at the expense of the cubic lines, and no change in position is observed. For both reactions, after annealing for a sufficient time, the final ordered structures are the same. The first type of reaction has been called a continuous reaction and the second a discontinuous reaction. It is clear that the coherency strains responsible for the required magnetic properties are associated with the continuous reaction, and that a knowledge of the temperature ranges over which the different types of ordering reactions occur is therefore of importance.

The work described here forms an initial stage of an investigation of structural and magnetic properties of ternary alloys similar to the binaries described above. One set of alloys of interest in this work is that in which the 50 at. % platinum is retained and the cobalt is partially replaced by iron, *i.e.* alloys in the pseudo-binary system CoPt FePt. This account gives the results of some investigations of the structural properties of such alloys.

ALLOYS AND METHODS OF MEASUREMENT

The alloys used for this work were provided by Messrs. Johnson, Matthey and Co. Ltd. The nominal compositions were chosen to cover the range from CoPt to FePt

References p. 389

in intervals of 10 at. %, *i.e.* (i) 10 at. % Fe, 40 at. % Co, 50 at. % Pt; (ii) 20 at. % Fe, 30 at. % Co, 50 at. % Pt; etc. The alloys were produced by argon-arc melting and cast in roughly cylindrical ingots of approximate diameter 1.25 cm and length 7.5 cm, ingots of this size being required for magnetic work. For each alloy, specimens suitable for X-ray powder photograph work were cut from the ends of the ingots by means of a carborundum wheel, rubbed down to a suitable shape (approximately 0.4 mm diameter and 1 cm long) on emery cloth and lightly etched in aqua regia. When the X-ray work was complete, typical specimens of each alloy were analysed by Messrs. Johnson, Matthey and Co. Ltd. and the results of the analyses are given in Table I.

TABLE I

COMPOSITION OF ALLOYS

Alloy No.	*Wt. % Fe*	*At. % Fe*	*Wt. % Co*	*At. % Co*	*Wt. % Pt*	*At. % Pt*
2	5.21	11.65	18.70	39.63	76.09	48.72
3	9.42	21.01	14.35	30.32	76.23	48.67
4	12.54	28.96	8.66	18.95	78.80	52.09
5	17.05	38.49	5.30	11.34	77.65	50.18

Initially, an attempt was made to quench in a high-temperature disordered phase for all of the alloys. This was done for CoPt by sealing a specimen under vacuum in a quartz tube, heating at 1000°C for approximately 1 hour, and then quenching rapidly in water. In order to obtain a rapid quench, thin wall 1 mm bore quartz tubing was used. To prevent any reaction of the specimen with the quartz at high temperatures, the tube was first "carbonized" on the inner surface. This was done by placing a few drops of acetone in a sealed tube and then baking the tube at 800°C for about 1 hour, thus producing the required protective layer of carbon on the walls of the tube. A further precaution taken with all specimens which had been heated or annealed was that they were lightly etched in aqua regia to remove any surface effects.

CoPt specimens quenched in this way showed the expected disordered face-centred cubic structure. As the iron content of the alloys increased however, progressively higher temperatures were required to produce disordering. The alloys were heated in a platinum-wound furnace giving a maximum practical temperature of operation of approximately 1400°C. In order to obtain rapid quenching, the furnace tube was held vertical, and the specimen supported by a thin platinum wire and weighted by a small block of suitable ceramic material. To quench, the wire was released and the specimen, wire, and weight fell some 30 cm into water. This method gave satisfactory results for the alloys of lower iron content, but for alloys of higher iron content was unsatisfactory in that no disordered phases were obtained, and hence higher temperatures from which to quench were required.

In an attempt to disorder the alloys of higher iron content, an eddy current heater was therefore used. The X-ray specimen was placed on a small carbon block inside a quartz tube, which was continuously evacuated, the carbon block and specimen then being heated by the eddy current heater. With this arrangement, sufficient heat could be developed in the carbon block to melt the specimen if necessary. The specimen was quenched by switching off the R.F. power, closing the vacuum system, and letting a stream of water flow through the quartz tube and over the specimen, thus giving a very rapid quench. The temperature of the specimen and carbon block was measured

References p. 389

when necessary by an optical pyrometer. This method allowed the disordered phase to be obtained for all alloys except FePt.

To determine the ordered phase of the various alloys, specimens were heated in the temperature range 500–600°C for about a week. All alloys were found by X-ray measurements to be completely ordered after this length of time. The lattice parameters of all ordered and disordered phases were determined by usual X-ray techniques using CuK_α radiation and a precalibrated 19 cm Unicam powder camera.

For the alloys which could be disordered relatively easily, an attempt was made to determine the ordering temperature by the use of X-ray methods. A specimen was first disordered, and then annealed for approximately an hour at a chosen temperature and finally rapidly quenched and X-rayed. Any sign of ordering in the specimen indicated that the chosen temperature was below the ordering temperature. (Because of the relatively rapid rates of ordering with these alloys, one hour annealing was sufficient for this work.) By investigating a suitable range of temperature it was possible in this way to estimate the ordering temperature for an alloy to within limits of approximately ± 5°C.

The types of ordering reaction occurring at various temperatures in the different alloys was also investigated. The specimen was annealed for a certain length of time at the chosen temperature, quenched and X-rayed, and then annealed for a further time, and so on. The time intervals were chosen if possible so that a series of X-ray photographs were obtained showing the development of the specimen from the disordered to the ordered state. This could be done without difficulty at low temperatures where the rate of ordering was slow, but a range of photographs was usually not possible at higher temperatures when complete ordering was obtained in a relatively short time. In order to present the results of these ordering reaction investigations, for each photograph the line profiles of the 311 and 113 lines were measured by means of a Hilger microphotometer. Of these lines, the cubic structure shows only a single 311 line while the tetragonal structure shows the two lines separately. The relatively large separation of these lines in the X-ray film enables the difference between continuous and discontinuous reactions to be detected without difficulty.

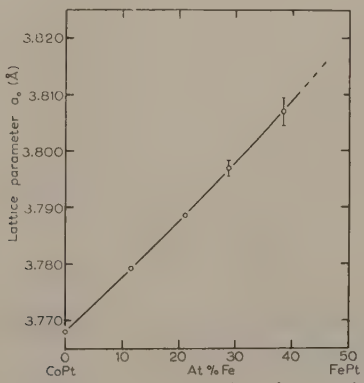

Fig. 1. Variation of lattice parameter a_0 as a function of composition for disordered alloys.

References p. 389

RESULTS AND DISCUSSION

The variation of cubic lattice parameter, a_0, as a function of at. % iron present in the alloy is shown in Fig. 1. It is seen that at low at. % iron where the disordered phase can be quenched in without difficulty, an accurate determination of a_0 is possible and the accuracy is better than ± 0.001 Å. Beyond approximately 25 at. % Fe (*i.e.* 50 mol. % FePt) however, even with rapid quenching, the disordered phase is difficult to retain and the X-ray lines obtained are blurred. The resultant inaccuracies in the values of a_0 are indicated in Fig. 1. In the case of the alloy containing 38.5 at. % Fe, the disordered condition was obtained only by quenching from the melt, while, as previously indicated, the disordered phase of FePt could not be obtained. Because of these difficulties, it is seen that the deviation of the parameters from a Vegard line cannot be discussed, although the results which are available do show some deviation from a straight line.

The results obtained by ordering the alloys are shown in Fig. 2. It is seen that in all cases an ordered face-centred tetragonal structure similar to that in CoPt and FePt occurs, and values of a_0 and c/a are plotted as a function of at. % iron in the alloy. In this case, no difficulty was experienced in obtaining the ordered structure and the accuracy of the a_0 values is estimated as ± 0.001 Å for all compositions. Again, the variation of the parameters with composition is not linear, but a factor which must be considered here is the variation of platinum content of the alloys. Ideally the alloys should all have contained 50 at. % Pt but difficulties in production resulted in deviations from this of up to 2 at. %. The results of NEWKIRK *et al.*[2] and MARTIN[5] have shown that in the case of Co–Pt alloys changes of composition of this amount can cause considerable variation in the lattice parameter values. The variation in parameter which could possibly occur because of the platinum content variation in the present series of alloys is demonstrated by arbitrarily assuming the variations which occur for Co–Pt alloys and calculating a corresponding value for each alloy concerned here, using the Pt percentage given in Table 1. The resulting values of a_0

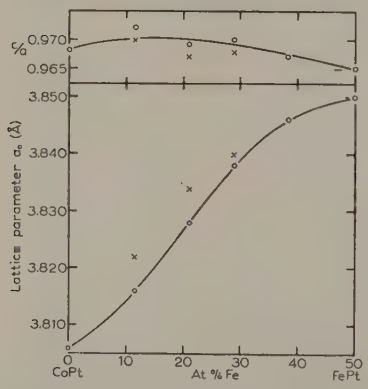

Fig. 2. Variation of lattice parameter a_0 and ratio c/a as a function of composition for ordered alloys. O Experimental results with actual alloys. × Estimated values for alloys of ideal composition.

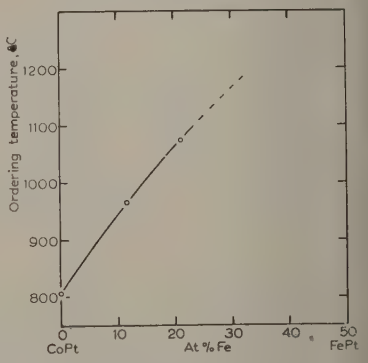

Fig. 3. Variation of ordering temperature as a function of composition.

References p. 389

and c/a are plotted in Fig. 2. The general form of the curves is not changed, but it is obvious that a detailed discussion of the form of the curves has no point at this stage.

In the work to determine ordering temperatures, it was found impossible to obtain values of any significance for alloys containing more than 25 at. % Fe. Fig. 3 therefore shows the values of ordering temperature determined for the three alloys of lower iron content. The accuracy of the temperatures is estimated to be ± 5°C.

In the case of the alloys for which the ordering temperature could be determined, investigations were also carried out to investigate the types of ordering reaction. Fol-

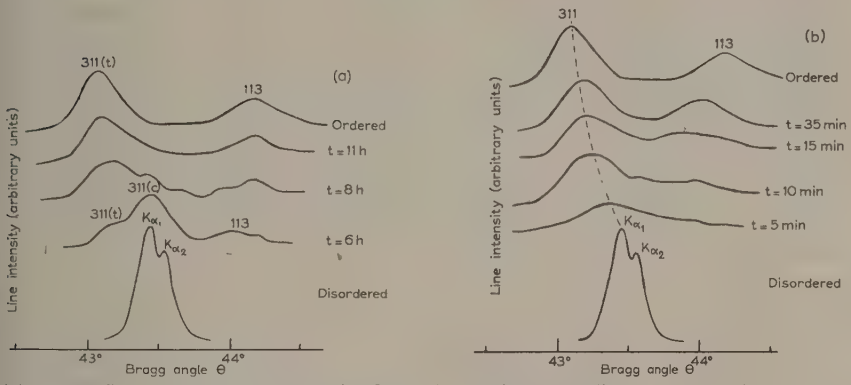

Fig. 4. Profiles of 311 and 113 lines for CoPt after various annealing treatments (t = time of anneal). (a) Annealed at 500°C. (b) Annealed at 700°C.

lowing the work of NEWKIRK *et al.*[2,4], different specimens of CoPt, initially disordered, were annealed at 500°C and 700°C respectively and in each case the ordering observed as described in section 2. Figs. 4a and 4b show the variation of the profile of the 311 and 113 lines for various times of anneal at 500°C and 700°C respectively. It is seen that the two types of reaction can be distinguished in these graphs, and that the

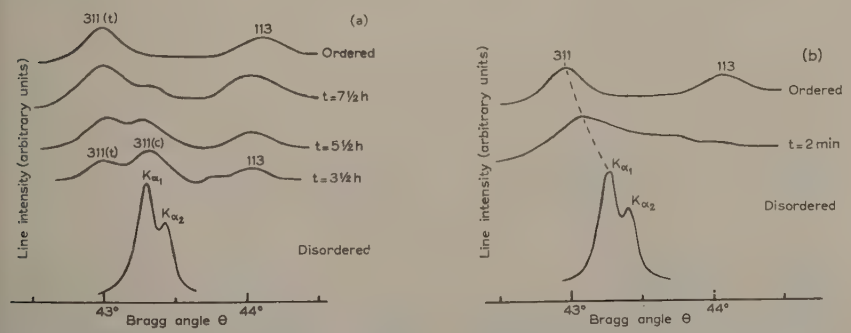

Fig. 5. Profiles of 311 and 113 lines for alloy No. 2 (nominal 40 Co, 10 Fe, 50 Pt) after various annealing treatments (t = time of anneal). (a) Annealed at 500°C. (b) Annealed at 750°C.

References p. 389

temperature range at which the transition from discontinuous to continuous reaction occurs must lie between 500°C and 700°C in this case.

Similar measurements were then made on alloy No. 2 (nominal 10 at. % Fe). Fig. 5a shows the profile variation with annealing at 500°C and this is clearly a discontinuous reaction. When results were obtained for annealing at 700°C, these were found to be indeterminate. The annealing temperature was therefore raised to 750°C. The results obtained, shown in Fig. 5b, were typical of a continuous reaction, but because of the increased rate of reaction as compared with the CoPt results due to (a) the increased temperature and (b) the increased iron content, very short annealing times were required and only one intermediate profile is shown in Fig. 5b, this representing 2 min annealing at 750°C. It appears, however, that the temperature at which the transition from discontinuous to continuous reaction occurs increases with increased iron content.

These results were confirmed by the measurements made on alloy No. 3 (nominal 20 at. % Fe). In this case annealing at 675°C produced a discontinuous reaction, as shown in Fig. 6a, although the annealing times required were shorter than those required for CoPt at 700°C. The profile obtained by annealing for 2 min at 750°C (Fig. 6b) was indeterminate but tended to indicate discontinuous behaviour. The

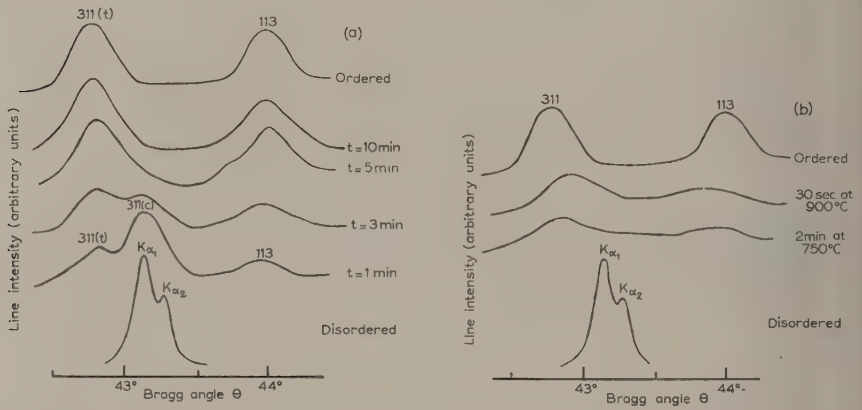

Fig. 6. Profiles of 311 and 113 lines for alloy No. 3 (nominal 30 Co, 20 Fe, 50 Pt) after various annealing treatments (t = time of anneal). (a) Annealed at 675°C. (b) Annealed at 750°C and 900°C.

other intermediate profile in Fig. 6b represents the results of annealing for nominally 30 sec at 900°C. The profile has the continuous form, but under these conditions the reaction rates are so rapid that times of anneal have little significance.

A further point of interest in the order–disorder reaction in these alloys is the degree of disregistry likely to occur when ordering takes place by the continuous reaction. No data have been obtained as to the actual cohabiting planes of the ordered and disordered structures, but it is of interest to calculate from the measured lattice parameters the possible percentage disregistry for various combinations of planes. As was shown by NEWKIRK *et al.*[2] the two combinations giving small disregistry values

References p. 389

TABLE II

PERCENTAGE DISREGISTRY CALCULATED FROM LATTICE PARAMETER VALUES

Alloy No.	*Nominal at. % composition*	*Percentage disregistry*	
		$(110)_{dis.}:(101)_{ord.}$	$(111)_{dis.}:(111)_{ord.}$
1	50 Co, 50 Pt	0.41	—0.14
2	40 Co, 10 Fe, 50 Pt	0.54	0.07
3	30 Co, 20 Fe, 50 Pt	0.53	0

Sign of disregistry given by $\Delta A = \text{Area}_{\text{ordered}} - \text{Area}_{\text{disordered}}$.

are $(110)_{\text{disordered}} : (101)_{\text{ordered}}$ and $(111)_{\text{disordered}} : (111)_{\text{ordered}}$, and Table II gives the percentage disregistry (ratio $\Delta A/A$ expressed as a percentage) for these two combinations, in the case of the three alloys for which accurate disordered parameters could be obtained. It is seen that contrary to the results of NEWKIRK *et al.*[2], from these measurements the $(111)_{\text{disordered}} : (111)_{\text{ordered}}$ gives the smallest disregistry in each case including CoPt.

CONCLUSIONS

The above results show that the ordering which occurs in CoPt and FePt and which is responsible for the hard magnetic behaviour of these alloys, also occurs throughout the whole range of composition of CoPt–FePt alloys. Thus, similar magnetic properties are to be expected for these ternary alloys. As far as structural properties are concerned, the three factors which are of importance in obtaining the most suitable magnetic properties from the technological viewpoint are (a) the value of the ordering temperature, (b) the temperature range in which a continuous ordering reaction occurs and (c) the probable disregistry values. A consideration of points (a) and (b) indicates that the alloys of small iron content will probably be of more interest technologically, since for alloys of high iron content the increase in ordering temperature and the associated increase in the minimum temperature at which a continuous reaction occurs, means that the necessary annealing times become very short, and thus a control of the degree of ordering and thereby of the magnetic properties of the alloys becomes correspondingly more difficult. Insufficient data are available for the influence of factor (c) to be considered, but the results show that for alloys of low iron content, there appears to be little variation of the disregistry values with composition.

ACKNOWLEDGEMENTS

We are indebted to Professor L. F. BATES for the facilities of his laboratory, and to Dr. M. E. HAINE of Messrs. Siemens Edison Swan Ltd. for a maintenance grant to one of us (B.B.). We also wish to thank Dr. J. C. CHASTON of Messrs. Johnson, Matthey and Co. Ltd. for the preparation and loan of the alloys used in the work.

REFERENCES

1 E. P. WOHLFARTH, *Advances in Phys.*, 8 (1959) 87.
2 J. B. NEWKIRK, R. SMOLUCHOWSKI, A. H. GEISLER AND D. L. MARTIN, *J. Appl. Phys.*, 22 (1951) 290.
3 H. LIPSON, D. SHOENBERG AND G. V. STUPART, *J. Inst. Metals*, 67 (1941) 333.
4 J. B. NEWKIRK, A. H. GEISLER, D. L. MARTIN AND R. SMOLUCHOWSKI, *Trans. Am. Inst. Mining Met. Engrs.*, 188 (1950) 1249.
5 D. L. MARTIN, *Trans. A.I.M.E.*, 212 (1958) 478.

ZUR FEINREINIGUNG DES GALLIUMS

H. MERKEL

Forschungslaboratorium der Siemens-Schuckertwerke A.G., Erlangen (Deutschland)

(Eingegangen den 22. Oktober 1959)

ZUSAMMENFASSUNG

Das Verhalten der Elemente gegen Stickstoff und gasförmiges Ammoniak ermöglicht ein Reinigungsverfahren für Galliummetall, bei dem Spurenverunreinigungen, insbesondere Eisen, Aluminium, Titan, Magnesium u.a., nitridiert und wirkungsvoll abgereichert werden.

Die Durchführung der Reinigung mit Ammoniak bei 800°C unter Verwendung einer Apparatur, die es auf einfache Weise gestattet, das reinigende Agens, NH_3, unter sauberen Arbeitsbedingungen auf feinverteiltes Gallium einwirken zu lassen, wird beschrieben.

SUMMARY

A method has been developed for the preparation of super-pure gallium metal. It is based on the behaviour of the elements to nitrogen and gaseous ammonia. Impurities that form nitrides, especially iron, aluminium, titanium, magnesium and others, are effectively removed.

A description is given of a purification process with ammonia at 800°C. This is performed in an apparatus that, in a simple way, enables the purifying agent, NH_3, to operate on very finely distributed gallium metal.

Mit dem Fortschreiten der technischen Entwicklung stellt die Industrie an die Reinheit ihrer Werkstoffe immer höhere Anforderungen. Dies gilt besonders für die in der Halbleitertechnik verwendeten Materialien, die allerhöchsten Reinheitsansprüchen genügen müssen. Ein ganz neuer Industriezweig ist entstanden und gewinnt von Jahr zu Jahr mehr an Bedeutung, der sich mit der Produktion sogenannter „semiconductor grade" Substanzen befasst. Man versteht darunter Stoffe, die — zum mindesten in Bezug auf elektronisch wirksame Verunreinigungen — reiner sein müssen als schlechthin spektralreine Stoffe.

In besonderem Masse befruchtend für diese Entwicklung wirkte sich die Entdeckung der Halbleitereigenschaften der $A^{III}B^{V}$-Verbindungen durch WELKER[1] aus. Diese Stoffklasse umfasst die Verbindungen zwischen den Elementen der 3. und 5. Gruppe des Periodensystems der chemischen Elemente. Im Rahmen unserer Untersuchungen über diese Halbleitergruppe wurde für die Synthese von GaN, GaP, GaAs und GaSb Gallium hoher Reinheit benötigt.

Das reinste im Handel erhältliche Gallium, das für diese Versuche zur Verfügung stand, hatte einen nominellen Reinheitsgrad von etwa 99.99%; es war für Halbleiterzwecke nicht geeignet.

Es erschien wenig aussichtsreich, die Konzentration der noch vorhandenen störenden Verunreinigungen auf nasschemischem Wege, etwa nach HOFFMAN[2], merklich

Literatur S. 395

weiter zu verringern. Der nasschemischen Beseitigung von Spurenmengen aus einer gegebenen Matrix sind grundsätzliche Grenzen gesetzt, die verhältnismässig hoch liegen und dadurch bedingt sind, dass es praktisch in den wenigsten Fällen möglich ist aus einer grossen Flüssigkeitsmenge, in der sich ein Lösungspartner nahe seiner Sättigungskonzentration befindet, während eine Reihe anderer in hoher Verdünnung vorliegen, die letzteren abzutrennen. Fällungsreaktionen bei diesen anomalen Bedingungen nehmen meist durch Komplexsalzbildung, Adsorptionserscheinungen und andere Störungen einen oft unerwarteten Verlauf; durch Extraktionen wird häufig die Ausbeute am gewünschten Stoff stark vermindert oder die Scheidung ist unzureichend; die für die Reaktionen erforderlichen Säuren, Laugen und sonstigen Chemikalien bedeuten eine Quelle für die Einschleppung neuer Verunreinigungen; die Operationen sind langwierig und der Zeitaufwand unverhältnismässig gross.

Bei der Betrachtung der Möglichkeiten, die Reinigung mittels physikalischer Methoden vorzunehmen, schied die Destillation des Galliums wegen seines niedrigen Dampfdruckes bei noch erträglicher Temperatur (einige 10^{-3} Torr bei 1000°C) von vornherein aus; auch unerwünschte Reaktionen des hoch erhitzten Galliums mit dem Gefässmaterial, z.B. Quarz, mussten sich dabei störend bemerkbar machen. Über die Feinreinigung des Galliums durch Kristallisation[3], fraktioniertes Ziehen von Einkristallen[4] oder durch Zonenraffination[5] wurde schon verschiedentlich berichtet. Eigene Versuche in dieser Richtung bestätigten den geringen, jedoch unbefriedigenden Erfolg dieser Massnahmen. Die hohen Diffusionsgeschwindigkeiten der metallischen Verunreinigungen im Gallium selbst bei niedrigen Temperaturen, müssen für das Versagen dieser gerade in der Halbleitertechnik häufig so erfolgreich eingesetzten Methode verantwortlich gemacht werden.

Gute Reinigungsergebnisse erzielten wir dagegen mit einem trocken-chemischen Verfahren. Es basiert auf dem Verhalten der Metalle gegenüber Stickstoff und gasförmigem Ammoniak, auf das im folgenden kurz eingegangen wird.

Nach bisher vorliegenden Untersuchungen[6] reagiert der freie, molekulare, rein thermisch angeregte Stickstoff mit den in Tab. I aufgeführten Metallen unter Nitridbildung.

TABELLE I

NITRIDBILDUNG MIT STICKSTOFF

untersuchtes Metall	*Nitr.-Bldg. bei °C*	*untersuchtes Metall*	*Nitr.-Bldg. bei °C*	*untersuchtes Metall*	*Nitr.-Bldg. bei °C*
Li	—55	Pr	700	B	1200
Ca	20	Nd	700	Si	1250
Ba	190	Zr	700	La	Rotgl.
Sr	300	Ge	800	V	Rotgl.
Mn	390	Ti	800	Nb	Rotgl.
Cr	500	Th	800	Ta	Rotgl.
Mo	500	Al	820	W	Rotgl.
Mg	600	Be	900		
Ce	620	U	1000		

In dieser Übersicht ist die tiefste Temperatur angegeben, bei der eine merkliche Umsetzung des betreffenden Elementes zu Nitrid beobachtet wurde. Lithium und Calcium reagieren danach bereits bei Zimmertemperatur. Bei den anderen Elementen setzt die Nitridbildung erst nach relativ hoher Erhitzung ein. Die zugeführte ther-

Literatur S. 395

mische Energie ist wegen der bekannten Reaktionsträgheit des molekularen Stickstoffes, für dessen Zerlegung in Atome etwa 200 kcal/Mol aufgewendet werden müssen, erforderlich. Es wäre möglich, die reaktionsfreudigen N-Atome durch elektrische Anregung zu erzeugen. Das lässt sich aber nicht ohne grösseren apparativen Aufwand bewerkstelligen. Eine andere, sehr einfache Art, die für die Nitridbildung erwünschten N-Atome zu erhalten, beruht auf der Verwendung von gasförmigem Ammoniak, das sich bei seiner Einwirkung auf Metalle bereits bei nicht zu hoher Temperatur teilweise in N- und H-Atome aufspaltet. Deshalb ist bei Verwendung von Ammoniakgas die für die Nitridbildung erforderliche Temperatur im allgemeinen erheblich niedriger als bei molekularem Stickstoff. Ausserdem ist es möglich, bei den in Tab. II aufgeführten Metallen, die nicht mit Stickstoff reagieren, mit Ammoniak Nitrid- bzw. (bei den Alkalimetallen) Amidbildung zu erreichen[6].

TABELLE II

NITRID(AMID)-BILDUNG MIT AMMONIAKGAS

untersuchtes Metall	*Amid-Bldg. bei °C*	*untersuchtes Metall*	*Nitr.-Bldg. bei °C*	*untersuchtes Metall*	*Nitr.-Bldg. bei °C*
Na	300	Fe	450	Cu	280
K	300	Co	380	Zn	600
Rb	200	Ni	445	Cd	600
Cs	120			Ga	900

Im periodischen System der chemischen Elemente lassen sich die mit Stickstoff und Ammoniak reagierenden Metalle zu einer geschlossenen Gruppe zusammenfassen (Tab. III).

TABELLE III

STELLUNG DER MIT N_2 UND NH_3 REAGIERENDEN METALLE IM PSE

1a	2a	3a	4a	5a	6a	7a	8			1b	2b	3b	4b	5b	6b	7b	0
																H	He
Li	Be											B	C	N	O	F	Ne
Na	Mg											Al	Si	P	S	Cl	Ar
K	Ca	Sc	Ti	V	Cr	Mn	Fe	Co	Ni	Cu	Zn	Ga	Ge	As	Se	Br	Kr
Rb	Sr	Y	Zr	Nb	Mo	Tc	Ru	Rh	Pd	Ag	Cd	In	Sn	Sb	Te	I	Xe
Cs	Ba	La	Hf	Ta	W	Re	Os	Ir	Pt	Au	Hg	Tl	Pb	Bi	Po	At	Rn
Fr	Ra	Ac	Th	Pa	U												

Die Geschwindigkeit der Reaktion mit Stickstoff ist bei den Elementen der ersten Gruppen (1a bis 3a), die thermische und chemische Beständigkeit sowie die Bildungswärme der Nitride bei jenen der mittleren Gruppen (3a bis 5a) im allgemeinen am grössten. Bei den Elementen der Gruppen 6a bis 8 nimmt die Stärke, mit der der Stickstoff am Metall gebunden ist, mit steigender Ordnungszahl ab (Ausnahme Uran). Relativ schwer zugänglich sind die leichtzersetzlichen Nitride des Kupfers, Zinks und Cadmiums[7] (1b und 2b).

Das Gallium, dessen Verhalten im Zusammenhang mit der vorliegenden Unter-

Literatur S. 395

suchung von besonderem Interesse ist, wird von Sticksotff selbst bei den höchsten Temperaturen nicht angegriffen; mit Ammoniak reagiert es ab etwa 900°C unter Nitridbildung.

Es muss demnach möglich sein, dem Gallium bei geeignet gewählter Temperatur eine Reihe von Verunreinigungen durch Nitridierung mit Stickstoff oder Ammoniak zu entziehen. Welches der beiden als reinigende Agentien verwendbaren Gase mit Vorteil eingesetzt werden kann, hängt von der Art der vorhandenen Verunreinigungen ab. Bei Anwesenheit von Eisen, das wir immer im Rohgallium fanden, ist einzig und allein die Reinigung mit Ammoniakgas sinnvoll, weil Eisen zu den in Tab. II aufgeführten, nur mit Ammoniak reagierenden Metallen gehört.

Die Nitridierungstemperatur soll dabei 900°C nicht überschreiten, um Galliumnitridbildung zu vermeiden. Vielfach bewährt hat sich die Durchführung des Verfahrens bei etwa 800°C. Erfahrungsgemäss lassen sich mit Ammoniak nicht nur Eisen, sondern auch andere im üblichen Handelsgallium vorkommende Verunreinigungen stark abreichern, so dass sich die Behandlung mit Stickstoff, die bei wesentlich höherer Temperatur, z.B. 1200°C, möglich ist, im allgemeinen erübrigt. Sie bleibt auf die seltenen Fälle beschränkt, bei denen Fremdstoffe wie etwa Be, B, U zu beseitigen sind. Verunreinigungen dieser Art haben wir allerdings bis jetzt noch in keinem Galliumpräparat feststellen können.

Die Behandlung des Galliums mit Stickstoff oder Ammoniak kann grundsätzlich nach zwei Verfahrensweisen vorgenommen werden:

(1) Leiten des Gasstromes durch erhitztes Gallium;
(2) der Gasstrom umspült feine Galliumtröpfchen, die im Innern eines senkrecht stehenden, auf die Arbeitstemperatur erhitzten Rohres herabfallen.

Die Ausführungsform nach (2) ist vorteilhafter und wirkungsvoller aus folgenden Gründen:

(1) Das Gallium kommt nicht mit der heissen Gefässwand, aus der es Verunreinigungen aufnehmen könnte, in Berührung;
(2) das Reinigungsgas ist immer im grossen Überschuss vorhanden;
(3) jedes Galliumtröpfchen durchfällt einen Temperaturbereich von der Arbeitstemperatur bis etwa Zimmertemperatur, in dem die für jedes verunreinigende Element optimale Bildungstemperatur seines Nitrides enthalten ist;
(4) die Erhitzungsdauer ist für jedes Galliumtröpfchen nur kurz, so dass auch Elemente, die leichtzersetzliche Nitride bilden, abgereichert werden (Cu, Zn);
(5) infolge der Verteilung des Galliums in feine Tröpfchen wird die Beseitigung flüchtiger Verunreinigungen durch Verdampfen begünstigt.

Auf Grund der vorstehenden Überlegungen wurde die Reinigung des Galliums unter Verwendung der in Fig. 1 skizzierten Apparatur vorgenommen.

Sie besteht im wesentlichen aus dem etwa 800 mm langen Reaktionsrohr aus Quarz von 30 mm Durchmesser. Das Rohr trägt oben einen Aufsatz aus Jenaer Geräteglas mit eingeschliffener Tropfvorrichtung und seitlichem Gasableitungsrohr. Am anderen Ende des Reaktors befindet sich ein Sammelbehälter (Auffänger) für das herabtropfende Gallium, in den das Gaseinleitungsrohr mündet. In seinem unteren Teil ist der Sammelbehälter bis auf einen Durchmesser von etwa 6 mm verjüngt und wie aus der Fig. 1 ersichtlich gebogen, so dass das Gallium, wenn es sich im Behälter bis zu einer bestimmten Höhe angesammelt hat, stetig in ein vorgelegtes Gefäss ablaufen kann.

Literatur S. 395

Vor Inbetriebnahme der Reinigungsvorrichtung gibt man in den Auffänger eine kleine Menge Galliummetall, welche die Apparatur nach unten verschliesst. Dann verdrängt man durch Einleiten von gereinigtem Ammoniak die Luft aus dem Reaktor und heizt den oberen Teil des Rohres auf 800°C. In die Tropfvorrichtung werden nun z.B. 300 g Roh-Gallium gegeben und die Auslauföffnung so einreguliert, dass feine

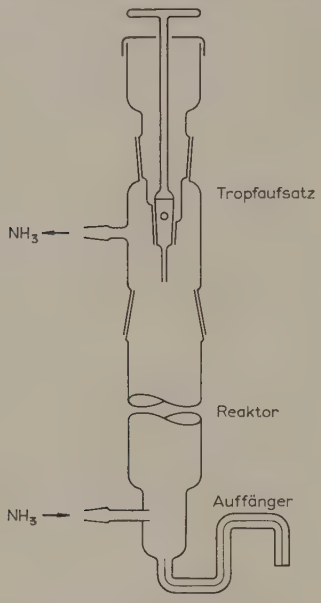

Fig. 1. Reinigungsapparatur.

Galliumtröpfchen in schneller Folge ausfliessen. Durch die Ausstrahlung des heissen Reaktionsrohres wird das zu vertropfende Metall (Smpkt. *ca.* 30°C) ohne besondere Heizung in dünnflüssigem Zustand gehalten. Die Vertropfung von 300 g Gallium benötigt in der angegebenen Apparatur etwa 15 min. Der Vorgang wird am besten mit dem selben Gallium mehrfach wiederholt.

Die in Nitride überführten Verunreinigungen sammeln sich nach der Reinigungsprozedur auf der Galliumoberfläche als dünne Haut (Schlacke) an. Sie kann bequem, sauber und ohne nennenswerten Galliumverlust am einfachsten dadurch vom Raffinat getrennt werden, dass man das flüssige Metall durch eine Kapillare von etwa 2 bis 3 mm lichter Weite fliessen lässt, wobei die Schlacke an der Gefässwandung haften bleibt. Auf der Innenwand des Reaktionsrohres entsteht während des Betriebes der Apparatur ein Belag, in dem neben den nitridbildenden Verunreinigungen auch Blei festgestellt wurde. Auch die reaktionsfähigen Metalle werden, mindestens zum Teil, verdampfen, ehe sie mit dem Ammoniak reagieren.

Versuche, auf analytischem Wege Aufschluss über das Verhalten der Spurenverunreinigungen bei der Nitridierung zu erhalten, führten zu den in Tab. IV aufgeführten Ergebnissen.

Literatur S. 395

TABELLE IV

ANALYSENERGEBNISSE

Beimengung	*Ga-Ausgangsmaterial*	*Ga-Endprodukt (nach 20 Durchgängen)*	*Schlacke + Rohrbelag*
Fe (ppm)	11	<(0.05)	700
Al (ppm)	<(7)	<(7)	35
Ti (ppm)	<12)	<(2)	30
Mg (ppm)	0,1	<(0,05)	2
Zn (ppm)	15	3	nicht best.
Cu (ppm)	9	5	3
Pb (ppm)	<(7)	<(7)	18

In dieser Übersicht geben die in Klammern stehenden Zahlen unsere derzeitigen analytischen Nachweisgrenzen für die betreffenden Elemente an. Da die Konzentrationen der Fremdstoffe schon im Ausgangsgallium klein sind bzw. bereits unterhalb der analytischen Erfassbarkeit liegen, erhält man bei manchen Spurenelementen erst nach Untersuchung der Schlacke einen Hinweis auf ihre Abreicherung. Diese ist am grössten beim Eisen und bei den Elementen, die thermisch stabile Nitride bilden. Die geringe Bildungstendenz der leicht zersetzlichen Nitride des Kupfers und Zinks verzögert die Ausscheidung dieser Metalle, deren Gehalt im Gallium nur durch häufige Wiederholung der Verfahrensschritte weiter erniedrigt werden kann.

Für unsere Zwecke war der aus Tab. IV ersichtliche Erfolg der Nitridierung jedoch völlig ausreichend, weil wir fanden, dass sich Kupfer und Zink sehr sicher und wirksam auf anderem Wege, über den noch berichtet werden soll, dem Gallium entziehen lassen.

LITERATUR

[1] H. Welker, *Z. Naturforsch.*, 7a (1952) 744; 8a (1953) 248.
[2] J. I. Hoffman, *J. Research Natl. Bur. Standards*, 13 (1934) 665.
[3] J. I. Hoffman und B. F. Scribner, *Metal Ind. (London)*, 47 (1935) 537.
[4] W. Zimmerman, *Science*, 119 (1954) 411.
[5] D. P. Detwiler und W. M. Fox, *J. Metals*, 7 (1955) 205.
[6] Gmelin, *Handbuch der anorganischen Chemie*, System Nr. 4: Stickstoff (1936), bzw. bei den betreffenden Elementen.
[7] R. Juza, *Die Chemie*, 58 (1945) 25.

AN INTERPRETATION OF SOME OF THE PROPERTIES OF THE TRANSITION METALS AND THEIR ALLOYS

D. A. ROBINS*

Tin Research Institute, Greenford, Middlesex (Great Britain)

(Received November 9th, 1959)

SUMMARY

The hypothesis is put forward that many of the properties of the transition metals can be interpreted in terms of a relationship between the co-ordination number of the metal atoms and the number of bonding electrons per atom. The electron resonance contribution to the bond strength is a maximum when the number of bonding electrons per atom is approximately equal to half the effective co-ordination number and it is postulated that the stability of this arrangement dictates very largely the alloying behaviour and crystal structure.

The alloying behaviour of transition metals and their interaction with hydrogen and other interstitial elements are considered in relation to the hypothesis.

1. INTRODUCTION

In the transition metals an incomplete group of eight electrons expands with increasing atomic number into a group of eighteen electrons and the s and p electron states of the outer shell overlap those of the incomplete d shell forming hybrid s.p.d. bonding orbitals. This makes the electronic structure of the transition metals so complex that the collective electron theory cannot, at the present time, be used to explain from first principles the properties of these elements. An alternative approach to the collective electron theory is that of considering the electrons to be localised around pairs of atoms and several theories have been proposed, based upon localised bonding, in which theoretical considerations and experimental observations are combined to correlate a number of specific properties. The interpretation of some of the properties of the transition metals in this paper has been stimulated by investigations of the characteristics of certain transition metal carbides and silicides[1,2,3] and, in particular, observations on the non-stoichiometry of tantalum carbide[3]. The interpretation is based upon the resonating covalent bond theory of PAULING[4,5,6] and its subsequent modifications by HUME-ROTHERY, IRVING AND WILLIAMS[7].

2. SOME PRELIMINARY OBSERVATIONS

HUME-ROTHERY, IRVING AND WILLIAMS[7] have suggested a scheme for the valencies of the transition metals in which the valencies in the metallic state are considered to be related to the valencies exhibited in inorganic chemistry (throughout this paper

* Previously at Research Laboratories of The General Electric Co., Ltd., Wembley, Middlesex.

References p. 410

the term valency of a metal is used to describe the average number of electrons per metal atom taking part in resonating covalent bonding). These authors agree with PAULING that the valency of the Group IIIA metals is three, of the Group IVA metals is four and of the Group VA metals is five but, for transition metals further to the right in the Periodic Table, HUME-ROTHERY and others[7] reject Pauling's idea of a constant valency of 5.78 since this is not in keeping with the physical properties of the elements. For the second and third transition series a valency of about six is accepted for molybdenum and tungsten and thereafter, on moving further to the right in the Periodic Table, the valency of the elements is considered to decrease progressively owing to the additional electrons entering non-bonding orbitals and having coupled with them electrons which previously contributed to the metallic bonding. In the first transition series the picture is rather more complex due to the increased stability of non-bonding orbitals causing electrons to enter non-bonding orbitals at an earlier stage. For this reason the hypothesis put forward in this present

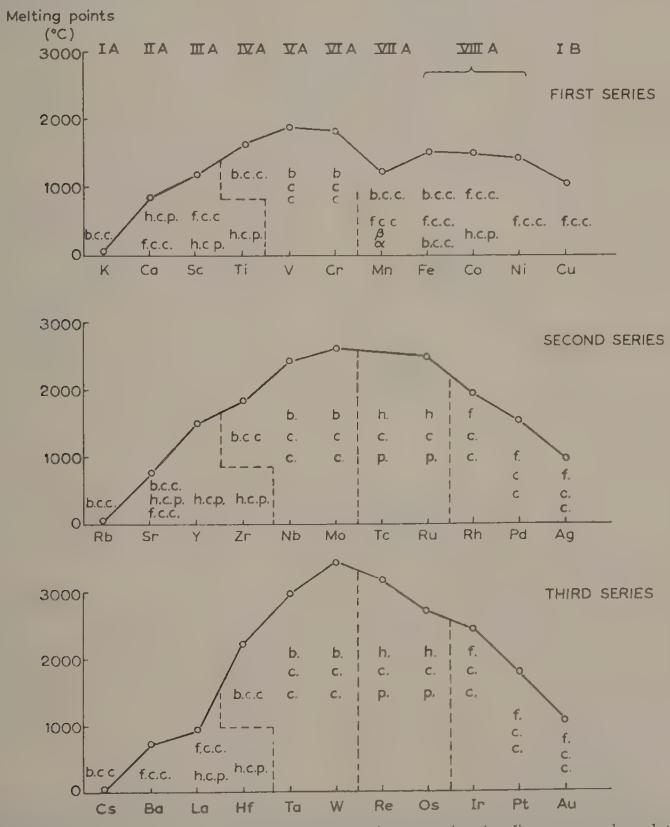

Fig. 1. Melting points and crystal structure of the elements in the first, second and third long periods: b.c.c. = body-centred-cubic; h.c.p. = hexagonal-close-packed; f.c.c. = face-centred-cubic.

References p. 410

paper cannot be applied in detail to elements in the first transition series beyond vanadium (or possibly chromium) although some of the general conclusions may still be applicable to these elements.

The important feature of HUME-ROTHERY, IRVING AND WILLIAMS' picture of the valencies of the transition elements in relation to the present work is that the addition of electrons to Group IIIA, IVA or VA elements will increase the valency of the metal whereas the addition of electrons to the Group VIA elements or those in Groups further to the right in the Periodic Table will produce a decrease in the number of electrons available for resonating covalent bonding.

When the melting points of the transition elements are plotted against atomic number, the second and third transition series show a systematic variation (Fig. 1). The melting point increases with increasing atomic number until Group VIA is reached and, thereafter, the melting point decreases. In the first transition series the picture is more complex although again elements to the left of Group VIA have melting points increasing with atomic number. For the third transition series the cohesive energies of the elements also show a maximum in Group VIA (Table 1).

TABLE I

HEATS OF FORMATION OF GASEOUS ATOMS AT 25°C
(kcal/g atom) [21]

Group IIA	*Group IIIA*	*Group IVA*	*Group VA*	*Group VIA*	*Group VIIA*	*Group VIIIA*			*Group IB*
Ca	Sc	Ti	V	Cr	Mn	Fe	Co	Ni	Cu
42	93	113	123	95	69	98	102	102	81
Sr	Y	Zr	Nb	Mo	Tc	Ru	Rh	Pd	Ag
39	103	142	177	156	140	160	138	93	68
Ba	La	Hf	Ta	W	Re	Os	Ir	Pt	Au
42	100	145	185	192	186	174	165	135	85

The available data suggests that the cohesive energy of the elements in the second transition series may behave in an irregular manner although the degree of irregularity is less than that for the first transition series. HUME-ROTHERY and his co-workers[7] have put forward a possible explanation for a maximum in bond energy in Group VIA as summarised below.

According to the resonating covalent bond theory of metals, the energy of a metal crystal is dependent both on the strength of the electron bonds and on the stabilising effect resulting from electron resonance between the different possible arrangements. If the number of bonding electrons per atom is v and the co-ordination number of the metal atoms is N, then the number of alternative arrangements between which resonance can occur is a maximum when $v = N/2$. In the face-centred-cubic metals and hexagonal-close-packed metals of ideal c/a ratio, the metal atoms have twelve nearest neighbours and, therefore, for these crystal structures a maximum in the bonding energy is to be expected when there are six bonding electrons, that is in Group VIA of the Periodic Table. The Group VIA elements possess the body-centred-cubic crystal structure, however, in which the metal atoms have eight nearest neigh-

References p. 410

bours and six additional atoms at a slightly greater distance. For co-ordination number of 8 and 14 the maximum bonding energies would be expected at an electron concentration of 4 and 7 electrons per atom respectively, and HUME-ROTHERY and his co-workers suggest that the maximum bonding energies in Group VIA can be understood if the effective co-ordination number has a value intermediate between 8 and 14.

Although no independent means have been found for determining the numerical value of an effective co-ordination number for crystal structures which are not face-centred-cubic or hexagonal-close-packed, the term is used in the present paper to convey the following concept. When a metal atom is surrounded by N atoms at a distance x (type A atoms) and N' atoms at a greater distance x' (type B atoms) then the A atoms will take part in the resonance process to a greater extent than the B atoms. If x' is considerably greater than x (as in the face-centred-cubic structure) then the co-ordination number is N but when x' is comparable to x then the effective co-ordination number from the point of view of resonance will be $N + k N'$ where k is less than one. Recently KUBASCHEWSKI[8] has introduced the idea of an effective co-ordination number and on the basis of two assumptions he obtains an effective co-ordination number of a little less than twelve (11.8) for the atoms in a body-centred-cubic structure. It should be pointed out that throughout much of his paper KUBASCHEWSKI uses an effective co-ordination number which includes an allowance for changes in bond lengths thereby including bond energies directly and on this basis he obtains an effective co-ordination number of a little more than twelve for a number of specific body-centred-cubic metals. The term effective co-ordination number used in this paper, as defined above, is concerned only with relative distances in a given structure.

For the purpose of the qualitative analysis presented in this paper it will be assumed that the effective co-ordination number of the atoms in a face-centred-cubic, body-centred-cubic or hexagonal-close-packed structure of ideal c/a ratio is in all cases approximately twelve. For the body-centred-cubic structure this is equivalent to saying that when $x'/x = 1.155$, $k = 2/3$.

3. ELECTRON CONCENTRATION AND CO-ORDINATION NUMBER

We postulate that the properties of the transition metals towards the centre of the transition series where high metal valencies are possible, are largely dependent on the tendency for the number of bonding electrons per atom to be equal to half the effective co-ordination number. This is equivalent to saying that for these elements the resonance contribution to the bonding is of considerable importance in determining, for example, bond strength and crystal structure.

According to this hypothesis elements which already possess the optimum condition for resonance (molybdenum and tungsten) will not be expected to accept or reject electrons readily since the optimum conditions would thereby be destroyed. Elements on either side of Group VIA can more nearly approach the optimum condition in two different ways. Either, for a given co-ordination number, the number of bonding electrons per atom may be altered by, for example, alloying or alternatively, for a given valency, the crystal structure will tend to be such as to give the required co-ordination number. These two alternatives will not be equally favour-

References p. 410

able, however, since any tendency to decrease the co-ordination number will be opposed by the tendency for a material with strong bonds which are not strongly directional, to possess a high co-ordination number. The importance of the resonance condition will decrease as the valency of the metal decreases and, therefore, the application of the hypothesis is limited to the elements towards the centre of the transition series.

If the hypothesis is correct it can be expected that elements to the left of Group VIA, having less than six bonding electrons per atom, will tend to accept electrons so as to approach more nearly the optimum concentration. Elements in Group IIIA should, therefore, be capable of accepting up to approximately three electrons per atom, Group IVA elements up to two electrons per atom and Group VA elements up to one electron per atom. On increasing the number of bonding electrons per atom it is to be expected that the stability of the metal lattice will increase provided the method of increasing the electron concentration does not introduce other considerations such as, for example, size factor effects. Those elements to the right of Group VIA in the Periodic Table will behave in the opposite manner to those on the left of Group VIA. Elements in Group VIIA, for example, will not readily accept additional electrons since additional electrons produce a decrease in effective valency and a decrease in bonding energy. These elements would tend, therefore, to behave as electron donors in an attempt to approach more nearly the Group VIA arrangement.

Both the face-centred-cubic and the ideal hexagonal-close-packed structures correspond to the closest packing of spheres, and, therefore, when strong bonding forces are present as in the transition metals these crystal structures would be expected. The elements in the centre of the transition series possess the body-centred-cubic structure, however, and ALTMANN, COULSON AND HUME-ROTHERY[9] have suggested that this crystal arrangement is due to the directional properties of the s.p.d. hybrid orbitals. If, as has been suggested, the body-centred-cubic structure possesses an effective co-ordination number of twelve then as far as the resonance contribution to bonding is concerned, the three common metal crystal structures are approximately equivalent provided the lattice is not distorted. On either side of Group VIA in the Periodic Table, the number of bonding electrons is less than the proposed optimum value of six for these common crystal structures, and it would be expected that these elements would tend to posses a structure of co-ordination number less than twelve. The hexagonal-close-packed structure is a crystal structure in which the effective co-ordination number can vary by varying the c/a ratio. For an ideal hexagonal-close-packed structure the c/a ratio is 1.633 and for any other value the effective co-ordination number must be less than twelve since six atoms will be at a distance x and six atoms at a greater distance x'. For example, if, as has been assumed, the effective co-ordination number of the body-centred-cubic structure is twelve so that $k = 2/3$ when $x'/x = 1.155$, an effective co-ordination number of less than twelve will be obtained for titanium with a hexagonal-close-packed structure of c/a ratio 1.587. Following the analysis by KUBASCHEWSKI[8], if the value of k decreases linearly with increasing x'/x over the range $x'/x = 1$ to $x'/x = 1.155$ then the effective co-ordination number of hexagonal-close-packed titanium is 11.75, in comparison with a value of 12.0 for a body-centred-cubic structure. It might be expected, therefore, that elements on either side of Group VIA would possess imperfect hexagonal-close-packed structures and that the c/a ratio would vary with the

References p. 410

number of bonding electrons per atom. The ideal ratio of 1.633 should be more nearly reached as the number of bonding electrons per atom approaches six.

An alternative way of reducing the effective co-ordination number in a given crystal structure is by substitutional solid solution of atoms having a different atomic radius from that of the solvent. A close-packed structure can no longer remain close-packed when atoms of a widely different size are introduced into the lattice and in a binary system in which there is a continuous series of solid solutions the distortion of the structure will be a maximum (and the effective co-ordination number a minimum) when there are approximately equal proportions of the two types of atoms, provided ordering does not take place.

Many of the properties of the transition metals can be interpreted on the basis of the ideas put forward above. The following examples, which are by no means exhaustive, are put forward to illustrate the usefulness of this method of approach.

4. THE SOLUBILITY OF HYDROGEN IN TRANSITION METALS

There is a considerable amount of experimental evidence to show that hydrogen in solution in a metal exists in an ionised state and this is to be expected from theoretical consideration[10]. The addition of hydrogen to a metal may be considered, primarily, therefore, as the addition of electrons to the metal atoms. The behaviour of the transition metals with hydrogen varies considerably both in the amount of hydrogen which can be dissolved or combined with the metal and in the thermodynamics of the process.

All the transition metals to the left of Group VIA in the Periodic Table dissolve hydrogen exothermically and form hydrides having a given limiting composition (Table 2). The only Group IIIA element for which there are data is lanthanum which is the first of the rare earth elements. Lanthanum forms a hydride of limiting composition corresponding to $LaH_{2.8}$ and if the electrons from the hydrogen atoms are taking part in the metal bonding, the optimum concentration of approximately six bonding electrons per metal atom for a metal–metal co-ordination of twelve, has been reached. The Group IVA elements form hydrides having a limiting composition corresponding to a little less than two hydrogen atoms for each metal atom so that again the number of bonding electrons is a little less than six. In Group VA, the limiting composition corresponds to a little less than equi-atomic proportions of hydrogen and metal and again the number of bonding electrons is approximately six. Since the presence of any additional electrons would produce a decrease in the bond energy, it can be seen why hydrides containing more hydrogen than corresponds to MH_3, MH_2 and MH for the Groups IIIA, IVA and VA metals respectively are not stable. The exothermic nature of the reaction can also be understood.

It is of interest to observe that the crystal structures of the hydrides of titanium and zirconium are either face-centred-cubic or distorted face-centred-cubic with the degree of distortion, at least for zirconium, varying with the hydrogen content[11]. The Group VA hydrides are, however, body-centred-cubic (or distorted body-centred-cubic) and yet, in spite of this difference between the Group IVA and the Group VA hydrides, the limiting electron concentration for their hydrides is a little less than six. This is consistant with the idea that the effective co-ordination numbers of the body-centred-cubic and face-centred-cubic structures are approximately the same.

References p. 410

TABLE II

THE REACTION OF TRANSITION METALS WITH HYDROGEN[22]

	Group IVA	*Group VA*	*Group VIA*	*Group VIIA*		*Group VIIIA*	
Element	Ti	V	Cr	Mn	Fe	Co	Ni
Limiting composition or solubility (cc/100 g)	$TiH^{*}_{1.99}$	$VH_{0.72}$	2.8 (1000°C)	30 (24°C)	3.2 (900°C)	3.4 (1000°C)	13.7 (1450°C)
Heat of sol. (kcal/mól)	—20	—15	25	—2	13	16	6
Element	Zr	Nb	Mo	Tc	Ru	Rh	Pd
Limiting composition or solubility (cc/100 g)	$ZrH^{*}_{1.92}$	$NbH^{**}_{0.94}$	0.5 (1000°C)	—	(low)	(low)	$PdH_{0.6}$
Heat of sol. (kcal/mol)	—35	—22	12.5	—	—	—	—1.7
Element	Hf	Ta	W	Re	Os	Ir	Pt
Limiting composition or solubility (cc/100 g)	—	$TaH^{**}_{0.80}$	(low)	(low)	(low)	(low)	0.2 (1000°C)
Heat of sol. (kcal/mol)	—	negative	—	—	—	—	35

* H. L. YAKEL, *Acta. Cryst.*, 11 (1958) 46.
** G. BRAUER AND R. HERMANN, *Z. anorg. Chem.*, 274 (1953) 11.

The titanium–hydrogen system is a typical example of the exothermic reaction of a transition metal with hydrogen. Hydrogen has a considerable solid solubility in β titanium and it depresses the α to β transition temperature[12]. This is to be expected since the hydrogen increases the effective number of bonding electrons per atom (see Section 6). The solubility in the α phase however, is very limited, a hydride phase being formed. The hydride has a composition range from TiH to $TiH_{1.99}$ and in this "compound" the metal atoms are arranged on a face-centred-cubic lattice. The low solubility of hydrogen in the α phase is to be expected since according to our interpretation, the hexagonal-close-packed structure of titanium only exists because of the small number of bonding electrons per atom (see Section 5). The addition of electrons from the hydrogen atoms causes the metal lattice to change to the close-packed face-centred-cubic structure found in the hydride. The hydride may be considered, therefore as a new titanium phase which has been stabilised with hydrogen. It is not understood why the face-centred-cubic structure is formed in preference to the body-centred-cubic structure characteristic of transition metals of high electron concentration but according to our approach the effective co-ordination numbers are the same. As is shown in a later section, the stabilising of the face-centred-cubic structure by the addition of electrons from interstitial elements is a quite general phenomenon. Titanium having changed phase to the face-centred-cubic structure will then continue to accept electrons until the number of bonding electrons per atom is approximately six.

The data on the solubility of hydrogen in the transition metals to the right of Group VA in the Periodic Table are very incomplete but from the electron concentration relationships it is to be expected that the addition of hydrogen will introduce electrons into non-bonding orbitals of the metal atoms and will have coupled with them electrons which previously contributed to the bonding. Group VIA elements already possess the optimum electron concentration for the co-ordination number and the reduction in the effective electron concentration by the addition of hydrogen will destroy this arrangement. An element such as rhenium which has already passed the optimum concentration will become still further removed from the optimum arrangement by the addition of hydrogen. Where experimental data are available they do, in general, confirm that for the elements to the right of Group VA the solubility for hydrogen is low and the solution takes place endothermically (Table 2).

5. THE CRYSTAL STRUCTURE OF THE TRANSITION METALS

All the Group VIA elements possess the body-centred-cubic crystal structure, (Fig. 1), with an effective co-ordination number of approximately twelve. The Group VA elements also possess the body-centred-cubic structure but, since there are only five bonding electrons per atom, for these metals the electron concentration is below the optimum for the co-ordination number. Apparently, however, the electron concentration is not sufficiently removed from the optimum value to produce a change in co-ordination number. For the Group IVA metals, the number of bonding electrons per atom is only four and the crystal structure changes to an imperfect hexagonal-close-packed arrangement, (Table 3). The c/a ratio for all the Group IVA metals is considerably less than the value for closest packing so that the effective co-ordination number is less than twelve. These elements, however, exhibit a phase

References p. 410

change to the body-centred-cubic structure at elevated temperatures suggesting that the difference in energy between the two structures is small.

TABLE III

c/a RATIOS FOR HEXAGONAL-CLOSE-PACKED STRUCTURES[9]

Group IIIA	*Group IVA*	*Group VIIA*	*Group VIIIA*
Sc	Ti	—	—
1.585–1.588	1.587	—	—
Y	Zr	Tc	Ru
1.585–1.588	1.592	1.604	1.583
La	Hf	Re	Os
1.61	1.587	1.615	1.579

Theoretical c/a ratio for an undistorted hexagonal-close-packed structure = 1.633.

The hexagonal-close-packed structure is again present at room temperature in Group IIIA and again the c/a ratio is considerably less than the ideal value (Table 3). At elevated temperatures, these elements change phase to the face-centred-cubic structure typical of elements at either end of the transition series where the valencies are low and our hypothesis is no longer applicable.

The considerations put forward for the Groups of elements to the left of the Group VIA in the Periodic Table apply also to the elements to the right of Group VIA except that in the first transition series, the stability of the atomic orbitals makes a detailed interpretation for these elements impossible at the present time. For the second and third transition series, however, the interpretation of changes in crystal structure is straightforward. On decreasing the number of bonding electrons to a value less than six in Group VIIA, a distorted hexagonal-close-packed structure is produced. The small degree of distortion of the hexagonal-close-packed structure exhibited by the Group VIIA, metals (Table 3) is, we suggest, due to the electron concentration being not far removed from the optimum value. On decreasing the number of bonding electrons per atom still further as in the case of osmium, the structure is again hexagonal-close-packed, but the c/a ratio is further removed from the theoretical value. The theory no longer applies to elements beyond osmium due to their low valencies.

If as described above, the crystal structure of the transition elements is governed by a relationship between electron concentration and co-ordination number, it should be possible to relate changes in crystal structure on alloying to changes in electron concentration. In the following two sections, it will be shown that the alloying behaviour of the transition metals can, at least in part, be understood in terms of the hypothesis.

6. ELECTRON CONCENTRATION AND ALLOYING BEHAVIOUR

In recent years, the alloying behaviour of titanium[12] and zirconium[13] has been studied extensively and the characteristics of binary alloy systems containing these elements will be used to illustrate the importance of electron concentration and co-ordination number in alloys of the transition metals. Both titanium and zirconium possess the hexagonal-close-packed crystal structure at room temperature with a

References p. 410

c/a ratio of 1.587 and 1.592 respectively. When any of the transition metals to the right of Group VIA in the Periodic Table are added to titanium or zirconium, the stability of the body-centred-cubic β phase is increased and according to our hypothesis t! is is due to the increase in the average number of bonding electrons per atom. The magnitude of the stabilising effect for a given additive would be expected to be dependent upon the number of electrons per atom donated to the solvent by the solute.

TABLE IV

THE LOWERING OF THE $\alpha+\beta/\beta$ PHASE BOUNDARY IN BINARY TITANIUM ALLOYS TO 700°C

System	At.-% of additive	Size factor	System	At.-% of additive	Size factor
Ti–V	12	—7.5	Ti–Cr	8	—13
Ti–Nb	18	0	Ti–Mo	10	—4.8
Ti–Ta	20	0	Ti–W	9	—4.2

Consider for example, the $(\alpha + \beta)/\beta$ phase boundary in titanium alloys containing a Group VA or VIA metal. Table 4 lists the atomic percentage of the additive necessary to reduce the $(\alpha + \beta)/\beta$ boundary to 700°C and the percentage differences in atomic diameters for each system are also included in this table. To reduce the phase boundary by equal amounts, twice as much niobium or tantalum is required as molybdenum or tungsten, since replacing one atom of titanium by a Group VA metal is equivalent to adding one electron, whereas the addition of a Group VIA atom is equivalent to adding two electrons. The picture is a little more complex for additions of vanadium and chromium owing to the large differences in atomic diameters and the contribution of lattice distortion produced in this way will be considered in the next section. No data are available on the effects of adding Group IIIA elements to titanium, but on this basis, it is expected that Group IIIA elements will stabilise the hexagonal-close-packed structure.

Increasing the number of bonding electrons per atom in titanium and zirconium by adding transition elements to the right of Group IVA, in addition to stabilising the β structure, should also increase the c/a ratio of the α phase so that it would more nearly approach the ideal value of 1.663. MAYKUTH[14] has shown that at 530°C. the α solubility of tantalum in titanium extends beyond 1.49 at.-% and that increasing additions of tantalum produce a linear expansion of the titanium lattice in the c direction whilst having no significant effect on the a parameter. No other data of this type are available for the titanium alloys due to the low solubility of most transition elements in the α titanium.

All the binary transition metal systems that possess a hexagonal-close-packed phase of which the variation of the c/a ratio with composition has been determined vary in the way expected from the change in electron concentration (Table 5). HELLAWELL AND HUME-ROTHERY[15] have studied in some detail the variation of the c/a ratio of dilute solutions of zirconium, niobium, molybdenum, rhodium and palladium in ruthenium and again the results are in agreement with the hypothesis. Regularities in the position of intermediate phases and solid solution limits in binary transition metal alloys has recently been summarised by HAWORTH AND HUME-ROTHERY[16] and, for the body-centred-cubic and hexagonal-close-packed structures,

References p. 410

TABLE V

HEXAGONAL-CLOSE-PACKED PHASES IN BINARY TRANSITION METAL ALLOYS

System	Upper valency limit		Lower valency limit		Ref.
	Composition (At.-%)	c/a ratio	Composition (At.-%)	c/a ratio	
V–Os	85* Os	1.595	100 Os	1.579	A
Nb–Os	85 Os	1.583	100 Os	1.579	A
Cr–Os	90* Os	1.598	100 Os	1.579	A
Mo–Os	75 Os	1.590	100 Os	1.579	A
Mo–Rh	47 Rh	1.605	85 Os	1.603	B
Mo–Ir	43 Ir	1.601	78 Ir	1.600	B
W–Ir	44 Ir	1.611	77 Ir	1.602	B

A — A. E. KNAPTON, *J. Inst. Metals*, 87 (1958) 28.
B — M. HANSON, *Constitution of Binary Alloys*, McGraw-Hill, New York, 1958.
* Limiting composition not yet known.

the experimental data are in keeping with our hypothesis. No attempt has yet been made to apply our relationship to the β W, σ or α Mn phases owing to the difficulty of determining an effective co-ordination number for these complex structures.

7. SIZE FACTOR EFFECTS

The Group IVA elements, titanium and zirconium, form a continuous series of solid solutions in both the α and β phases but in the centre of the phase diagram, the α to β transition temperature is lowered considerably. This cannot be related to a change in valency since both titanium and zirconium possess four bonding electrons per atom, but the phenomenon is in keeping with the present theory. The sizes of the titanium and zirconium atoms differ by approximately 8% and, therefore in an alloy, the effective co-ordination number in either the α or β phase will be reduced, producing an increase in the stability of the β phase. The distortion of the structure will be a maximum towards the centre of the phase diagram and, therefore, it is to be expected that the α to β transition temperature will exhibit a minimum in this region, as is the case.

When an element other than zirconium or hafnium, is added to titanium, according to the hypothesis the resulting change in the α/β transition will be due both to the change in effective valency and the change in effective co-ordination number brought about by the presence of atoms of different sizes. Consider, for example, titanium alloys containing Group VA elements. As has already been pointed out, approximately 20 at.-% of niobium or tantalum is required to reduce the $(\alpha + \beta)/\beta$ phase boundary to 700°C (Table 4). The size factor in both these systems is zero, so that no change takes place in the effective co-ordination number. In the titanium–vanadium system, however, the addition of vanadium both increases the valency and decreases the effective co-ordination number (size factor = —7.5) and, therefore, the stabilising effect on the β phase is increased. The same considerations apply to titanium with the Group VIA metals, but the size factor effect is reduced in relation to the changes in electron concentration.

References p. 410

8. INTERSTITIAL ELEMENTS OTHER THAN HYDROGEN IN TRANSITION METALS

When transition metals dissolve or form metallic compounds with bo on, carbon, nitrogen or silicon, experimental evidence is consistent with the idea that some electron transfer is taking place from the non-metal atoms to the metal atoms[2,17,18,21,23,24]. This is possibly also true for oxygen in dilute solution[25]. Although the solution of these non-metallic elements in transition metals cannot be considered simply as the additions of electrons since metal–non-metal and non-metal–non-metal bonding may also be present, the change in electron concentration is considered to be of considerable importance. A more detailed account of these ideas, as applied to the carbides, has already been published[18].

Since the Group IVA elements possess only four bonding electrons per atom, a high affinity for boron, carbon, nitrogen and oxygen is to be expected and the addition of these elements to the hexagonal-close-packed phase should cause the c/a ratio to approach more nearly the value for close-packing. The solubility of interstitial elements in titanium decreases in the order oxygen, nitrogen, carbon,

TABLE VI

ELECTRONEGATIVITY OF INTERSTITIAL ELEMENTS AND THEIR SOLUBILITY AT 700°C IN TITANIUM

	*Electronegativity**	*Solubility at 700°C (at.-%)*
Oxygen	3.5	33
Nitrogen	3.0	13
Carbon	2.5	1
Boron	2.0	0.2

* L. PAULING, *The Nature of the Chemical Bond*, 2nd Ed., Cornell University Press, Ithaca, N.Y., 1958, p. 64.

boron and this order corresponds to decreasing electronegativity of the added element (Table 6). Oxygen can only be a weak electron donor, and, therefore, a considerable quantity of oxygen in solution is required to produce a phase change to a perfect close-packed structure. (TiO, TiN and TiC all possess the NaCl type crystal structure in which the metal atoms are arranged on a face-centred-cubic lattice.) The ability to donate electrons increased in the order oxygen, nitrogen, carbon, boron, and therefore, the amount of these elements required to produce a phase change decreases in this order. The same pattern of behaviour is shown by the variation of the c/a ratio of the α phase (Table 7). All the interstitial elements increase the c/a ratio as expected and the magnitude of the effect for a given amount of impurity increases in the order, oxygen, nitrogen, carbon and boron.

TABLE VII

THE EFFECT OF INTERSTITIAL ELEMENTS ON THE LATTICE PARAMETERS OF α TITANIUM

Added element	*Parameter change per unit wt.-%*	
	a	c
Oxygen	0.000	0.015
Nitrogen	0.002	0.023
Carbon	0.013	0.049

References p. 410

As for hydrogen, interstitial elements cause the metal to favour the face-centred-cubic structure in preference to the body-centred-cubic structure for an electron concentration approaching six bonding electrons per atom possibly due to the interstitial elements reducing or destroying any directional properties of the s.p.d. bonding orbitals.

Since, according to the hypothesis put forward in this paper the existence of a distorted hexagonal-close-packed structure in titanium and zirconium is due to the low electron concentration, the number of additional electrons per atom required to produce a change in phase should be independent of the method of addition. For example, a given amount of hydrogen in solution in zirconium is required to produce a phase change, but if the electron concentration has already been increased by other interstitial elements in solution, the amount of hydrogen necessary will be reduced. The effect of oxygen, nitrogen and carbon on the solubility of hydrogen in zirconium has been studied (McQUILLAN AND McQUILLAN[12]) and the results support the theory. The solubility of hydrogen is reduced by the presence of other interstitial elements in solution and the magnitude of the decrease for a given atomic percentage of non-metal increases in the order oxygen, nitrogen, carbon, the order of decreasing electronegativity.

Detailed information on the solubility of interstitial elements in Group VA metals is not available, but the solubility of oxygen in vanadium, niobium and tantalum is of the order of a few atomic percent. In general, therefore, interstitial elements can be accepted into the lattice of elements to the left of Group VIA, although when the added element is a strong electron donor a change of phase of the metal may be produced at an early stage. These borides, carbides, nitrides and silicides exhibit metallic properties and as the theory predicts the compounds of greatest stability are formed with Group IVA or VA metals, whereas the transition elements of maximum melting point are found in Group VIA.

In the elements molybdenum and tungsten the maximum number of bonding electrons per atom has already been attained and any increase in the electron concentration reduces the effective number of bonding electrons. Therefore, the addition of oxygen or carbon to molybdenum for example, is energetically unfavourable resulting in low solubility[19]. The solubility of interstitial elements in the transition metals to the right of Group VIA will also be low and the stability of any interstitial compounds will be lower than the corresponding compounds containing Group IVA or Group VA elements.

9. THE SEGREGATION OF INTERSTITIAL ELEMENTS

It has been shown that, on the basis of our hypothesis, the addition of electrons to the transition metals in Group VIA and elements further to the right in the Periodic Table will be energetically unfavourable. We will now consider in more detail the addition of, for example, hydrogen to an element such as molybdenum.

When a hydrogen atom is introduced into an otherwise perfect molybdenum lattice, the effective valency of the surrounding metal atoms will be decreased and, since in molybdenum the optimum electron concentration for the co-ordination number already exists, the hydrogen atoms will tend to be in an unstable position. A local reduction in the effective electron concentration by the addition of hydrogen will, in fact, favour, a lower co-ordination number for the metal atoms. This means

References p. 410

that hydrogen atoms will have a low solubility in the perfect molybdenum lattice but that hydrogen will segregate and be bound to those points in the crystal where the metal co-ordination number is already reduced such as at dislocations and grain boundaries. It should be emphasised that this suggested segregation effect is not associated with the relief of lattice strain but is an electron concentration effect. The same analysis applies not only to the Group VIA elements but also to Group VIIA and possibly some Group VIIIA elements since again the addition of electrons decreases the effective metal valency. There is a considerable amount of experimental evidence which suggests that, in transition metals which dissolve hydrogen endothermically, the solution of hydrogen takes place preferentially at faults in the lattice[20].

Interstitial atoms other than hydrogen will also be attracted electronically to faults in the lattice of, for example, molybdenum or tungsten whereas no electronic bonding will be present in elements to the left of Group VIA. In fact, in the Group IVA and VA elements the reverse will be true since the optimum electron concentration for the co-ordination number has not been reached. It is suggested that this difference between the elements to the left of Group VIA and those to the right of Group VA may account for marked differences in mechanical properties between for example, the Group VA elements and the Group VIA elements. Tantalum in Group VA and tungsten in Group VIA both possess the body-centred-cubic structure and have comparable melting points. However, tungsten is difficult to work and exhibits a ductile-to-brittle transition temperature in contrast with tantalum which is ductile and under a wide range of conditions does not exhibit a ductile-to-brittle transition. In both these materials interstitial impurities are influencing the movement of dislocation as is shown by the marked variation of yield stress with temperature but the difference in ductility cannot be explained on the basis of elastic interaction between interstitial atoms and dislocations since the elastic interaction in the two metals should not be very different. As described above, however, the difference in electron concentration should result in interstitial impurity atoms having a much greater effect in tungsten than in tantalum.

On the basis of electron concentration segregation as described above, it may be possible to explain why the embrittling effect of an interstitial impurity depends upon the particular element in solution.

10. CONCLUSIONS

The hypothesis is put forward that many of the properties of the transition elements can be interpreted in terms of a relationship between the co-ordination number of the metal atoms and the number of bonding electrons per atom. The electron resonance contribution to the bond strength is a maximum when the number of bonding electrons per atom is approximately equal to half the effective co-ordination number and it is postulated that, although this optimum condition cannot always be achieved, the stability of this arrangement dictates very largely alloying behaviour and crystal structure. The effect is greatest towards the centre of the transition series, the importance of the electron concentration/co-ordination relationship decreasing with increasing separation of the element under consideration from Group VIA of the Periodic Table.

The stability of a closely packed structure of metal atoms having approximately

References p. 410

six bonding electrons per atom results in transition elements to the left of Group VIA accepting additional electrons until a concentration of approximately six bonding electrons per atom has been reached. Elements to the right of Group VA, however, will not accept additional electrons and will behave as electron donors when in solution in a metal requiring additional electrons. The effects of alloying together two transition metals is dependent on changes in average electron concentration and, when the difference in atomic diameters is large, on changes in the effective co-ordination number of the metal atoms.

In support of the hypothesis it is shown that it leads to an understanding of the behaviour of transition metals with hydrogen; the hypothesis leads to a partial understanding of the crystal structure of the transition metals in the centre of the transition series and some examples are given of the way the hypothesis can be applied to alloys. The hypothesis is relevant to the interaction of elements such as carbon and nitrogen with transition metals and it follows logically that, in transition metals to the right of Group VA, interstitial elements will be bound electronically to faults in the metal lattice.

The applications of the hypothesis discussed in this paper illustrate the potential value of this new approach to the transition element although the analysis has been, on the whole only qualitative and, so far, no serious attempt has been made to apply the theory to intermetallic compounds. It is considered however, that in both these respects, considerable development of these ideas will be possible.

REFERENCES

1 D. A. ROBINS AND I. JENKINS, *Acta Met.*, 3 (1955) 598.
2 D. A. ROBINS, *Phil. Mag.*, 3 (8th series) (1958) 313.
3 D. A. ROBINS, The Physical Chemistry of Metallic Solutions and Intermetallic Compounds, *Natl. Phys. Lab. Symposium No. 9*, Vol. II, paper 7B, H.M. Stationary Office, London, 1959.
4 L. PAULING, *Phys. Rev.*, 54 (1938) 899.
5 L. PAULING, *J. Amer. Chem. Soc.*, 69 (1947) 542.
6 L. PAULING, *Proc. Roy. Soc. (London)*, 196A (1949) 343.
7 W. HUME-ROTHERY, H. M. IRVING AND J. R. P. WILLIAMS, *Proc. Roy. Soc. (London)*, 208A (1951) 431.
8 O. KUBASCHEWSKI, The Physical Chemistry of Metallic Solutions and Intermetallic Compounds, *Natl. Phys. Lab. Symposium, No. 9*, Vol. I, paper 3C, H.M. Stationary Office, London, 1959.
9 S. ALTMANN, C. COULSON AND W. HUME-ROTHERY, *Proc. Roy. Soc. (London)*, 240A (1957) 145.
10 I. ISENBERG, *Phys. Rev.*, 79 (1950) 736.
11 D. A. VAUGHAN AND J. R. BRIDGES, *Trans. A.I.M.E.*, 206 (1956) 528.
12 A. D. MCQUILLAN AND M. K. MCQUILLAN, *Titanium*, Butterworths Scientific Publications, London, 1956.
13 G. L. MILLER, *Zirconium*, Butterworths Scientific Publications, London, 1954.
14 D. J. MAYKUTH, *J. Inst. Metals*, 81 (1953) 426.
15 A. HELLAWELL AND W. HUME-ROTHERY, *Phil. Mag.*, 45, 7th series (1954) 797.
16 C. W. HAWORTH AND W. HUME-ROTHERY, *Phil. Mag.*, 3, 8th series (1958) 1013.
17 G. W. WIENER AND J. A. BERGER, *Trans. A.I.M.E.*, 203 (1955) 360.
18 D. A. ROBINS, *Powder Met.*, 1 (1958) 172.
19 W. E. FEW AND G. K. MANNING, *Trans. A.I.M.E.*, 194 (1952) 271.
20 D. P. SMITH, *Hydrogen in Metals*, Univ. Chicago Press, Chicago, 1948.
21 O. H. KRIKORIAN, *Univ. Calif. Rep. No. U.C.R.L. 2888*, (1955).
22 C. J. SMITHELLS, *Metals Reference Book*, Butterworths Scientific Publications, London, 1955, Vol. II, p. 536.
23 P. DAVAL AND L. S. DARKEN, *Trans. A.I.M.E.*, 188 (1950) 1156.
24 K. H. JACK, *Proc. Roy. Soc.*, 195A (1948) 34.
25 N. SCHONBERG, *Acta. Chem. Scand.*, 8 (1954) 221, 240, 617, 620, 627, 630, 932.

LOSS OF METAL FROM CHROMIUM AT ELEVATED TEMPERATURES IN AIR

G. R. WILMS AND T. W. REA

Australian Defence Scientific Service, Defence Standards Laboratories, Department of Supply, Maribyrnong (Australia)

(Received November 13th, 1959)

Since advances in gas turbine and rocket design are now demanding engineering materials that operate at temperatures in excess of 1000°C, increasing attention is being directed to the oxidation and vaporization behaviour of metals and alloys. In many studies of oxidation and vaporization reported in the literature, metal specimens are merely heated in an electric furnace exposed to a supposedly static air atmosphere, the specimens being weighed before and after the heating. Adopting the same procedure to study the behaviour of chromium in our laboratories, a considerable scatter in results was obtained.

Cylindrical test specimens, 0.4 in. dia., 1½ in. long and weighing 22 g, were heated in air at constant temperatures in the range of 1000°–1100°C for 200 h in commercial electric furnaces. Tests were done in triplicate, care being taken to ensure temperature uniformity. Heating in the above temperature range resulted in a loss of metal, but the relative roles of oxidation and vaporization are not at present known.

Typical results, given in Table I, show that the average metal loss is markedly increased with increase in furnace size (see A and B in Table I). Furthermore, there are differences in metal loss between individual specimens heated in the same environment, these differences being more pronounced for the larger furnace. This scatter

TABLE I

VARIATION IN LOSS OF CHROMIUM AFTER HEATING IN AIR AT 1100°C FOR 200 h

Method of heating	*Loss of weight*, g*	*Reduction in diameter*, in.*
A. Furnace X	0.766	0.0050
(Heating chamber: 2.3 cu. ft.)	1.122	0.0057
	0.270	0.0016
B. Furnace Y	0.102	0.0003
(Heating chamber: 0.3 cu. ft.)	0.126	0.0004
	0.129	0.0005
C. Furnace Y	0.112	0.0004
(Stream of air blown into heating chamber through	0.784	0.0040
thermocouple port by external circulation fan.)	0.595	0.0030

* Figures do not include oxide layer, since a non-adherent scale was formed at 1100°C.

References p. 412

in results is apparently due to variations in convective air flow through the respective furnaces, since, when heating in the smaller furnace, both the average metal loss and the difference in metal loss between individual specimens can be substantially increased by introducing a gentle stream of air (see B and C in Table I).

Similar results have been obtained on mild steel[1,2], in that scaling increased rapidly with gas flow rate over a range of very low gas velocities; a critical velocity, dependent on temperature, gas composition and surface area, was reached above which further increases in the gas velocity produced no further increase in scaling. It would evidently be of interest to determine whether a similar critical velocity exists for chromium. The essential point of the investigation on chromium to date, however, is that the atmosphere in commercial electric furnaces is not truly static, and that relatively small variations of air flow at very low flow rates can have a considerable effect on the high temperature behaviour of metals.

ACKNOWLEDGEMENTS

The authors wish to thank Mr. J. I. NISH for his helpful advice, and the Chief Scientist, Australian Defence Scientific Service, Department of Supply, Melbourne, Australia, for permission to publish this work.

REFERENCES

1 C. UPTHEGROVE, *Univ. Mich. Eng. Research Inst. Eng. Research Bull.*, 25 (1933) 18.
2 H. C. MILLETT AND J. W. COBB, *Trans. Inst. Gas Engrs.*, 85 (1935–36) 626.

CONTENTS

A study of rhodium(III) oxalates by paper electrophoresis, paper chromatography, ion-exchange chromatography and spectrophotometry
by S. K. SHUKLA (Paris) 333

The constitution of manganese base alloys with metals of the second transition series
by A. HELLAWELL (Oxford) 343

Die Beeinflussung der Warmverformbarkeit von Ti–Al-Legierungen durch Wasserstoffzusätze
von H. W. SCHLEICHER UND W. JUNG-KÖNIG (Frankfurt/Main) 348

Some measurements on the thermoelectric power of plutonium metal
by J. A. LEE AND R. O. A. HALL (Harwell) 356

The ordered crystal structure of In_2Te_3
by J. C. WOOLLEY, B. R. PAMPLIN AND P. J. HOLMES (Nottingham and Aldermaston) 362

A survey of the rhenium–carbon system
by J. E. HUGHES (Aldermaston) 377

Ordering in CoPt–FePt alloys
by J. C. WOOLLEY AND B. BATES (Nottingham) 382

Zur Feinreinigung des Galliums
von H. MERKEL (Erlangen) 390

An interpretation of some of the properties of the transition metals and their alloys
by D. A. ROBINS (Greenford) 396

Loss of metal from chromium at elevated temperatures in air
by G. R. WILMS AND T. W. REA (Maribyrnong) 411

All rights reserved

ELSEVIER PUBLISHING COMPANY, AMSTERDAM

Printed in The Netherlands by

NEDERLANDSE BOEKDRUK INRICHTING N.V., 'S-HERTOGENBOSCH

FILED IN STACKS

ELSEVIER'S

SCIENTIFIC JOURNALS

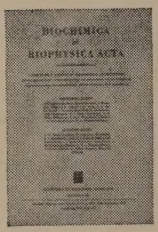

ANALYTICA CHIMICA ACTA

BIOCHIMICA ET BIOPHYSICA ACTA

JOURNAL OF CHROMATOGRAPHY

CLINICA CHIMICA ACTA

ICSU REVIEW

TROPICAL AND GEOGRAPHICAL MEDICINE

EPILEPSIA

JOURNAL OF ELECTROANALYTICAL CHEMISTRY

WEAR - USURE - VERSCHLEISS

Specimen copies are available

ELSEVIER PUBLISHING COMPANY
110-112 SPUISTRAAT — AMSTERDAM — THE NETHERLANDS